ROBUST COMMUNICATIONS IN LARGE AND HETEROGENEOUS VEHICLE-TO-VEHICLE NETWORKS

by

BIN CHENG

A dissertation submitted to the

School of Graduate Studies

Rutgers, The State University of New Jersey

In partial fulfillment of the requirements

For the degree of

Doctor of Philosophy

Graduate Program in Electrical and Computer Engineering

Written under the direction of

Marco Gruteser

And approved by

_____

_____

_____

_____

New Brunswick, New Jersey

January, 2019

ABSTRACT OF THE DISSERTATION

Robust Communications in Large and Heterogeneous Vehicle-to-Vehicle Networks

by BIN CHENG

Dissertation Director:

Marco Gruteser

Dedicated Short-Range Communications (DSRC) is a wireless communication technology designed to support periodic information sharing between vehicles. With the shared information, a car can enhance its situational awareness and thus improve driving safety. However, as DSRC moves rapidly towards large-scale real-world deployments, several challenges remain. One particularly challenging scenario is DSRC in heterogeneous networks where different protocols/technologies coexist. These coexistence scenarios can arise when: 1) the protocols of DSRC evolve to a newer version and thus two versions of DSRC coexist in one network during a transition period; 2) DSRC shares its licensed spectrum with other unlicensed users, e.g., Wi-Fi devices; 3) Multi-technology and multi-band vehicular communications enable other emerging technologies, e.g., mmWave, on the same car.

Since DSRC was originally designed for sole operation, coexistence could degrade its performance. However, it remains unknown to what extent the DSRC performance will be degraded and whether the performance degradation can be mitigated or controlled to an acceptable level. To fill this void, this dissertation quantifies the performance of DSRC in these coexistence scenarios via accurate simulations whose simulation models were developed and calibrated based on the data collected from a set of experiments

with up to four hundred DSRC transmitters, identifies the main challenges of preserving the DSRC performance and further proposes solutions to reduce the experienced performance degradation.

Specifically, for the evolved DSRC scenario, we consider two DSRC congestion control protocols as an example, CAM-DCC as the legacy DSRC protocol and LIMERIC as the evolved DSRC protocol. We first show that the CAM-DCC vehicles can experience doubled packet latency after introducing the LIMERIC vehicles into the network and identify that the performance degradation can be controlled by adjusting LIMERIC's parameters. We then propose an adaptive algorithm to maintain the performance degradation within an acceptable level.

For the DSRC-Wi-Fi spectrum sharing scenario, we first identify delayed detection, unilateral hidden terminals and backoff countdown collisions are the main challenges of preserving the performance of the legacy DSRC when applying three recently proposed spectrum sharing mechanisms to share the DSRC spectrum with unlicensed Wi-Fi devices. Simulation results indicate that sharing the DSRC spectrum by using the three mechanisms can cause more than 30% extra packet losses of DSRC transmissions. To reduce the DSRC performance degradation, we then suggest adding an extra idle period to the Wi-Fi inter-frame period and preventing Wi-Fi transmissions upon DSRC detection.

For the mmWave scenario, we show that mmWave coordination is possible via DSRC without affecting existing DSRC traffic. The driving status shared via DSRC can be further utilized to estimate the usefulness of sensing information shared via mmWave. When scheduling mmWave transmissions, these transmissions carrying more useful information can then be scheduled with a higher priority. Compared to a simple broadcast strategy, our approach significantly improves the mmWave information sharing efficiency by up to 50%.

Acknowledgements

I have been very fortunate to spend my PhD time at WINLAB, Rutgers University. There are many people to whom I am very grateful for providing various forms of guidance and support during my time as a doctoral student.

First, I would like to express my gratefulness to my advisor, Marco Gruteser. Marco is not only a tremendous advisor, but also an incredibly caring and supportive mentor. He uses the sharp critiques and incisive suggestions to take my work to its next level, and also steered me back on track every time I was lost. He always generously shares his experiences and suggestions to guide me through many crossroads during my PhD journey. Marco is definitely my role model in my future career. I deeply feel fortunate to have Marco as my advisor.

I would also like to thank Prof. Roy Yates and Prof. Dipankar Raychaudhuri for serving on my dissertation committee and proposal defense committee, respectively. Their insightful suggestions and valuable comments have greatly improve the quality and completeness of my work.

I am also honored to have the opportunity to be mentored by and work with Dr. John Kenney, my internship mentor at Toyota InfoTechnology Center. I admire him for his sharp mind, enthusiasm and wholeheartedness.

Special thanks to Ali Rostami, who has worked with me for more than five years and was always willing to give me hand when I needed help. I am very lucky to be surrounded by a brilliant group of peers and friend at WINLAB – Gorkem Kar, Shubham Jain, Viet Nguyen, Hongyu Li, Luyang Liu, Ines Ugalde.

Words cannot describe my gratitude to my family. I have always been feeling that I have the best parents in the world. Though I am their only child, they encouraged me to go abroad to see the world. No matter how many difficulties I met, I never lose

Dedication

To my family.

Table of Contents

List of Tables

List of Figures

Chapter 1

Introduction

In the U.S., over thirty-two thousand people die in car accidents with about 100 times more injured or disabled each year [8]. Globally, these numbers increase to 1.3 million and 50 million, respectively [9]. Therefore, necessary actions are urgently required to reduce the number of car accidents. Vehicle-to-vehicle (V2V) safety communications have been long envisioned as one efficient solution to improve the driving safety. With V2V communications, cars are able to "talk to" each other and exchange vehicle status information. Many safety applications can then leverage the shared information to assist drivers in expanding their horizon of awareness, predict imminent car collision threats, and avoid accidents or reduce the severity of their consequences. Given the potential safety benefits, V2V communications, in particular, Dedicated Short-Range Communications (DSRC), have been investigated for many years for real-world deployment. For example, in the U.S., the Federal Communication Commission (FCC) has allocated 75 MHz in the 5.9 GHz band for intelligent transportation systems (ITS) [10]. A series of projects have been initiated by the National Highway Traffic Safety Administration (NHTSA) [11–15] to evaluate the performance of DSRC-based communication systems in different environments and also study the reliability of safety applications built upon such communication systems. The outcomes of these projects validated the effectiveness of DSRC-based V2V communication systems in preventing potential car collision and thus improve the driving safety.

However, while DSRC technology moves rapidly towards real-world deployment, several challenging issues remain to be resolved. This dissertation is concerned with DSRC performance in heterogeneous networks where different protocols/technologies coexist. Such coexistence scenarios can arise, because:

- Driven by the requirements of different applications and the needs of technology evolution, DSRC protocols may evolve from one version to an upgraded one. During the transition period, protocols from different development stages may coexist in the same network.

- According to [16], it is possible that DSRC will share its spectrum with unlicensed Wi-Fi devices in the near future. Consequently, different technologies share the same spectrum and coexist in the same network.

- In the near future, multi-technology and multi-band V2V scenarios are enabled on vehicles. In this scenario, DSRC is expected to coexist with other emerging V2V technologies, e.g., millimeter wave communications (mmWave).

A large body of existing research has studied various heterogeneous networks, such as Wi-Fi coexisting with Bluetooth and Zigbee [17–19], Wi-Fi coexisting with Long Term Evolution (LTE) [20–22], LTE coexisting with second generation (2G)/third generation (3G) mobile systems [23], newer version of Wi-Fi protocols coexisting with legacy Wi-Fi protocols [24] and unlicensed devices coexisting in the TV white space [25]. However, the safety-critical nature of DSRC makes its coexistence scenarios special. When coexisting with DSRC systems, the newly introduced protocols/technologies are required to provide adequate protection to the legacy DSRC systems. Although this is not unique in DSRC coexisting scenarios as unlicensed users are also required to provide protection to the coexisting licensed users in primary-secondary users coexisting scenarios, the safety-critical nature of DSRC heightens the requirement. That is, the coexisting protocols/technologies with DSRC are expected to introduce none or negligible performance degradation to the legacy DSRC system. Otherwise, the effectiveness of V2V safety applications will be impaired and potentially lead to failures in preventing imminent car accidents.

Introducing another protocols/technologies to DSRC networks can predictably degrade the performance of the legacy DSRC system since DSRC was designed for operating alone and the newly introduced protocols/technologies may not be well compatible

with the legacy DSRC. However, it remains unknown to what extent the DSRC performance will be degraded . Moreover, it has not been identified whether the performance degradation of the legacy DSRC can be mitigated or controlled to an acceptable level. Motivated by these questions, this dissertation studies the performance of the legacy DSRC in heterogeneous networks via accurate network simulations.

Specifically, we investigate DSRC performance in three different DSRC coexistence scenarios: 1) a DSRC protocol ready to be deployed on day one coexisting with an upgraded version for later deployment; 2) DSRC sharing its licensed spectrum with unlicensed Wi-Fi devices; 3) DSRC coexisting with emerging communication technologies (e.g., mmWave communications) for sharing a large amount of sensing information. For these coexisting scenarios, we quantitatively study the performance degradation of the legacy DSRC via detailed simulations and identify the fundamental challenges of preserving the DSRC performance. Based on the studied results and identified challenges, we then propose solutions or suggestions to reduce experienced performance degradation of the legacy DSRC.

In this dissertation, we have learned that introducing new protocols/technologies can result in significant performance degradation of the legacy DSRC in several studied near-worst cases. We also show that such performance degradation is possible to be controlled to an acceptable level if the newly introduced protocol can carefully adjust its parameters and carefully design its mechanism of accessing the legacy DSRC networks in order to provide sufficient protection to the legacy DSRC. We also show that DSRC is possible to collaboratively coexist with mmWave communications in a multi-technology and multi-band V2V scenario by help mmWave improve its data sharing efficiency.

The contributions of this dissertation are summarized as follows:

Develop an accurate network simulator for V2V communication: The primary research tool used in this dissertation is a network simulator. However, the validity of the simulation results is frequently questioned. To lay the research foundation of this dissertation, we first develop an ns-3 based network simulator for V2V communications and calibrate it based on the data collected in a set of experiments with up to 400 DSRC transceivers. We show that it is possible to achieve 88% simulation accuracy

with marginal increases in simulation run-time.

Harmonize coexistence of DSRC packet generation protocols from different deployment stages: We use two DSRC congestion control protocols as an example to study the impact of protocol evolution on the performance of the legacy DSRC. A reactive congestion control protocol is expected to be deployed on day one, and an adaptive control protocol, which outperforms the reactive solution regarding effectiveness, convergence, and fairness, is under consideration for day two deployment. During a transition period, the two protocols may coexist in one network. We identify that in such a heterogeneous network, cars with the legacy reactive protocol can experience doubled packet latency. Facing the issue, we then propose a mechanism which can automatically adjust the algorithm parameters of the evolved adaptive protocol such that the performance degradation of the legacy reactive protocol is controlled to an acceptable level with only a negligible impact on the performance of the evolved adaptive protocol.

Identify fundamental challenges when DSRC sharing the spectrum with Wi-Fi: We identify main challenges of preserving the performance of the legacy DSRC when applying three recently proposed spectrum sharing protocols to share the DSRC spectrum with unlicensed Wi-Fi devices: 1) self-interference of Wi-Fi transmissions can temporarily prevent Wi-Fi devices from detecting DSRC transmissions, resulting in potential packet collision between DSRC transmissions and Wi-Fi transmissions; 2) DSRC, as the primary user of the channel, has no obligation to detect Wi-Fi transmissions. This can further lead to a unilateral hidden terminal problem; 3) even DSRC and Wi-Fi can mutually detect each other, the MAC layer backoff countdown collision can further cause extra DSRC packet losses. We find that adding a few hundreds of microseconds extra idle time in the Wi-Fi inter-frame idle period can significantly improve the performance of Wi-Fi detecting DSRC, especially when the Wi-Fi traffic load is close to saturated. We also suggest that the Wi-Fi devices are desired to leave the DSRC channels upon detecting DSRC transmissions. It is because, after detection, the unilateral hidden terminal problem can still cause more than 30% extra packet losses of DSRC transmissions. Also, backoff countdown collisions that are inherent to the IEEE

802.11 MAC protocol can cause 32% extra packet losses to the DSRC transmissions.

Propose a DSRC-assisted mmWave sensor data sharing mechanism: In a multi-technology and multi-band V2V scenario, we show that DSRC can collaboratively coexist with emerging mmWave communications. Due to its large capacity and high throughput, mmWave communication is a good candidate for sharing a large amount of sensor data between vehicles. Instead of letting vehicles simply broadcast sensing information to all nearby vehicle without considering the value of the shared information, we propose a DSRC-assisted mmWave sensor data sharing mechanism which utilizes the information shared via DSRC to estimate the usefulness of a mmWave transmitter's sensing information to its intended receiver. When scheduling the mmWave transmissions, mmWave transmissions carrying more useful information are scheduled with higher priorities. Compared to a simple broadcast strategy, the proposed mechanism significantly improves the mmWave information sharing efficiency by up to 50%.

The rest of this dissertation is organized as follows. Chapter 2 introduces the technical knowledge of DSRC-based V2V communications. We present our methodology and experience of calibrating a network simulator for accurate V2V simulations in Chapter 3. In Chapter 4, we study the coexistence scenario where an earlier deployed DSRC protocol operates with an evolved protocol in the same network. In Chapter 5, we investigate the DSRC performance in a coexistence scenario where DSRC shares its spectrum with unlicensed Wi-Fi. In Chapter 6, a DSRC-assisted mmWave sensor data sharing mechanism is proposed and evaluated. The dissertation is concluded in Chapter 7.

Chapter 2

DSRC-based Vehicle Safety Communications

In 2002, the U.S. Department of Transportation (USDOT) partnered with Crash Avoidance Metrics Partnership (CAMP) and initiated a Vehicle Safety Communications (VSC) project in order to estimate the potential benefits of communication-based vehicle safety applications and define their communication requirements [26]. In the VSC project, 34 safety application scenarios were identified and studied. The study indicated that many of the safety applications require communication latency in order of 100 ms. Compared to alternative technologies including 2.5/3G cellular systems, Bluetooth, radar systems and ultra-wideband communications, DSRC technology demonstrated its potential capability of supporting low-latency communications. In addition, the feasibility of several V2V safety applications has been proven, including forward-collision warning (stopped vehicle ahead), emergency electronic brake lights (hard-braking vehicle ahead), blind spot warning, intersection movement assist, do-not-pass warning and control-loss warning [4].

Since the VSC project, a number of research activities have been dedicated to vehicle safety communications, e.g., project DRIVE-C2X funded by the European Union with 120 vehicles and 450 drivers in seven locations across Europe [27], project Safety Pilot Model Deployment in the U.S. with approximately 3000 vehicles [14], and an ongoing project in the U.S. where USDOT and CAMP joined forces to investigate the interoperability and scalability of DSRC-based V2V safety communications [15].

In this dissertation, we particularly study one type of VSC which is based on a single-hop broadcast by DSRC technology. This chapter provides background information on DSRC technology as far as it is helpful to understand the research problem and the contributions of this dissertation.

2.1 DSRC Frequency Band

The U.S. FCC has allocated a dedicated 75 MHz frequency band between 5.850-5.925 GHz for intelligent transportation systems. In this band, the microwaves spectral environment and propagation characteristics can provide a sufficient data rate for a wide range of DSRC safety applications.

The DSRC spectrum is divided into a guard band of 5 MHz and seven channels, each with 10 MHz bandwidth. As illustrated in Fig. 2.1, each channel is designated as either a service channel or as the control channel [4]. Specifically, the control channel 178 is used to exchange common safety-related messages and announcements of service provided on other service channels. In the U.S., the safety-related messages, e.g., Basic Safety Message (BSM), traffic light signal phase and timing data, are transmitted on the service channel 172. Channel 180 is reserved for high power public safety applications. The rest of the service channels are exploited for data exchange of non-safety applications. The current DSRC experiment practice primarily focuses on 10 MHz channels since such narrow-band communications are reported to be more suitable to inhibit inter-symbol interference in the vehicular environment [28].
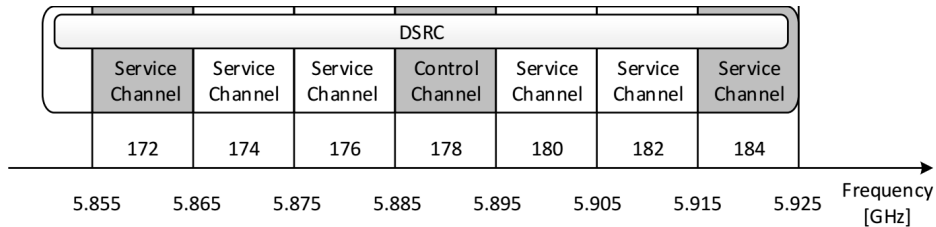
Figure 2.1: Spectrum and channel allocation for DSRC in the U.S. [3]

2.2 DSRC Protocol Stack

The Institute for Electrical and Electronics Engineers (IEEE) and the Society for Automotive Engineers (SAE) have defined a set of protocols and standards for DSRC technology. Fig. 2.2 provides an overview of the protocol stack and corresponding standards for DSRC for the layers of the ISO/OSI network model [29].

The lower four layers of the protocol stack are typically referred to as Wireless
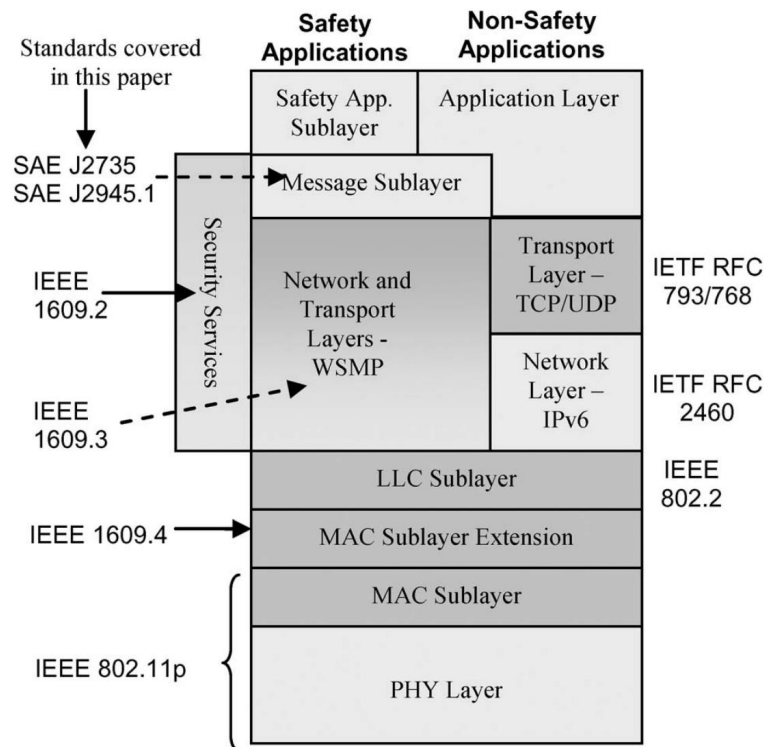
Figure 2.2: Overview of the protocol stack and corresponding standards for DSRC [4]

Access in Vehicular Environments (WAVE). In particular, the IEEE 802.11p standard defines the PHY and MAC layer behaviors of DSRC. In the MAC sublayer extension, the IEEE 1609.4 allows a radio to switch between different channels and introduces concepts of control and service channels, i.e., radios are synchronized alternating between 50 ms control channel periods and 50 ms service channel periods [30]. Due to this channel switching operation, only 46% of the total time is available for safety message exchange (50 ms channel occupation time minus 4 ms guard interval). To gain higher channel capacity for safety applications, the IEEE 1609.4 has been made optional in the U.S. Next to the MAC sublayer extension, the IEEE 802.2 Logical Link Control (LLC) sublayer is employed to establish a connectionless, unacknowledged data transfer service [31].

Two types of network and transport layer protocols are defined in the DSRC protocol stack, one for safety communications and the other for non-safety communications. In the U.S., the safety communications focus on one-hop message exchange. Consequently, a lightweight transport layer protocol, named WAVE Short Message Protocol (WSMP)

has been developed [32] and the routing functionality has been omitted. However, for non-safety communications, the protocols for the Internet are employed, including Internet Protocol (IP), Transmission Control Protocol (TCP) and User Datagram Protocol (UDP).

The upper layer protocols specify the safety message generation rate and the transmission power, the accuracy of the sensor and position information, the minimum performance requirements of safety applications. The PHY/MAC layer protocol and the upper layer protocols are more relevant to this dissertation. More information will be provided in the following.

2.3   DSRC PHY/MAC Layer Protocol—IEEE 802.11p

The IEEE 802.11p is developed based on the IEEE 802.11a protocol [33]. More specifically, for the PHY layer, the IEEE 802.11p inherited the Orthogonal Frequency-Division Multiplexing (OFDM) technology form the IEEE 802.11a, with adjusted parameters for 10 MHz channels in contrast 20 MHz channels used by the typical IEEE 802.11a communications. The IEEE 802.11p offers eight data rates, ranging from 3 Mbps to 27 Mbps, see Table 2.1. Each data rate results from a combination of a modulation scheme, which decides how the information is conveyed by the physical waveform, and a coding rate, which defines the ratio of the number of data bits to the total number of transmitted bits (the non-data bits are designed for error correction).

Table 2.1: Available data rates in the IEEE 802.11p with 10 MHz channels

Modulation	Coding rate	Data rate [Mbps]
BPSK	1/2	3
BPSK	3/4	4.5
QPSK	1/2	6
QPSK	3/4	9
16-QAM	1/2	12
16-QAM	3/4	18
64-QAM	2/3	24
64-QAM	3/4	27

With respect to the MAC layer specifications, the IEEE 802.11p introduces a new

communication mode, i.e., Outside the Context of a BSS (OCB), with the purpose of reducing the communication latency. This new mode allows stations to directly communicate with each other, without establishing or join a Basic Service Set (BSS). The medium access control of the IEEE 802.11p follows the Distributed Coordination Function (DCF) of the IEEE 802.11 standards augmented by the Enhanced Distributed Channel Access (EDCA) mechanism. The DCF employs Carrier Sense Multiple Access (CSMA), a contention-based channel access mechanism based on the principle of "listen before talk". Before transmitting a frame, a station is required to listen to the channel for a certain period. If the channel is sensed idle during this period, the station is allowed to access the channel. If the channel is sensed busy, the station has to wait from a random number of idle time slots before attempting to access the channel again. This procedure is called backoff. The initial random number of idle time slots is uniformly chosen between zero and the size of the contention window. The backoff time decreases once the channel is sensed idle and the decrement is halted once the channel becomes busy again. It is clear that the size of the contention window can affect the CSMA efficiency and effectiveness. If the contention windows size is relatively small comparing to the number of stations competing for the channel, many stations may access the channel at the same time leading to a large probability of packet collision. However, if the contention window size is too large, each station has to wait longer before it can access the channel. This increased delay can potentially lead to degraded performance of safety communications whose latency requirements are stringent. The IEEE 802.11 protocols employ the binary exponential backoff procedure. In this procedure, the contention window size is doubled upon the detection of a frame collision until reaching the maximum value of the contention window size CW_{max}. Recall that the vehicle safety communication primarily relies on one-hop broadcast, i.e., no frame acknowledgments are required. Consequently, the binary exponential backoff procedure is not applicable to vehicle safety communications. Thus, the contention window size keeps at its minimum value CW_{min}.

The EDCA mechanism in the IEEE 802.11p prioritizes between different types of

messages based on their Quality of Service (QoS) requirements. The EDCA mechanism includes four Access Categories (ACs), i.e., background (AC_BK), best effort (AC_BE), video (AC_VI) and voice (AC_VO), in the ascending order of priority. Each AC operates as an independent DCF station and the main differences between different ACs are their EDCA parameter configurations, i.e., the configurations for CW_{min}, CW_{max} and Arbitration Interframe Space (AIFS). AIFS is a combined interval of a Short Interframe Spacing (SIFS) and a number of time slots (The default slot time in the IEEE 802.11p for 10 MHz channel is 13 μs). The number of time slots, denoted as AIFS Number (AIFSN), can affect the size of AIFS and further determine the priority of the frames to be sent. The default EDCA parameters of the IEEE 802.11p are summarized in Table 2.2.

Table 2.2: Default EDCA parameters of the IEEE 802.11p in [1]

Access Category	CW_{min}	CW_{max}	AIFSN
AC_BK	15	1023	9
AC_BE	15	1023	6
AC_VI	7	15	3
AC_VO	3	7	2

2.4 DSRC Application Layer Protocols—Application Layer Congestion Control

The safety message in the U.S., BSM, has a mandatory Part I with vehicle operation status, like position, speed, heading, and an optional Part II with additional information, e.g., map, path history [4]. The transmission of a BSM can be scheduled periodically or triggered by an event. Recently, the BSM transmission policy, the minimum requirements of sensor accuracy, the minimum performance requirements of safety applications are specified in the SAE J2945.1 standard draft.

The counterpart to the BSM in Europe is Cooperative Awareness Message (CAM). Similarly, the CAM also has mandatory and optional parts. The mandatory part contains the frequently changing vehicle information. The optional part contains long-term characteristics of the vehicle like its physical size as well as additional information like

path history. The generation of a CAM is determined by a set of generation rules, which primarily examine changes in the heading, position, and speed since the last generated CAM. These generation rules are further shaped by Decentralized Congestion Control (DCC) by setting a lower bound to the CAM interval according to channel congestion.

Chapter 3

Accurate Simulation of Dense Scenarios with Hundreds of Vehicular Transmitters

The network simulator is the primary research tool used in this dissertation. This chapter reports our methodology of developing and calibrating a V2V network simulator based on the data collected from a set of experiments with up to four hundred DSRC transmitters. With most of these transmitters in communication range, this represents an extremely dense wireless configuration that challenges radio and interference models. Field test and simulations were conducted in tandem and iteratively to facilitate model selection and configuration as well as to allow a detailed evaluation of simulation accuracy.

3.1 Motivation

Given the increase of programmable wireless hardware, mobile networking research has shifted over the past decades from a heavy reliance on simulation towards a more experiment-driven methodology. Yet, network simulators remain an important tool, for example, for complementing studies of large-scale networks with hundreds or thousands of wireless nodes that require significant resources to fully evaluate experimentally. The validity of such simulation results is frequently questioned, and, however, little data exists for verifying the accuracy of modern network simulators in such settings.

To fill this void, this chapter reports on our methodology and experience from a multi-year effort to cross-validate a vehicular network experiment with four hundred DSRC transmitters through ns-3 simulations. The primary use case for DSRC technology is for vehicles to periodically exchange their status information (including position,

(a)

(b)
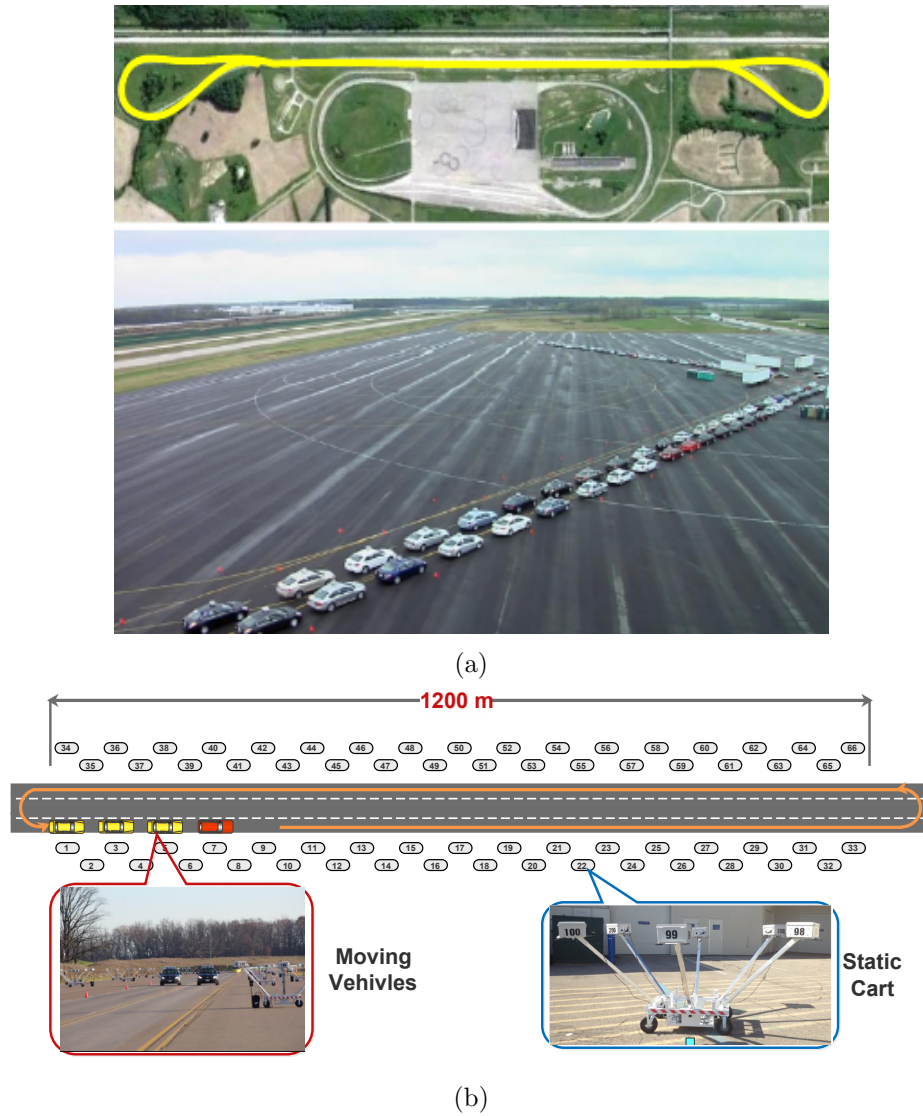
Figure 3.1: (a) The phase 1 testing environment illustration: the bird's eye view of the phase 1 testing facility (top) and an illustration of the vehicle distribution in one test (bottom); (b) the carts and moving vehicles layout in the phase 2 test

speed, heading, etc.) with other nearby traffic participants, thereby improving situational awareness among all traffic participants, whether human-driven or self-driving. This technology should also support safety applications with coverage and latency requirements that would be challenging to accommodate on cellular networks. Given the likely government mandate[1] and current deployment plans, it is possible that hundreds, even thousands, of periodically transmitting vehicles will congregate within communication range in future traffic situations. Such V2V communication experiments can, therefore, serve as a particularly dense case study of wireless network simulations. In addition, the safety-related character of the system leads to a heightened need for validation of results, which has made it possible to conduct field test with two hundred vehicles and up to four hundred prototype transmitters.

To date, simulation accuracy has only been studied with a relatively small number of nodes [36–39]. Over the years, many model improvements have been proposed for network simulators. As to the receiver modeling, Chen et al. [5] proposed a novel receiver model for the ns-2 simulator. This model first introduced the frame capture effect into the network simulator. Based on [5], Bingmann et al. [6] developed a similar receiver model for the ns-3 simulator. Going beyond a packet-level simulator, Papanastasiou et al. [40] proposed models to mimic the device's behavior at a signal level, which promises more accuracy but significantly increases the computational load, particularly in large-scale simulations. As to the propagation modeling, many channel models have been proposed for characterizing the signal propagation in a V2V environment. Some of them were derived based on the gained experience in mobile cellular networks [41]. Many of them were derived based on the data from field measurements, e.g., [42–46]. However, the scale of these measurements was normally small, i.e., none of them involved hundreds of vehicles. Other large-scale testbeds, such as the Michigan Safety Pilot [14] also use large numbers of vehicles but they are distributed over a large geographic region, so that network load and interference effects usually remain negligible.

---

[1]The United States National Highway Traffic Safety Administration (NHTSA) has issued an advance notice of proposed rulemaking with an intention to require V2V capability in new cars since 2020 [34]. The secretary of the United States Department of Transportation (USDOT) has also announced an aggressive regulatory plan for V2V deployment in the near future [35].

We are not aware of any large-scale evaluation of simulation accuracy for any of these models or datasets.

In this effort, we, therefore, co-developed an experiment design and simulator model that would allow simulation accuracy comparisons in V2V scenarios with hundreds of nodes — the key components that a V2V network simulator primarily relies on are: a network traffic generator, a node mobility manager, a packet reception controller (via receiver models) and a channel and signal propagation emulator (via propagation models). In a V2V network, the primary network workload is simply periodic broadcast messages, the basic safety messages, which simplifies the implementation of the network traffic generator. For node mobility, we use a trace-driven approach that relies on the Global Position System (GPS) readings from the field experiment. The receiver and propagation models require more attention, and therefore we focus on these models. In particular, we studied the accuracy that can be obtained with different model complexities, confirmed exact receiver parameters through hardware lab testing, and studied the sensitivity to the choice of receiver and propagation parameters.

In this work, we have learned

- The existing simulation models with default parameters may only achieve 15% simulation accuracy in term of packet error ratio. However, with calibrated parameters, the accuracy of these models can improve by $\sim 20\%$.

- Adjusting the complexity of propagation models and receiver models can result in 10-20% improvements in simulation accuracy with 8% overhead in simulation runtime and for well-calibrated models, it is possible to achieve 88% accuracy.

- The calibration process is helpful in identifying implementation errors of simulators. A calibrated simulator can assist researchers in validating, planning and predicting the field experiments results.

More details will be discussed in the following sections.

3.2   Background Knowledge of Field Tests and Simulations

3.2.1   Field Experiment Setting

To investigate the V2V scalability issue and study the congestion control, the Crash Avoidance Metrics Partnership (CAMP) Vehicle Safety Communications 3 (VSC3) Consortium, in partnership with USDOT, has conducted a series of V2V experiments in several testing facilities to evaluate seven driving conditions.

In these field experiments, each DSRC transceiver broadcasted safety messages several times per second (the default rate is 10 Hz) at data rate 6 Mbps on channel 172 with 10 MHz bandwidth and 5.9 GHz center frequency, using Atheros 802.11p chips. The packet size of safety messages varied from 310 to 390 Bytes due to different frame payload size.

Two major field test activities were conducted in this project. The phase 1 test involved up to 200 On-Board Equipment devices (OBEs). Each OBE was mounted on the roof of a car, acting as a DSRC transceiver. Each OBE acquired its position from an integrated GPS device at rate 10 Hz. In the phase 1 test, six primary driving configurations were tested: highway, intersection, V2V safety application, high dynamics winding road, hidden node and sudden loading effect. In each test trial, the vehicles were driving along a predefined route at a nearly constant speed with the intention of maintaining the separation distance between two adjacent moving vehicles constant. Fig. 3.1a provides a bird's eye view of the testing facility and a snapshot of the vehicle distribution in one field experiment.

As an extension to the phase 1 test, the phase 2 test increased the number of OBEs to 400. The test was conducted in an open-space environment, and it primarily relied on the use of OBEs mounted on stationary carts, each of which held up to six OBEs, leading 400 OBEs to mount on 66 carts. These carts were placed in two rows on each side of a straight track and evenly spaced within each row. The length of the track was 1200 m and the spacing between two neighboring carts was 37.5 m. This test used a combination of stationary OBE carts and a small number of vehicles. In the majority of test trials, four moving vehicles were used. The speed of these moving vehicles was

set to 40 km/h and the separation distance between two adjacent moving vehicles was 75 m. The layout of the carts and the moving vehicles is illustrated in Fig. 3.1b.
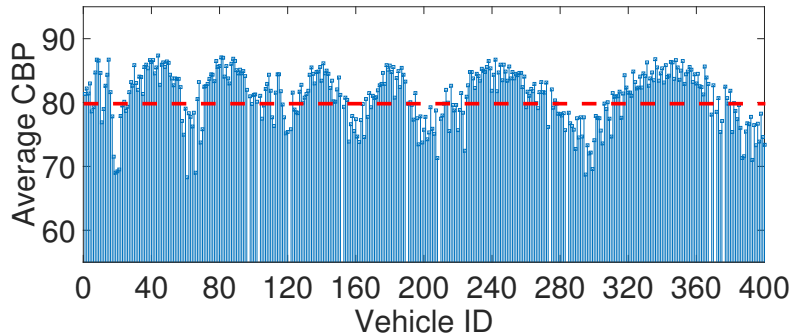
Figure 3.2: Average CBP measured by each OBE

The phase 2 test models a highway traffic jam where most vehicles are stationary and move forward only rarely. The moving vehicles mimic cars driving on less congested lanes, e.g., a carpool lane. Such a scenario of a high density of stationary vehicles and a few fast-moving vehicles is a particularly challenging scenario in V2V safety communications since reliable and low-latency communications need to be maintained for the fast-moving vehicles in this high-density situation. With such a large number of transmitters in the test, the channel was highly congested. The channel condition was indicated through channel busy percentage (CBP), which is defined as the percentage of the period during which the channel is measured as busy. As shown in Fig. 3.2, more than 88% OBEs observed that their average CBP was higher than 75%. To produce even higher channel loads, higher transmission rates (up to 50 Hz) were used by each OBE to emulate up to 2000 transmitters on the channel. To avoid unnecessary redundancy while analyzing the performance of each OBE, a subset of OBEs, named loggers, were selected as representatives for data collection and performance evaluation. The selected 33 loggers were uniformly distributed in the experiment area. Due to various link distances between loggers, the link quality, indicated by the Received Signal Strength Indicator (RSSI) measurements, varied in a wide range, from -55 dBm to -95 dBm. Fig. 3.3 illustrates the connected links between several loggers and the average RSSI for each link.

It required a significant amount of time (nearly one day for the CAMP team) to
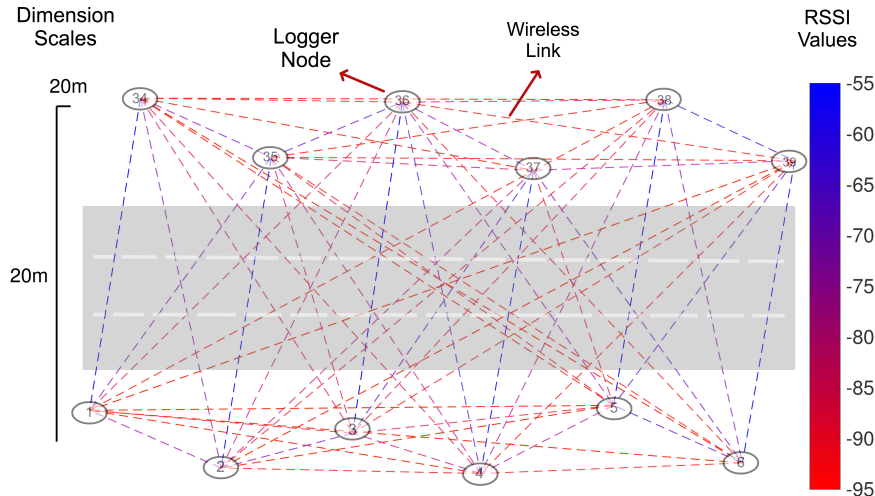
Figure 3.3: Link connections between a subset of loggers

deploy such a large-scale network over the experiment area. Thereby, for this multi-day test, the devices had to stay on the testing ground overnight. Due to the dropped temperature at night, icing occurred on the surface of the OBE boxes, which could cause temporary port connection issues (e.g., a port supplying the power to the OBE) while booting the OBEs in the next morning. However, note that all the data were collected when no device malfunctions occurred. Also to control this large-scale network and monitor the network operation in real time, a separate control network was built via a Wi-Fi router integrated into each OBE and several access points. With this control network, the control center was able to notify OBEs to load configurations, to start/stop tests at approximately the same time. Meanwhile, the operating status of each OBE was reported to the control center and displayed through visualization tools. In this way, any device failure or misbehavior could be detected and monitored in real time.

In this work, we primarily focused on simulating the phase 2 test because it provided a higher transmitter density and a more congested channel.

3.2.2 Simulating Signal Propagation

In a network simulator, the propagation model is responsible for reflecting the environmental effects on the channel, such as signal blockage and reflection, and then

determining the power and delay of a transmitted signal at a receiver. The main factors of a propagation model are the distance-dependent path loss and the fading. The distance-dependent path loss captures how the average received power level varies with distance to the transmitter. The fading captures how the instantaneous signal level fluctuates over time, frequency, and space. Typically, a statistical modeling framework of the received signal power (RSSI in dB) at a random time point and for a given distance of a transmitter-receiver pair is given by

$$RSSI = P_t + [10 \log_{10} g_{med} + 10 \log_{10} F_{sh}] + 10 \log_{10} F_{mp}$$

In this equation, the bracketed term is the locally averaged path loss for a particular transmitter-receiver distance d; $g_{med}(d)$ is the median value of the path loss over all transmitter-receiver links of length d. This term is distance-dependent. One simple model for this term is the **log-distance model**, where the path loss in dB changes linearly with the log-distance, $Gmed = 10 \log_{10} gmed = A - 10Blog10(d)$ [47]. If there are no or only small obstacles between the transmitter and the receiver, the received signal could consist of a line of sight signal component and multiple reflected signal components dominated by a ground reflected signal. This effect can be modeled by the **two-ray model** [47]. To model a complex signal propagation environment, multiple models can be applied jointly, e.g., before a distance breakpoint, the two-ray model is applied. After that point, the log-distance model is applied. For a particular link, F_{sh} represents the large-scale fading which varies slowly with physical locations depending on the structures (e.g., buildings) in the environment. Several previous works [47, 48] have suggested the large-scale fading follows the Gaussian distribution. F_{mp} represents the small-scale fading due to multipath, and it can be modeled by the Nakagami or the Gaussian distributed random variable.

3.2.3 Simulating Receiving Behaviors

A wireless receiver starts the reception of a packet with looking for a known pattern of the preamble. If such pattern is found, the receiver then attempts to decode the Physical Layer Convergence Procedure (PLCP) header, which contains details of this

transmission including data rate, frame length, etc. If the receiver decodes PLCP header successfully, it can next demodulate the frame body. Until the end of the frame body duration, all the incoming signals fluctuate the receiving packet's Signal-to-Interference-and-Noise-Ratio (SINR) and thus affect the current reception. At the end of the reception of a packet, a CRC code check is performed to determine if this packet can be received correctly.

In a network simulator, the receiver model typically determines whether a packet is received successfully based on the packet's SINR. As in [5, 6], the receiver's behaviors are normally modeled by identifying different states, e.g. TX, IDLE, CCA_BUSY, and RX.

A node is in TX state if it is transmitting a packet. If the receiver is in this state while a new packet arrives, the receiver will drop the newly arrived packet.

If a node is neither in transmission nor reception of a packet, it is in IDLE or CCA_BUSY state. If the receiver is in one of these states when a packet with high enough power arrives (e.g., higher than -94 dBm), an SINR check for PLCP header decoding is scheduled. If the SINR of the receiving packet passes the check, the reception continues. Otherwise, it aborts. At the end of the reception of this packet, another SINR check for frame body decoding is performed to determine whether the packet is received successfully.

If a node is receiving a packet, it is in RX state. If the receiver is in this state when a new packet arrives, the decision whether to switch to the new signal is made by the frame capture policy. Instead of directly ignoring newly arrived packet, the **frame capture effect** enables a receiver to switch to a stronger signal during the reception of a weaker one. If a newly arrived packet has high enough signal strength (e.g. 4 dB greater while receiving the preamble portion of the current packet and 10 dB greater while receiving the frame body portion), a receiver can then pick and lock to the new signal. The switch is allowed in both preamble duration and frame body duration. If the capture occurs, the earlier reception is terminated immediately.

3.3   Simulation Approaches

The main components of a V2V network simulator are the node mobility manager, the network traffic generator, the propagation model and the receiver model. Our calibration process involved all these four components but focused on the propagation and the receiver models. In this section, we describe our methods for calibrating these components in detail.

3.3.1   Mobility Manager Calibration

In the field experiments, each OBE relied on the frequent GPS readings to obtain its location and speed information. The information was further piggybacked in safety messages and shared with nearby OBEs. To accurately recreate the same mobility pattern in simulations, these GPS readings were collected and organized into a GPS trace file. This trace file was then converted to a format which can be directly processed by the ns-3 simulator. By using this approach, the movement of each node in the simulation is scheduled according to the input trace file. Thereby, the logged node position from simulations is expected to be same as that logged in the experiment. However, the default ns-3 mobility scheduler extrapolates nodes to their new positions by primarily using current speed vectors and previously extrapolated positions with an assumption that the speed and heading are constant. As shown in Fig. 3.4, this speed-dependent scheduling approach can introduce an accumulative error between a node's position in the simulation and its position in the input trace file. It is because the speeds in the trace file were instantaneous reading by the GPS and with instantaneous speeds as well as constant speed/heading extrapolation in the simulation, there is no guarantee that the node reaches the trace-reported position at each position update time. Such undesired error can further have a negative impact on calibrating the signal propagation. To eliminate such position error, we introduced the position-dependent scheduling along with the default speed-dependent scheduling, such that the nodes are relocated to the trace-reported position at each position update time. A slight discontinuity in the nodes trajectory can occur. However, we did not observe any adverse effect of these

discontinuities on the simulation results. This two-level scheduling method improves the accuracy of the trace-driven approach and guarantees that the trace-reported positions are replayed in the simulations.
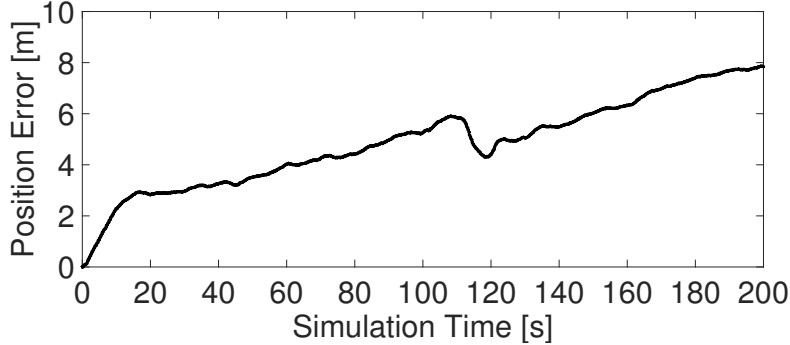
Figure 3.4: Cumulative position error of a moving vehicle between its position in the field experiment and in the simulation at a given time

3.3.2 Traffic Generator Calibration

In the field experiment, the network traffic was simply periodic transmissions. However, to reproduce a similar network traffic in simulations, several simulation parameters including the transmission power, the transmission rate and jitter, the channel bandwidth and its center frequency, the packet length, the noise floor, the threshold for clear channel assessment (CCA) detection, the threshold for energy detection require correct configurations. A hardware lab test was conducted by the CAMP VSC3 team to clarify some of the radio characteristics of the DSRC transceivers and help to determine the correct values for these parameters. As to the packet size, it varied in the field experiment. We believe it would be highly inefficient to reproduce the exact packet size for every packet in the simulations since the packet size is relatively small and it has a marginal impact on the system performance. Instead, we unified packet size to 316 Bytes which was the mode value of all the packet sizes.

3.3.3 Propagation Model Calibration

Since a propagation model consists of two main components, i.e. the distance-dependent path loss model and the fading (large-scale and small-scale), our calibration efforts
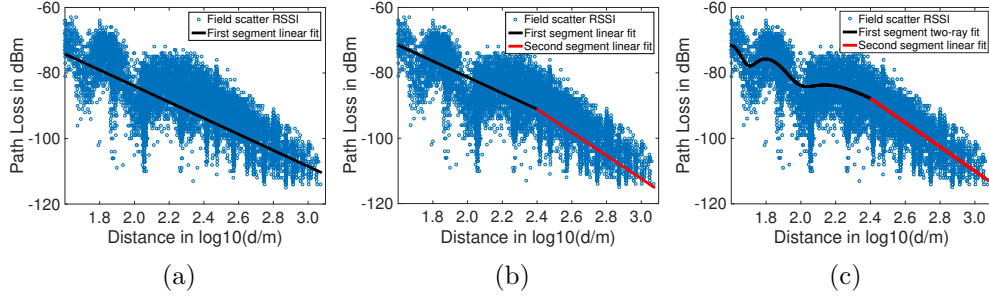
Figure 3.5: Different fitting models: (a) One-segment log-distance; (b) Two-segment log-distance; (c) Two-segment, two-ray for the first segment, log-distance for the second segment

primarily targeted these components. Given that the calibrated model was expected to be used in large-scale simulations, model complexity should be taken into account as well as model accuracy. Therefore, our model calibration started with commonly used low complexity models.

Choices for Distance-dependent Path Loss

One-segment log-distance model: Recall that the one-segment log-distance model is simple with only two fitting parameters in it, i.e. the parameter A and B, which can be obtained by minimizing the mean-square deviation of the calculated path loss to the field test data. This one-segment model was a conscious decision to avoid overfitting the RSSI measurement noise which was mostly present for longer distances since the signal strength was approaching to the noise floor. However, as the field test data included RSSI measurements for longer distances (up to 1200 m), the fitted path loss exponent (the parameter B) tended to be smaller for longer distances. It is because the RSSI samples were normally biased towards higher values at the longer distances, resulting in a gradual decrease in the path loss. Therefore, applying a single value for the path loss exponent can be problematic since it is difficult to accurately represent the path loss for the large distances.

    Two-segment log-distance model: As an enhancement to the one-segment log-distance fit, a two-segment log-distance regression was considered, where a distance break point d_{br} was defined. This two-segment model allowed us to provide separate

fits for shorter distances and longer distances. The shorter distances and the longer distances were identified via a distance threshold d_{br}. However, it is important to emphasize that this model does not capture local effects such as the null effect at ∼100m from the transmitter (see Fig. 3.5) while the two-ray model does so.

Two-ray two-segment model: From the field test data, we have observed that in some testing scenarios (e.g., highway scenario), the spacing distance between vehicles was comparatively small and thus the ray reflected by the ground was blocked by multiple metallic obstacles (i.e., car bodies) along its signal path. In these scenarios, the null effect was weak as the signal strength of the reflected ray was weak. The two-segment log-distance model would be a good fit to the data from these testing scenarios. However, in the phase 2 test, very few metal structures were present on the signal propagation path. As a result, the direct and the reflected ray can interact with opposite phase and thus the null effect was prominent. Therefore, we assumed that the two-ray model would be a good fit for the shorter distances range. For longer distances, the effect of two-ray superposition diminished and thus we kept using the log-distance model. In our calibrated model, the distance breakpoint is 250 m.

Fig. 3.5 illustrates the fitting performance of the three models. The blue dots represent RSSI samples collected in the field experiments while the solid lines indicate fitted models. In general, the one-segment linear model performs worse than the two-segment model. It is mainly because that the path loss exponents are normally different for shorter and longer distances. The one-segment model is not able to capture this characteristic. Due to the null effect, the RSSI scatter points show a winding shape in the first 250 m. As mentioned above, the linear model is not sufficient to model the null effect, while the two-ray model is a better choice to follow the winding trend. After the breakpoint, the RSSI scatter points form a dense, fairly uniform cloud whose trend is downward with increased distances. This indicates that the log-distance model is competent to model the median value of RSSI samples after the breakpoint.
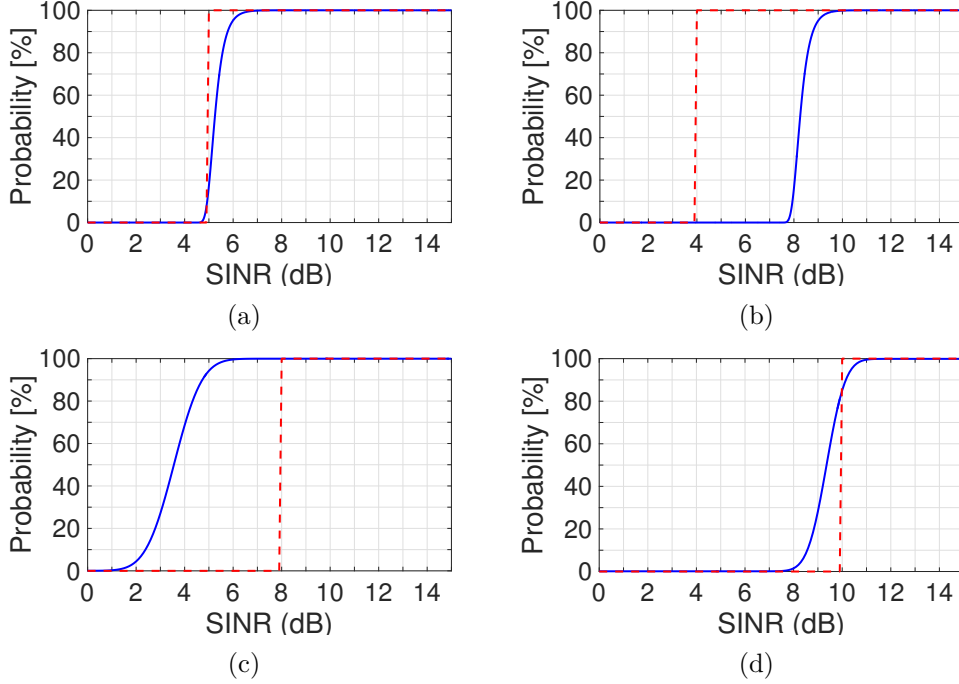
Figure 3.6: Fitted probability model v.s. the threshold-based model in [5, 6]: (a) preamble decoding; (b) preamble capture; (c) frame body decoding; (d) frame body capture - blue solid line for the fitted probability-based model, red dash line for the threshold-based model

Large-scale Fading and Small-scale Fading

With respect to the fitted model of the distance-dependent path loss, the variation of the field RSSI scatter points was captured by the fading model. In our models, it was represented as σu, where u was a zero-mean, unit variance Gaussian random variable, and σ was the standard deviation of the variation. Note that the fluctuating due to multipath was also included in each RSSI sample, and thus the variance computed from the field test data is actually $\sigma^2 = \sigma_{sh}^2 + \sigma_{mp}^2$, that is, the variances of the two kinds of fading were highly coupled. To decouple them, we first ascertained the distribution of the small-scale fading. The details of exacting the distribution have been presented in [49]. Based on the estimated σ_{mp}, the large-scale fading σ_{sh} can then be computed.

3.3.4   Receiver Model Calibration

CAMP VSC3 hardware lab test results have indicated that the transmitters used in the field test supported the frame capture effect. Unfortunately, This feature is not modeled

in the default ns-3 simulator yet. Some previous work [5,6] proposed a receiver modeling framework which considered the implementation of the frame capture effect. In that receiver model, a binary decision of whether a packet can be received successfully or whether the receiver can switch to a stronger signal is made by comparing the packet's SINR with specific thresholds. However, many existing works [50, 51] have identified the probabilistic nature of the packet reception. The CAMP lab test results also showed a similar probabilistic characteristic of the device's packet reception and capture. That is, between 0% and 100% successful reception, a comparatively large transition region exists. Within this region, packets are successfully received/captured with a certain probability for a given SINR value. Therefore, it is desired to model the packet reception and capture with a probability function of SINR and then create such a transition region between unsuccessful and successful receptions. We defined two probability models for the preamble reception and the frame body reception, respectively. The model for the preamble reception and capture was obtained by empirically adjusting the default ns-3 probability model for decoding the Orthogonal Frequency Division Multiplexing (OFDM) 6 Mbps signal for improving agreement of the simulation results with the field test results. The model for frame body reception and capture was derived by fitting the following equation to the CAMP hardware test results.

$$p = \frac{2a}{\sqrt{\pi}} \int_0^{(SINR-b)/c} e^{-z^2} dz + d$$

where a, b, c and d are the parameters to be fitted. A comparison between the threshold-based model and the fitted probability-based model is depicted in Fig. 3.6.

3.4 Accuracy & Lessons Learned

Next, we quantitatively analyze the simulation accuracy improvement introduced by the calibrated models and the increased model complexity. The Packet Error Ratio (PER) is selected as the primary evaluation metric because the effectiveness of V2V safety communication relies heavily on successful message exchanges. The Inter-Packet Gap (IPG) latency, which is defined as the elapsed time between two consecutive successful receptions from one particular transmitter, is introduced as the secondary metric

supporting the observations from the PER evaluation. The simulation accuracy of a particular link is defined the match to the field experiment results in terms of these evaluation metrics, e.g., for PER, it is $(1 - |\frac{PER_{sim} - PER_{exp}}{PER_{exp}}|) \times 100\%$, where PER_{sim} and PER_{exp} are the PER of a specific link in the simulation and in the field experiment, respectively.

3.4.1 Accuracy Gain of Model Calibration

To investigate the accuracy improvements introduced by the model calibration, three propagation models, i.e., one-segment log-distance, two-segment log-distance, and two-segment two-ray, were selected and tested with the default ns-3 receiver model. The default ns-3 simulator has provided the uncalibrated versions of the log-distance models. Although our calibrated two-segment two-ray model and the Nakagami model described in [5] differ somewhat in the way the median path loss is modeled, two approaches are essentially the same since they share the same distribution of the ratio of instantaneous receiver power to transmission power. Thereby, the Nakagami model in [5] was selected as the uncalibrated version of the two-segment two-ray model. Fig. 3.7 depicts the average simulation accuracy of all logged links in term of PER and average IPG. With the default model parameters, the three propagation models can only achieve 15%, 27%, 31% PER accuracy and 22%, 35%, 42% IPG accuracy. However, with the calibrated model parameters, the simulation accuracy improves by 25%, 21%, 28% regarding PER and 24%, 18%, 20% regarding average IPG, respectively.

The receiver model calibration follows a similar trend. The model described in [6] and the default ns-3 receiver model were selected as the uncalibrated version of the threshold-based and the probability-based approach, respectively. Note that the frame capture effect was not implemented in the default ns-3 model and to the best of our knowledge, we are not aware of any existing work describing a probability-based frame capture model which can be implemented jointly with the default ns-3 receiver model to serve as the uncalibrated version of the probability-based model. The selected receiver models were tested with our calibrated propagation model. As shown in the bottom plot of Fig. 3.7, with the calibrated thresholds, the threshold-based approach gains 5% - 6%
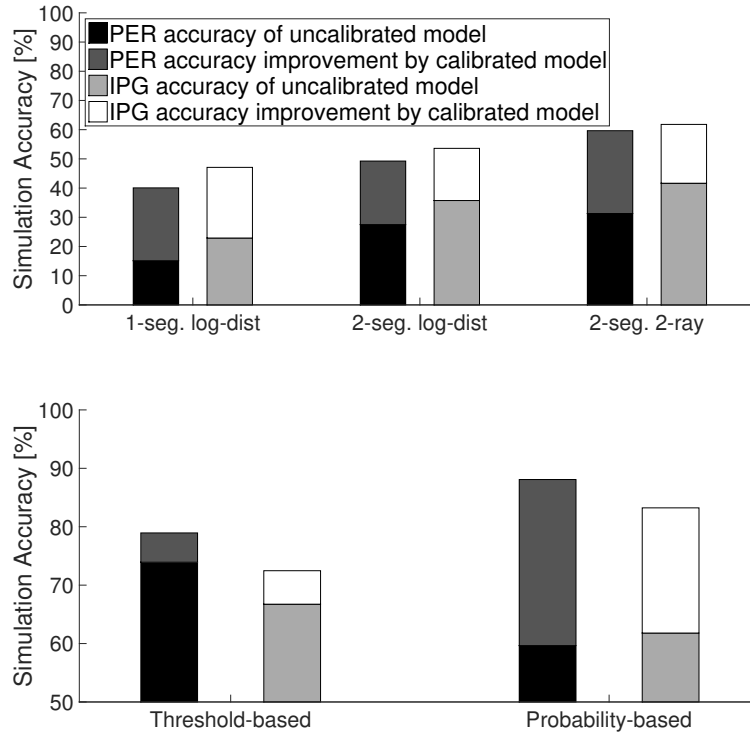
Figure 3.7: The improvement of simulation accuracy with different : (a) propagation models (top); (b) receiver models (bottom)

more accuracy in both terms of PER and IPG. As to the probability-based approach, the PER and the IPG accuracy improve by 29% and 21%, respectively, comparing to the default ns-3 receiver model.

These results show that the accuracy gain of switching to a more sophisticated model without parameter calibration is lower than the gain of calibrating the parameters of a simpler model. This underscores the need for careful model parameter choices in simulations.

3.4.2 Accuracy of Well-calibrated Models

Generally speaking, our calibrated propagation and receiver model were developed based on the models in existing literature. Then, according to the extracted features from the field test data, we selected the models which can largely capture these features and carefully adjust their model parameters. The results in Fig. 3.7 indicate that with
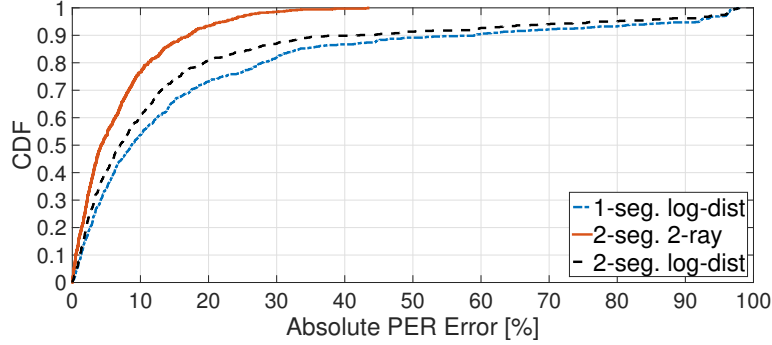
Figure 3.8: CDF of absolute PER errors of simulations applying different propagation models

well-calibrated models, it is possible to achieve 88% simulation accuracy regarding PER and 84% accuracy regarding IPG.

The calibration process was complicated by us having to rely primarily on the collected RSSI samples for the model calibration. Using RSSI samples in such a dense setting creates two challenges. First, the RSSI measures the total power in the full system bandwidth. Thereby, it is possible that the interference power is also included in the RSSI samples. This issue becomes much more severe when the interference power is strong. Second, the RSSI was reported only for packets sufficiently clean to be accurately received. Thus, many RSSI samples may have been lost due to weak received power or strong interference. To extract useful models from experiment RSSI data, we have developed methods for decoupling the interference from fading effects and for counteracting the effects of biased RSSI values [52].

Link-level accuracy. Fig. 3.8 depicts the per-link CDF of the absolute simulation errors in terms of PER obtained from the simulations where the three calibrated propagation models were tested with the calibrated probability-based receiver model. We observe that while the median errors are less than 10%, the largest error for the two-ray model is $\sim 43\%$, but over 98% for the log-distance models. This reflects the stochastic nature of the propagation model: links are assigned random fading values that match the distribution observed in the field-test but not necessarily the exact fading characteristics of a link. This primarily affects links with weak signals near the reception threshold. For example, for links with only a small subset of packets received

successfully in the field experiment, the log-distance models fail to reproduce these successful receptions in the simulation and wrongly treat these weak links as broken links, then resulting in larger errors. We also notice that for the two-ray model, the simulation error of about 78% links is less than 10%, but only 54% and 60% links in the one-segment and the two-segment log-distance simulations can achieve the same level of accuracy.

Two aspects of complexity were discussed in the receiver modeling: 1) with v.s. without the frame capture implementation; 2) the threshold-based v.s. the probability-based approach. Since the frame capture effect is expected to primarily benefit these links with higher signal strength, the performance of links with length less than 100 m was investigated in three types of simulations: the calibrated threshold-based model without and with the frame capture effect, and the calibrated probability-based model. As shown in Fig. 3.9, the simulation accuracy are 2%, 76%, and 87%, respectively. These results indicate that the implementation of the frame capture significantly affects the accuracy given that this feature has already been supported by the field test devices. Completely without modeling, this feature in the simulations can potentially lead to low accuracy. Further, if the probabilistic nature of packet reception and capture is modeled, the simulation accuracy can be improved by 11%.

Runtime tradeoffs. More detailed models can lead to higher computational loads and increased simulation runtime. The runtimes for simulating 400 nodes for 260 seconds using these aforementioned models on a machine with a 2.4 GHz Intel Xeon E7 CPU is listed in Table 3.1. When using the two-ray model, the runtime increases by 8.3% comparing to the log-distance model, due to the more complex propagation equation. Further, in the two-ray simulation, more nodes may receive interference by a transmission due to the changed propagation range. These additional nodes then start the receiving procedure which also increases the computational load. Second, for the calibrated probability-based model, the runtime increases by 8.7% comparing to the default ns-3 model. It is because both the threshold-based and the probability-based model introduce additional procedures for handling the frame capture and the probability-based model uses a more complex implementation. We find these tradeoffs
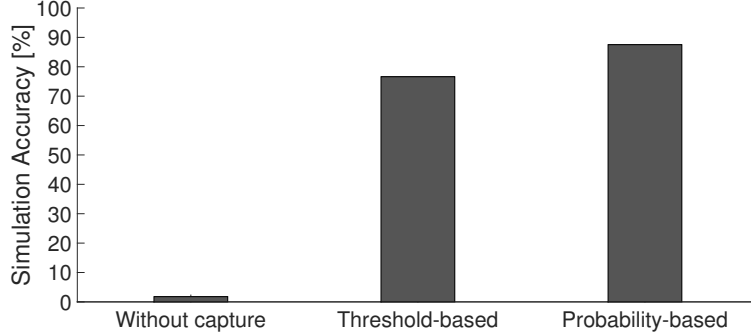
Figure 3.9: PER accuracy of links with link distance less than 100 m

acceptable for simulations with several hundreds even thousands of nodes given the improvements in simulation accuracy.

Table 3.1: Runtime comparison of simulation models

Models	Runtime
One-segment log-distance, default receiver	48 min
Two-segment log-distance, default receiver	48 min
Two-segment two-ray, default receiver	52 min
Threshold-based, two-ray propagation	54 min
Probability-based, two-ray propagation	57 min

3.4.3 Cross-validation of Simulation and Field Experiment

The calibration process is helpful in identifying errors in simulations. While examining the behaviors of the MAC layer in the default ns-3 simulator, we have identified that the implementation of the backoff timer countdown in the Enhanced Distributed Channel Access (EDCA) function does not follow the descriptions in the IEEE 802.11 standard [1]. This incorrect implementation can enlarge the queuing time of each packet in the MAC layer and increase the mismatch to the field experiments. We have shared these corrections with the ns-3 maintainers.

The process of joint experiments and simulations also helps in validating, planning, and predicting the field experiment results. Once a level of credibility of the calibrated simulator is established, we found the simulator useful in planning additional experimental tests. As an example, recall that in some field experiments, the OBEs

were configured to transmit at higher rates (up to 50 Hz instead of 10 Hz) in order to emulate more nodes that were actually available (emulating 2000 transmitters on the channel). There was uncertainty whether this emulation method is valid, which was greatly reduced by simulating 2000 vehicles and comparing the results simulations of the emulation as well as with the field test. We found that up to 30 Hz the emulation method was accurate but 40 Hz and higher queuing issues compromised its accuracy. Moreover, with a calibrated simulator, one can predict field test results before the test is conducted and study possible issues that may be encountered. Simulations can also be used to explore a large number of mobility and propagation scenarios to identify candidates for future experimental study.

3.5 Discussion

In this work, the simulation models were calibrated for the particular field experiments. However, we believe these calibrated models can be to some extent generalized to other scenarios.

The field experiments were conducted in open-space environments with few large obstacles. Such environments are commonly seen in many rural or highway communication scenarios. We expect that our calibrated propagation model for the field experiment is still suitable for other similar open-space environments. Moreover, as briefly mentioned in Section 3.3.3 while calibrating the propagation model, we have developed a set of techniques to process the collected RSSI data for model fitting, e.g., decoupling the interference from the fading effect in the collected RSSI samples, counteracting the effect of biased RSSI samples. We believe these techniques are also useful for fitting experiment RSSI data to statistical models in other propagation environments.

The packet recovery and capture parameters are not defined in the IEEE 802.11 standards, instead, they are radio chipset dependent. In theory, receivers should perform similarly if their chipsets are from the same vendor and of the same model. Our receiver model is calibrated for an Atheros AR5414 chipset. We believe such chipsets have been used in many other Wi-Fi devices, which means that our model should match

these devices' receiver behaviors as well.

3.6 Summary

In this chapter, we share our experience in evaluating a dense V2V network through joint large-scale field tests with hundreds of nodes and simulations and then reflect on the state of network simulation. We have learned that: the default propagation and receiver models were not able to produce a good match to the field experiment results despite the relatively straightforward open-space simulation environment. However, with well-calibrated parameters and models from the literature, the simulation accuracy improves by about 20% and the stochastic simulation achieved 88% accuracy in term of PER in this scenario. Such accuracy can be achieved with existing models from the literature and at a relatively small additional runtime overhead 8.7%, although we did not find implementations of these models readily available in the ns-3 simulator. We have shared our models and corrections with the ns-3 maintainers to facilitate wider availability[2].

---

[2]The ns-3.16 implementation of our models are available in http://www.winlab.rutgers.edu/ gruteser/projects/patch/patch-list.html.

Chapter 4

Evolution of Vehicular Congestion Control Without Degrading Legacy Vehicle Performance

Based on the experience and knowledge gained in the previous chapter, we focus on studying the impact of the evolved DSRC protocol on the performance of the legacy DSRC. Mainly, we consider two DSRC congestion control protocols [1] as an example, CAM-DCC protocol as the legacy DSRC protocol and LIMERIC protocol as the evolved protocol. Situations could arise where vehicles with different protocols operate in the same network. In this chapter, we first investigate the performance of CAM-DCC and LIMERIC in this mixed network and identify that the CAM-DCC vehicles can experience performance degradation after introducing the LIMERIC vehicles into the network. We then propose a CBP target adjustment mechanism to automatically adjust the CBP target of LIMERIC vehicles according to vehicle density and mixing situation of the two protocols in the network.

4.1 Motivation

To enable Intelligent Transportation System (ITS) applications, especially safety applications, each vehicle has to frequently exchange safety messages including its vehicle state (e.g., position, heading and speed) with other neighboring vehicles via V2V communications. These safety messages are referred to as CAMs in Europe [53] and BSMs in the U.S. [54]. Once the number of V2V equipped vehicles is large, congestion can arise on the wireless channel, which leads to dropped or delayed safety messages, and affects the reliability of ITS applications. Several algorithms have been proposed to

---

[1]As previously mentioned, the congestion control protocols studied in this chapter is to determine when a packet should be generated at the application layer.

control the congestion, reduce packet error rate and improve the reliability of safety applications [55–58]. A recent European Telecommunication Standards Institute (ETSI) standard, ETSI TS 103 175, V1.1.1 [59], presents two algorithms that can satisfy Decentralized Congestion Control (DCC) requirements, one state-based reactive approach, which we refer to as CAM-DCC [60] for consistency with earlier literature since it is the original CAM-DCC algorithm and one linear adaptive approach, which is based on the Linear MEssage Rate Integrated Control (LIMERIC) algorithm [61]. We refer to the linear adaptive control in the DCC framework as LIMERIC.

At a future point, one may expect that the system will need to transition to improved versions of congestion control algorithms. Such considerations can already be found in the final report of the C-ITS Deployment Platform [62]. While CAM-DCC is recommended for day one deployment, the report also implies that more sophisticated DCC solutions for more demanding applications should be realized in the future. Due to its better performance in convergence, fairness, and stability, LIMERIC is considered as one of such sophisticated DCC solutions for future deployment.

Hence, due to such system evolution issues, a situation could arise where vehicles with two different algorithms operate in the same network, a situation that we refer to as mixed networks. Since neither CAM-DCC nor LIMERIC was designed for coexistence operation, the performance of CAM-DCC vehicles, as the legacy vehicles, can be degraded in the mixed network compared to an all CAM-DCC network. This raises the question whether such performance degradation can be limited, if not eliminated.

To answer this question, we first quantitatively evaluate the performance of CAM-DCC in mixed networks and understand the severity of the performance degradation. We then propose a CBP[2] target adjustment mechanism for LIMERIC which controls the performance degradation of existing CAM-DCC vehicles to a desired level. The main idea is to adjust the CBP target of LIMERIC vehicles according to vehicle density and mixing situation in a network such that LIMERIC vehicles spare enough channel capacity for CAM-DCC vehicles to transmit as in an all CAM-DCC network. The proposed

---

[2]CBP, Channel Busy Percentage, is defined as the fraction of time during which the channel is measured as busy, and it serves as an indicator of the channel condition

mechanism estimates at which CAM-DCC state the CAM-DCC vehicles are desired to operate in the mixed network and then adjust the CBP target in a way such that the steady-state CBP of the network is within the CBP range associated with that state. Extensive simulation results show that with the target adjustment, the performance of CAM-DCC vehicles in mixed networks can preserve while the performance of LIMERIC vehicles is better or similar.

4.2   CAM-DCC & LIMERIC

Inspired by the ETSI standardization considerations [59], we study a scenario where the original state-based CAM-DCC algorithm is deployed initially, and then vehicles with the original LIMERIC algorithm plus CAM message generation are introduced at a later time. At least for a transition phase, it is possible that vehicles with different algorithms could mix on the road and form what we refer to as a mixed network.

As defined in current standards, both algorithms serve as gatekeepers to regulate the CAM message generation process [53]. In essence, a vehicle generates CAMs based on its kinetic status, i.e., changes in its position, speed or heading. The maximum rate at which those messages are sent is then limited by the congestion control algorithms. Both algorithms use CBP measurements as algorithm input. However, the two algorithms differ in fundamental design philosophy. The CAM-DCC algorithm maps a measured CBP to a transmission rate through a predefined look-up table. LIMERIC instead implements an adaptive controller to drive CBP towards a target that maximizes the network throughput.

4.2.1   CAM Generation Rules

DCC does not only shape the traffic into the MAC layer but also limits CAM generation in the facilities layer [60]. The CAM generation rules are defined in EN 302 637-2 [53]. The specific generation times of CAMs are determined by vehicle dynamics and can be restricted by the DCC algorithm if necessary. The time interval between two generated CAMs should be within the range of 100 ms to 1000 ms (i.e., generation rate

38

is between 1-10 Hz). Generally, a new CAM shall be generated when the following two conditions are satisfied: (a) the elapsed time since the last generated CAM generation is larger than the message interval, which is provided by DCC through the parameter *T_GenCam_DCC*; (b) one of the following vehicle dynamics criteria is met: 1) heading changed $> 4^o$; 2) position changed > 4 meters; 3) magnitude of speed changed > 0.5 m/s

If the above two conditions are not met for 1 second after the last CAM generation, a CAM is generated immediately. When a CAM is generated due to one of these dynamics criteria, a second and third (the actual number is controlled by *N_GenCam*. The default value of *N_GenCam* defined in EN 302 637-2 is 3) CAM shall be generated at the same interval unless a shorter interval is allowed.

4.2.2 State-based Control (CAM-DCC)

As a state-based reactive approach, the CAM-DCC algorithm defines a RELAXED, multiple ACTIVE and a RESTRICTIVE state. The ACTIVE state can be further divided into several sub-states. Each state (sub-state) specifies a transmit rate for controlling the channel load. The transition between different states is driven by the channel load, locally measured by each vehicle during a sampling interval. To prevent frequent transitions between states, inertia is introduced in the form of two parameters (i.e., *NDL_TimeUp* and *NDL_TimeDown*) dictating for how long a state shall last. Through a table look-up, a CAM-DCC vehicle uses the transmission rate whose associated CBP range includes the measured CBP. Table 4.1 presents the states defined in [59] and used in our simulations.

Table 4.1: CAM-DCC look-up table

State Index	CBP	State	Packet Tx Interval	Packet Tx Rate
4	**<30%**	RELAXED	100 ms	10 Hz
3	**30-39%**	ACTIVE 1	200 ms	5 Hz
2	**40-49%**	ACTIVE 2	400 ms	2.5 Hz
1	**50-59%**	ACTIVE 3	500 ms	2 Hz
0	**≥ 60%**	RESTRICTED	1000 ms	1 Hz

4.2.3   Linear Adaptive Control (LIMERIC)

LIMERIC is a distributed and adaptive linear rate-control algorithm where each vehicle adjusts its transmission rate in a way such that the total channel load converges to a specified target [61]. The transmission rate of vehicle j at time t (denoted as $r_j(t)$) is adapted according to the following equation:

$$r_j(t) = (1 - \alpha)r_j(t - 1) + \beta(r_{target} - r_C(t - 1)) \tag{4.1}$$

where r_C is the aggregate rate of all K vehicles within an interference range,; r_{target} denotes the defined target for total rate. α and β are the adaption parameters that control stability, fairness and steady state convergence. For a given target r_{target}, the converged aggregate rate is determined by:

$$r_{converge} = \frac{K\beta r_{target}}{\alpha + K\beta} \tag{4.2}$$

In order to achieve global fairness, i.e., all vehicles contributing to congestion at a given location should participate in congestion control in a fair manner, the PULSAR information dissemination functionality [63] has been added to LIMERIC. PULSAR requires each vehicle piggybacks a high precision CBP in its safety message. Thus, CBP_m in Eq. 4.1 is defined to be the maximum CBP reported by its 2-hop neighbors. In this way, all vehicles running LIMERIC are ensured to contribute to congestion control in a fair manner.

4.3   Performance Degradation of CAM-DCC in Mixed Networks

We use the packet error rate (PER) and the 95% inter-packet gap (IPG) as the main performance metrics to evaluate the performance of the two algorithms in mixed networks. The PER is defined as the ratio of the number of missed packets at a receiver from a particular transmitter to the total number of packets sent by that transmitter. The IPG is defined as the elapsed time between two consecutive successful packet receptions from a particular transmitter.

The performance of the two algorithms in a mixed network is studied via network simulations in a winding highway scenario. More details of the scenario setting are described in Section 4.5. Note that all results presented in this section are based on transmissions carried out on the winding part of the road and organized into distance bins according to the distance between the transmitter and the receiver. That is, for a pair of transmitter and receiver, if the transmitter is currently on the winding part of the road when the receiver is receiving packets from that transmitter, the distance between them will be calculated and binned by a certain distance (The bin size is 50 m in all calculations). Each bin collects data from all these pairs and then calculates the metrics. The calculation of the metrics is divided between CAM-DCC transmitters and LIMERIC transmitters. The CAM-DCC results are labeled "CAM-DCC_x%" and the LIMERIC results are labeled "LIMERIC_y%", where, x and y indicate the percentage of vehicles running CAM-DCC and that of vehicles running LIMERIC in the mixed network, respectively. If $x + y = 100$, the results for CAM-DCC and LIMERIC are obtained from the same mixed network.

4.3.1 Packet Error Ratio Performance

Fig. 4.1 depicts the PER for CAM-DCC vehicles and LIMERIC vehicles in both homogeneous and mixed network scenarios with different vehicle densities. From Fig. 4.1a to Fig. 4.1d, the total number of vehicles in the network is 300, 500, 1000 and 1500 respectively. For each vehicle density, CAM-DCC 100%, i.e., all the vehicles in the network are running CAM-DCC, shows the lowest PER in all distance bins. As the number of LIMERIC vehicles is increasing, the PER values are also increased. The average increment is 5-10%. This is because after LIMERIC vehicles are introduced into the network, they are trying to push the channel load towards a comparatively high target. As shown in Fig. 4.2c, before LIMERIC vehicles are introduced, the average CBP is 48-50%. As the percentage of LIMERIC vehicles increases to 20%, the average CBP is also increased to 55%, and it further reaches to 68% as the percentage of LIMERIC vehicles increased to 80%. Normally, a higher CBP should lead to a higher PER. Hence, comparing to CAM-DCC 100%, CAM-DCC vehicles in mixed networks
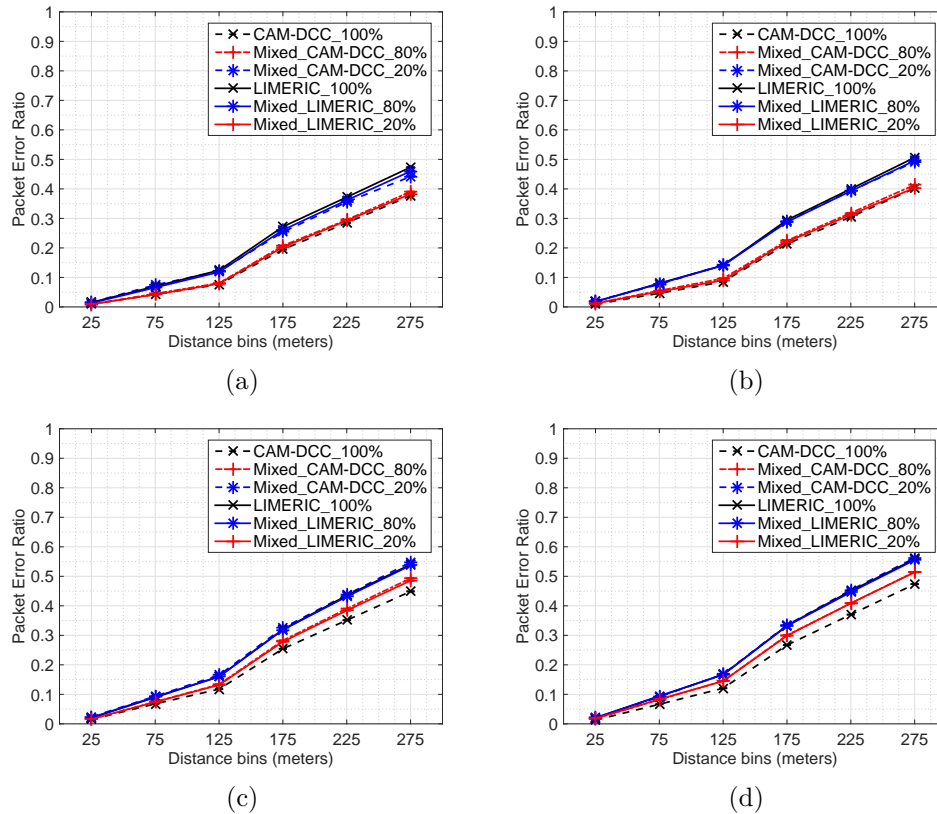
Figure 4.1: PER of mixed networks with different total number of vehicles: (a) 300 vehicles; (b) 500 vehicles; (c) 1000 vehicles; (d) 1500 vehicles

generally have higher PER values. However, it is concluded in [64] that the optimal network throughput is associated with CBP values in the range of approximately 60-70%. LIMERIC controls CBP to be in that range in order to maximize the number of safety messages a vehicle hears from its neighbors while keeping PER in a moderate range.

4.3.2 Inter-packet Gap Performance

The 95% IPG results of both homogeneous and mixed network scenarios with different vehicles densities are shown in Fig. 4.3. For each vehicle density, we observe that the 95% IPG values of both CAM-DCC and LIMERIC vehicles are increased as the percentage of LIMERIC vehicles is increasing in the network. For example, in Fig. 4.3a, the IPG value of CAM-DCC 100% at the first distance bin is 0.2s. As the percentage of LIMERIC vehicles increases to 20%, the IPG of CAM-DCC vehicles at the first distance
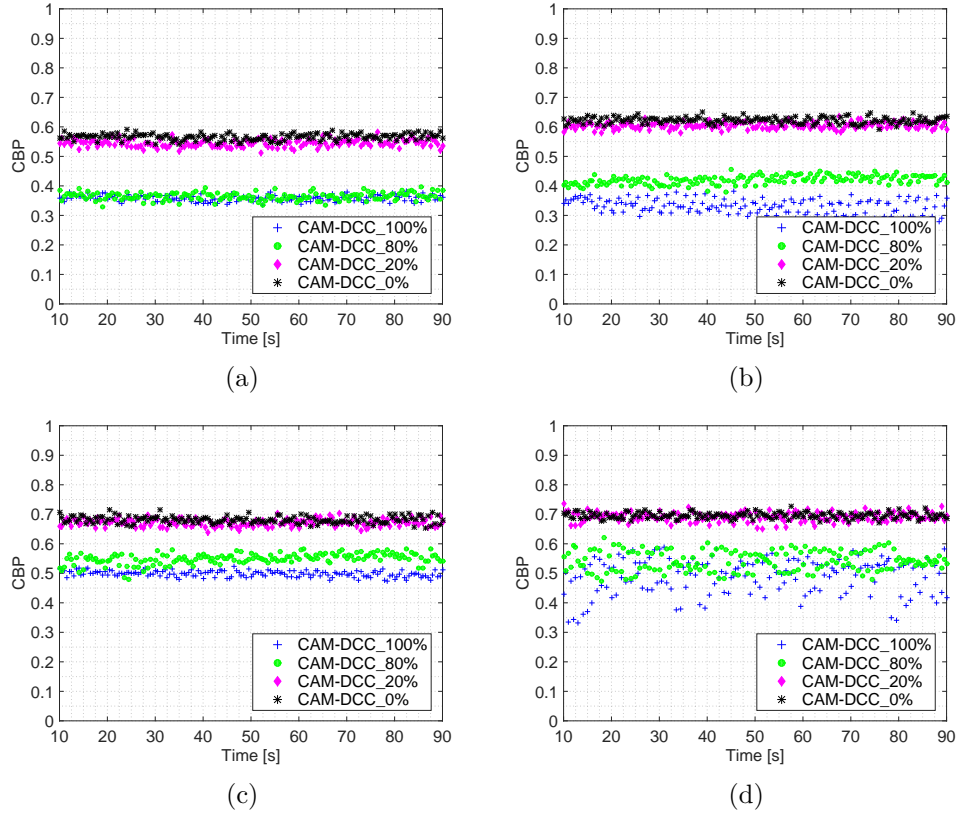
Figure 4.2: Average CBP over one second of mixed networks with different total number of vehicles: (a) 300 vehicles; (b) 500 vehicles; (c) 1000 vehicles; (d) 1500 vehicles

bin becomes 0.4s. When the percentage of LIMERIC vehicles reaches to 80%, the IPG of CAM-DCC vehicles at the first distance is 0.5s. In general, IPG is determined by the transmission rate and the PER. The higher the transmission rate is and the lower the PER is, the more frequently the message can be successfully received and the lower the IPG is. As shown in Fig. 4.1a, the PER value is comparatively low at the first distance bin. Therefore, these changes in IPG values are dominated by the changes in transmission rates. Fig. 4.4a shows that the transmission rate of CAM-DCC 100%, CAM-DCC 80%, and CAM-DCC 20% cases are 5 Hz, 2.5 Hz, and 2 Hz respectively, which supports our IPG analysis. These changes in transmission rate are primarily caused by the increasing CBP values as more LIMERIC vehicles are contributing to driving CBP towards the target. As to LIMERIC vehicles, each vehicle can transmit at a lower rate as the percentage of LIMERIC vehicle is increasing since more and more LIMERIC vehicles can help to push the CBP towards the target. However, the
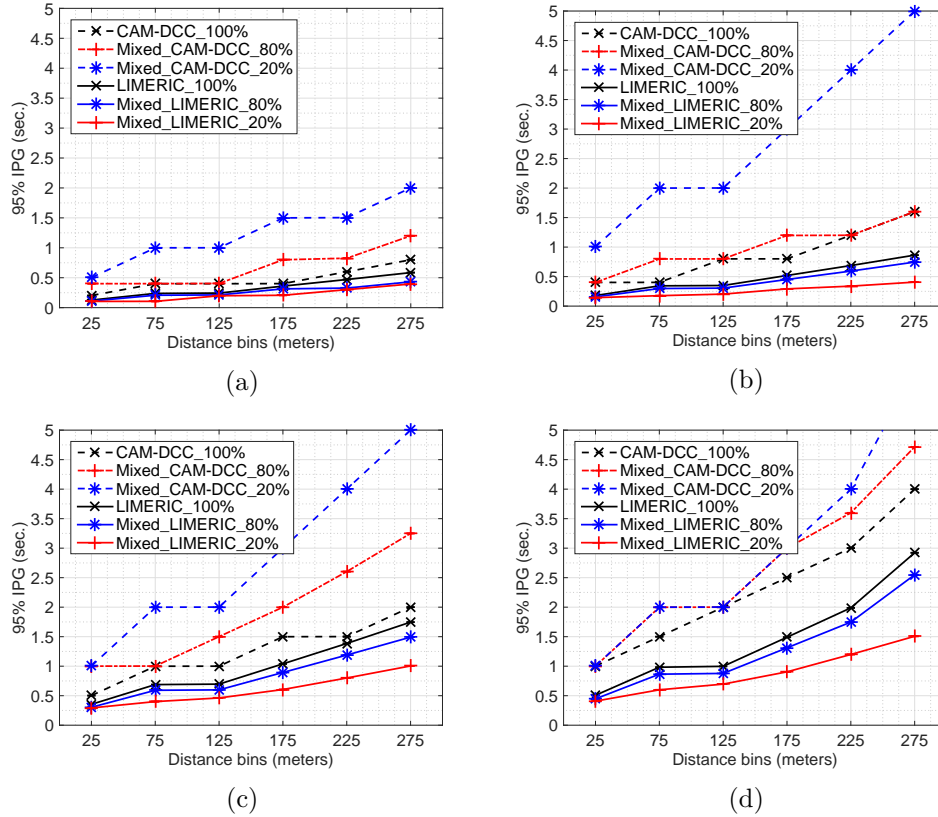
Figure 4.3: 95% IPG of mixed networks with different total number of vehicles: (a) 300 vehicles; (b) 500 vehicles; (c) 1000 vehicles; (d) 1500 vehicles

performance difference between CAM-DCC and LIMERIC in the same mixed network can be observed, e.g., the transmission rate of LIMERIC 80% in Fig. 4.4b is 6.7 Hz, while that of CAM-DCC 20% is only 1 Hz. The difference in transmission rate further leads to as large as a 4.5s difference in IPG. Actually, the performance difference is expected due to the reactive and the adaptive characteristics of the two algorithms. Unfortunately, in low vehicle density scenarios, i.e., the total number of vehicles in the network is 300 and 500, the performance degradation of CAM-DCC vehicles is noticeable after LIMERIC vehicles are introduced into the network. Fig. 4.4a shows that in the CAM-DCC 100% scenario, the CAM-DCC vehicles transmit messages at 5 Hz. However, as the percentage of the LIMERIC vehicles increases to 80%, the transmission rate of CAM-DCC vehicles drops to 2 Hz. Similarly, Fig. 4.4b shows that the transmission rate of CAM-DCC vehicles can drops from 2.5 Hz to 1 Hz. While for 1000 vehicles and 1500 vehicles cases (see Fig. 4.4c and Fig. 4.4d), the decrement

in transmission rates of the CAM-DCC vehicles after the LIMERIC vehicles shrinks and eventually diminishes. It is because in these cases the CBP is high enough to push CAM-DCC vehicles always operate in RESTRICTIVE state or a state close to the RESTRICTIVE state even without the participation of the LIMERIC vehicles.
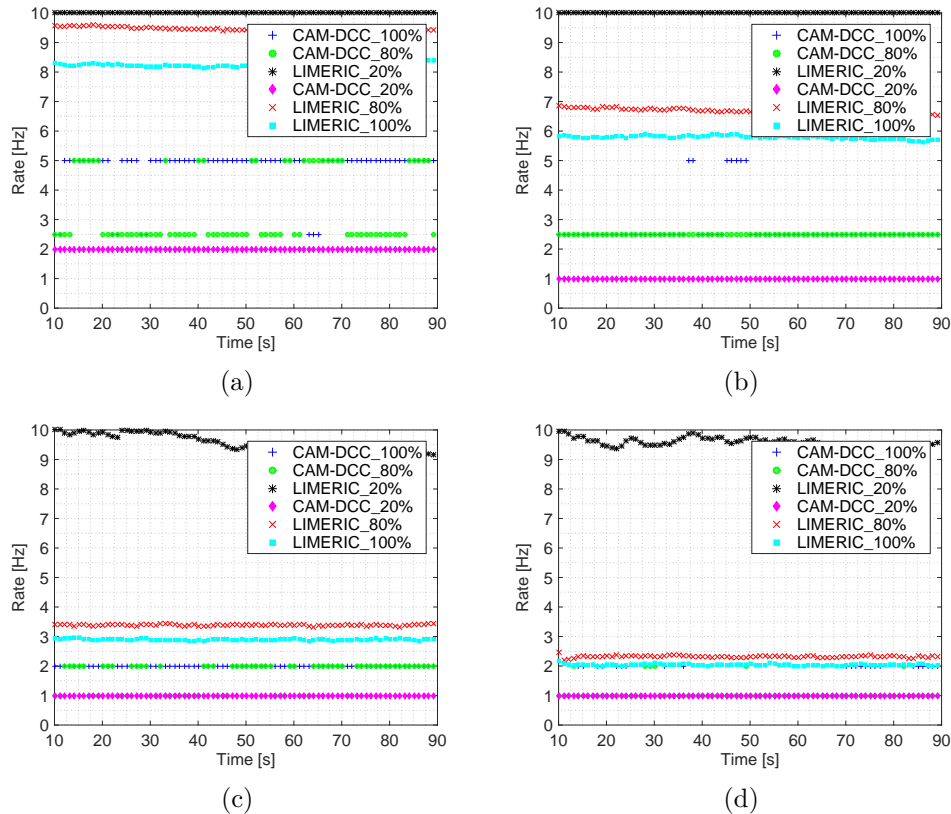
Figure 4.4: Transmission rate of mixed network with different total number of vehicles: (a) 300 vehicles; (b) 500 vehicles; (c) 1000 vehicles; (d) 1500 vehicles

4.3.3 Near-worst Case of Performance Degradation

The results from the previous subsection have demonstrated that in certain scenarios, introducing LIMERIC vehicles into the network can result in a noticeable performance degradation of CAM-DCC vehicles. However, a question could arise that what the worst or the near-worst case of this performance degradation caused by LIMERIC vehicles can be. To explore this question, a simulation study is performed. In this set of simulations, all the vehicles are static and uniformly distributed in an 800m × 100m area. This configuration aims to create an interference region of vehicles located at

the center area. The total number of vehicles is gradually increased from 10 to 300. Note that CAM generation rules are not applied in these simulations. The CBP values observed by the two algorithms and the determined rates of vehicles located at the center area are plotted in Fig. 4.5a and Fig. 4.5b, respectively. From Fig. 4.5a, it is observed that compared to the CBP in CAM-DCC 100% case, the CBP in CAM-DCC 20% case is about 20% higher. The increased CBP can consequently lead to a decrease in the transmission rate. As shown in Fig. 4.5b, the relatively large rate changes occur when the number of vehicles is 130-140 and 260-300. The corresponding rate changes of the CAM-DCC vehicles are 3 Hz and 2.5 Hz, respectively, which are close to the rate changes shown in Fig. 4.4a and Fig. 4.4b. In this study, we only test the limited number of vehicles densities and the percentage of LIMERIC vehicles in the network. Therefore, the identified large rate changes may not be the worst case of all scenarios. However, we believe this study can help to demonstrate that the significant performance degradation of CAM-DCC vehicles in mixed networks occurs typically when the vehicle density is low, and the transmission rate can decrease by 2.5 to 3 Hz, which is the near-worst case.

The primary reason for the performance degradation of the CAM-DCC vehicles is that the default LIMERIC algorithm targets at a high CBP (the default value is 76%), which drives CAM-DCC vehicles into more restrictive congestion control states. Our previous work [65] has also demonstrated that such performance degradation reduced in a specific scenario through a careful manual selection of LIMERIC's CBP target. The ideal target is dependent, however, on vehicle density and mixing ratio. This raises the question, whether the target can be automatically adapted to the network scenario so that CAM-DCC performance degradation is limited in all scenarios, if not eliminated.

4.4 Target Adjustment Mechanism

In this section, we present a CBP target adjustment mechanism that automatically adjusts the CBP target of LIMERIC vehicles according to vehicle density and mixing situation of the two algorithms in a network, to reserve sufficient channel capacity for CAM-DCC and thereby limit the performance degradation to a desired level. As the
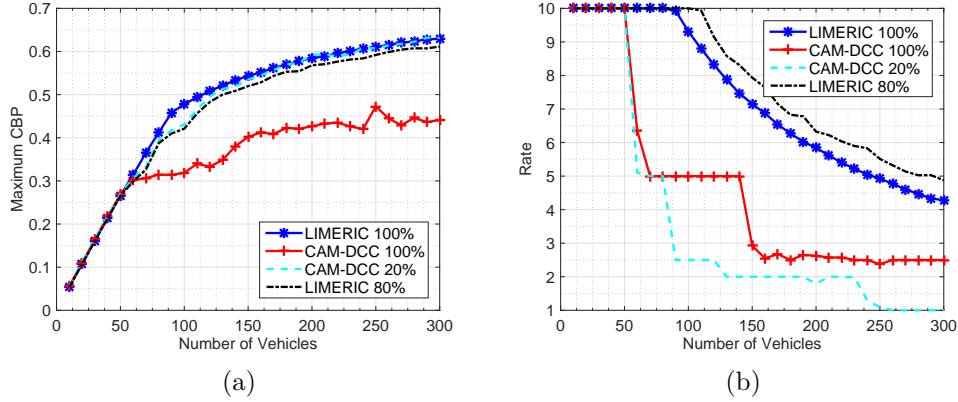
Figure 4.5: Near-worst case performance unfairness study: (a) CBP; (b) transmission rate

basis of the proposed mechanism, we first present the theoretical results of the steady-state CBP of a mixed network.

4.4.1 Steady-state CBP of a Mixed Network

Assume that the total number of vehicles within the same interference range in a mixed network is $K = K_{limeric} + K_{camdcc}$, where $K_{limeric}$ denotes the number of the LIMERIC vehicles, and K_{camdcc} denotes the number of the CAM-DCC vehicles. The transmission rate of a vehicle j, denoted by r_j $(j = 1, 2, ..., K)$, can be modeled as a fraction of the total channel capacity. Thus, the fraction of the network capacity allocated in aggregate to all K vehicles, represented in the number of transmitted messages per second, is $r_C(k) = \sum_{j=1}^{K} r_j(k)$. For mixed networks, r_C can be rewritten as:

$$r_C = r_{limeric}K_{limeric} + r_{camdcc}K_{camdcc} \tag{4.3}$$

Based on Eq. 7 in [61], $r_{limeric}$ is determined by

$$r_{limeric} = \frac{\beta(r_{target} - r_{camdcc}K_{camdcc})}{\alpha + \beta K_{limeric}} \tag{4.4}$$

where $r_{target} - r_{camdcc}K_{camdcc}$ is the actual CBP target of the LIMERIC vehicles in a mixed network. Due to CAM-DCC vehicles' share of the channel capacity, LIMERIC vehicles have to first exclude the channel load contribution of CAM-DCC vehicles from

the predefined target. α and β are adaption parameters that control LIMERIC's stability, fairness and convergence. Applying Eq. 4.4 into Eq. 4.3, we have

$$r_C = r_{target} - \frac{\alpha}{\beta}r_{limeric} \tag{4.5}$$

r_C presents the number of transmitted messages per second on the channel. There is a one-to-one relationship between r_C and the measured CBP [61]. According to this mapping, Eq. 4.5 can be written as

$$CBP_C = CBP_{target} - \frac{\alpha}{\beta * \delta}r_{limeric} \tag{4.6}$$

where CBP_{target} is the CBP target which the LIMERIC vehicles will use in their rate adaptation equation; CBP_C is the CBP of a mixed network when LIMERIC vehicles reach to the steady state; δ represents the near-linear mapping from the number of messages per second to CBP.

4.4.2 Design of the Mechanism

The proposed target adjustment mechanism consists of four main components:

1. Estimating the number of vehicles within the interference range

2. Estimating the pure CAM-DCC state, i.e., the CAM-DCC state at which a CAM-DCC vehicle would operate if all the vehicles use CAM-DCC algorithm

3. Determining new CBP targets for LIMERIC vehicles

4. Sharing new CBP targets with other LIMERIC vehicles over a two-hop range

The LIMERIC vehicles run this mechanism periodically and synchronously. With a relatively short period, each LIMERIC vehicle is able to collect the required information frequently and then react to changes in channel condition in a timely manner. The synchronous operation[3] ensures the LIMERIC vehicles within the same interference

---

[3]Synchronization can be achieved via GPS synchronization techniques.

Table 4.2: Notations used in the mechanism description

Notation	Description
$r_{limierc}$	The steady-state transmission rate of LIMERIC vehicles
r_{camdcc}	The steady-state transmission rate of CAM-DCC vehicles
R	The estimated LIMERIC's mixing ratio
K	The estimated number of vehicles within the interference range
$r^{table}_{camdcc}[\cdot]$	The function returns the corresponding transmission rate for an input CAM-DCC state according to Table 4.1
$mapToTxCount(\cdot)$	The function maps the measured CBP to the number of transmissions generating such a CBP value
$mapToCBP(\cdot)$	The inverse function of $mapToTxCount(\cdot)$
$level_{deg}$	The degradation level is allowed by the CAM-DCC vehicles in a mixed network
$CBP^{table}_{desired}[\cdot]$	Given a state which CMA-DCC vehicles desire to operate at, this function returns the CBP value to which the channel load should converge

range observe the same channel condition and mixing situation at the same time and then adjust to similar targets. The details will be described in the following. Table 4.2 lists the notations used in the mechanism description.

Estimating the Number of Vehicles in the Interference Range

First, a receiver is assumed to be able to distinguish whether the sender of the received packet is using LIMERIC or CAM-DCC. There could be several methods to identify the sender's algorithm type, e.g., the sender can explicitly indicate its algorithm type via one bit in its packet header, or the receiver can implicitly tell the algorithm type by checking the received packet's header structure, since a LIMERIC packet piggybacks the shared CBP values in its packet header, while a CAM-DCC packet does not. With such a capability, a receiver is able to count the number of the LIMERIC vehicles and the CAM-DCC vehicles within its one-hop range separately, and then estimate the LIMERIC's mixing ratio. Meanwhile, a receiver can also infer the sender's transmission rate based on the packet sending time and the packet id piggybacked in each received packet. One simple implementation for doing so could be: 1) For each sender, the receiver keeps recording the packet sending time and the packet id of the latest received packet from that sender; 2) Once a new packet from that sender is received, the receiver respectively examines the differences in packet sending time and the packet id between this packet and the latest packet from the same sender; 3) Based on the number of

packets transmitted during the elapsed time, the transmission rate of the sender can be estimated.

We believe that this mixing ratio within the reception range is also a good estimation for the mixing ratio within the interference range. For estimating the number of vehicles within the interference range, we exploit the locally measured CBP and the estimated LIMERIC's mixing ratio. As aforementioned, there exists a one-to-one near-linear mapping between the measured CBP and the number of transmissions contributing to this CBP value. $mapToTxCount(CBP)$ implements this mapping as a function of the measured CBP. If assuming K vehicles are within the interference range, we then have

$$r_{limeric} \cdot K \cdot R + r_{camdcc} \cdot K \cdot (1 - R) = mapToTxCount(CBP)$$

The terms on the left side represent the number of transmissions sent by the LIMERIC and the CAM-DCC senders, respectively. They are expected to be equal to the total number of transmissions which contribute to the measured CBP. Here, $r_{limeric}$, r_{camdcc}, R and CBP can be obtained via local measurements. Note that $r_{limeric}$ and r_{camdcc} are estimated via the average rate. Thus, K can be computed from this equation, and consequently, the number of the LIMERIC vehicles and the CAM-DCC vehicles are $K \cdot R$ and $K \cdot (1 - R)$, respectively.

Estimating the Pure CAM-DCC State

In this step, all the vehicles in the network are assumed to use CAM-DCC algorithm, and thus the CAM-DCC state of CAM-DCC vehicles (called pure CAM-DCC state) in this homogeneous network can be estimated. For each CAM-DCC state defined in Table 4.1, the maximum number of vehicles which can be tolerated in that state is calculated through the upper bound of the corresponding CBP range and the defined transmission rate for that state. For example, the ACTIVE 1 state defines the transmission rate as 5 Hz and the corresponding CBP range as 30%-39%. The maximum number of vehicles tolerated in this state is $mapToTxCount(39)/5$. We then compare, in turn, K with the maximum number of vehicles tolerated in each defined state, starting from the RELAXED state. The first state whose maximum number of tolerated

---

Algorithm 1 CBP Target Adjustment Mechanism

1: **Input:** $r_{limeric}, r_{camdcc}, CBP_{measured}, R, level_{deg}\ r_{camdcc}^{table}[\cdot], maxTolerateTx[\cdot]$
2: **Output:** CBP_T'
3: $CBP_T' = CBP_T$
4: $K \cdot (r_{limeric} \cdot R + r_{camdcc} \cdot (1 - R)) =$
   $mapToTxCount(CBP_{measured})$
5: Estimate the pure CAM-DCC state index, $dcc\_stateIndex\_pure$
6: $dcc\_stateIndex\_exp = dcc\_stateIndex\_pure - level_{deg}$
7: **if** $\qquad mapToTxCount(CBP_{desired}^{table}[dcc\_stateIndex\_exp])\qquad\qquad <$
   $r_{camdcc}^{table}[dcc\_stateIndex\_exp] \cdot K)$ **then**
8: $\qquad CBP_{desired} =$
   $mapToCBP(r_{camdcc}^{table}[dcc\_stateIndex\_exp] \cdot K)$
9: **else**
10: $\qquad CBP_{desired} = CBP_{desired}^{table}[dcc\_stateIndex\_exp]$
11: **end if**
12: $r_{limeric}^{exp} = (mapToTxCount(CBP_{desired}) -$
   $r_{camdcc}^{table}[dcc\_stateIndex\_exp] \cdot K \cdot (1 - R))/(K \cdot R)$
13: $CBP_T' = CBP_{desired} + \frac{\alpha}{\beta} \cdot r_{limeric}^{exp}$

---

vehicles is greater than K, will be selected as the pure CAM-DCC state.

Determine the New CBP Target for LIMERIC Vehicles

To drive the CAM-DCC vehicles to operate at a specific state, their measured CBP values have to fall into the CBP range associated with that state. In the mixed network, the LIMERIC vehicles and the CAM-DCC vehicles within the same interference range share a similar CBP value. Therefore, the CBP target is adjusted such that the LIMERIC vehicles' steady-state CBP is within the CBP range associated with the desired state. The choice of the new CBP target also depends on the allowed degradation level, which indicates how much degradation the CAM-DCC vehicles can accept in a mixed network in terms of CAM-DCC states. For instance, the state of the CAM-DCC vehicles in a mixed network is the ACTIVE 2 state, while the pure CAM-DCC state is the ACTIVE 1 state. The degradation level, in this case, is one. With the estimated pure CAM-DCC state and the allowed degradation level, the LIMERIC vehicles are able to estimate the expected state of the CAM-DCC vehicles in the mixed network, denoted as dcc_state_exp.

Given the expected CAM-DCC state, the LIMERIC vehicles will try to push their

steady-state CBP into the associated CBP range of the expected state. To achieve this goal, the LIMERIC vehicles have to determine to what exact value within this range the CBP will converge at the steady state. With considering the measurement variation of CBP, we conservatively designate the middle point of the CBP range as the steady-state CBP for the associated CAM-DCC state. However, if $mapToTxCount(CBP_{desired}^{table})$ is less than the number of transmissions generated by K vehicles transmitting at rate $r_{camdcc}^{table}[dcc\_stateIndex\_exp]$, the designated CBP is replaced by $mapToCBP($ $r_{camdcc}^{table}[dcc\_stateIndex\_exp] \cdot K)$ as shown in line 8 in Algorithm 1. This is because if the number of transmissions corresponding to the designated CBP ($mapToTxCount($ $CBP_{desired}^{table}))$ is smaller, it indicates that the transmission rate of the LIMERIC vehicles is potentially smaller than that of the CAM-DCC vehicles (i.e., $r_{camdcc}^{table}[dcc\_stateIndex\_exp]$), which can further result in performance degradation of the LIMERIC vehicles. The final designated CBP is denoted as CBP_{desire}.

After adjusting the CBP target, the equation in line 12 in Algorithm 1 is used to predict the LIMERIC vehicles' transmission rate. In this equation, the term $mapToTxCount($ $CBP_{desired})$ is considered as the resource which is allocated to all the vehicles within the interference range. The term $r_{camdcc}^{table}[stateIndex] \cdot K \cdot (1 - R)$ denotes the resource share of the CAM-DCC vehicles. Thanks to the PULSAR mechanism, the LIMERIC vehicles can fairly share the resource. Thereby, the rest portion of the resource is evenly allocated to $K \cdot R$ LIMERIC vehicles. According to Eq. 4.6, the new CBP target is determined as $CBP_T' = CBP_{desired} + \frac{\alpha}{\beta} \cdot r_{limeric}^{exp}$. Note that due to the errors in measurement and prediction, it is possible that in some cases, the new target could lead the LIMERIC vehicles to transmit at a lower rate than the expected rate of the CAM-DCC vehicles (i.e., $r_{camdcc}^{table}[dcc\_stateIndex\_exp]$). If such a case is detected, the LIMERIC vehicles start to transmit at rate $r_{camdcc}^{table}[dcc\_stateIndex\_exp]$ despite the calculated transmission rate.

CBP Target Sharing

To preserve the fairness between LIMERIC vehicles, a CBP target sharing mechanism is applied to share the CBP target over two-hop neighbors. Each LIMERIC vehicle inserts its own CBP target ($targetCBPSelf_{pkt}$), the received CBP target from its one-hop neighbors ($targetCBP1Hop_{pkt}$), and the index of the CAM-DCC state (idx_exp_{pkt}) at which the neighboring CAM-DCC vehicles expect to operate. Via the PULSAR mechanism, the sender's local CBP measurement ($CBPSelf_{pkt}$) and the received CBP value from its one-hop neighbors ($CBP1Hop_{pkt}$) are also shared with other LIMERIC vehicles. Once a new LIMERIC packet arrives, the LIMERIC receiver extracts the values of $CBPSelf_{pkt}$ and $CBP1Hop_{pkt}$ from the packet, and then compare them with the locally stored values of $CBP1Hop_{local}$ and $CBP2Hop_{local}$. Only if the CBP values piggybacked in the packet is larger, the CBP targets in the packet are considered being accepted. The rationale behind this design is that the senders in a more channel-congested region (i.e., the region with higher CBP) hold a higher priority for being assisted in controlling the congestion, and thereby their CBP targets should be considered with priority as well. The LIMERIC receiver then examines the CBP target piggybacked in the packet. Recall that a new CBP target is determined according to which state the neighboring CAM-DCC vehicles are desired to operate at. Different desired CAM-DCC states can result in different CBP targets. We believe it is fairer to consider the CBP targets for different desired CAM-DCC states separately. $targetCBP1HopArray$ and $targetCBP2HopArray$ are used to hold the CBP targets for different CAM-DCC states over a two-hop range. For the same CAM-DCC state, if the CBP target in the received packet is smaller, the held CBP target is updated to the value in the packet. The reason for selecting the smaller CBP target is that a vehicle with a higher CBP tends to determine a smaller CBP target. At the end of each target sharing window, each LIMERIC vehicle decides the new CBP target by two steps: 1) Find the most restrictive CAM-DCC state corresponding to the received CBP targets; 2) Select the minimum value of CBP targets for that state.

Algorithm 2 CBP Target Sharing Mechanism

1: **Input:** $targetCBPSelf_{pkt}$, $targetCBP1Hop_{pkt}$, $CBPSelf_{pkt}$, $CBP1Hop_{pkt}$, idx_exp_{pkt}, idx_exp_{local}

2: **if** $CBPSelf > CBP1Hop_{local}$ or $CBP1Hop > CBP2Hop_{local}$ **then**

3:      **if** $targetCBPSelf_{pkt} < targetCBP1HopArray[idx\_exp_{pkt}]$ **then**

4:          $targetCBP1HopArray[idx\_exp_{pkt}] = targetCBPSelf_{pkt}$

5:          $targetCBP1Hop_{local} = targetCBP1HopArray[idx\_exp_{local}]$

6:      **end if**

7:      **if** $targetCBP1Hop_{pkt} < targetCBP2HopArray[idx\_exp_{pkt}]$ **then**

8:          $targetCBP2HopArray[idx\_exp_{pkt}] = targetCBP1Hop_{pkt}$

9:      **end if**

10: **end if**

11: At the end of each monitoring period

12: **for** $stateIndex = 0 : idx\_exp_{local}$ **do**   ▷ The smaller index is, the more restrictive state is

13:      $tmpCBPSelf = targetCBPSelfArray[stateIndex]$

14:      $tmpCBP1Hop = targetCBP1HopArray[stateIndex]$

15:      $tmpCBP2Hop = targetCBP2HopArray[stateIndex]$

16:      **if** $tmpCBPSelf$!= NULL or $tmpCBP1Hop$!= NULL or $tmpCBP2Hop$!= NULL **then**

17:          $CBP_T = min(tmpCBPSelf, tmpCBP1Hop, tmpCBP2Hop)$

18:      **end if**

19: **end for**

4.5 Performance Evaluation

4.5.1 Evaluation in MATLAB Simulations

In the MATLAB evaluation, the nodes are deployed in a relatively small area so that all the nodes observe the same channel condition. The total number of the nodes in the network increases from 100 to 1000, and for each node density, the LIMERIC's mixing ratio varies from 0% to 100%.

As shown in Fig. 4.6a, without adjusting the CBP target, the CAM-DCC vehicles degrades one to two levels in almost all the scenarios where the total number of nodes is less 800. This is because, in these scenarios, the LIMERIC vehicles attempt to push the CBP towards a comparatively high target. While reacting to the increasing CBP values, the CAM-DCC nodes operate at more restrictive states. However, as the node density increases, the degradation level decreases. This is because, in these high node density scenarios, the CBP is high enough such that even without the participation
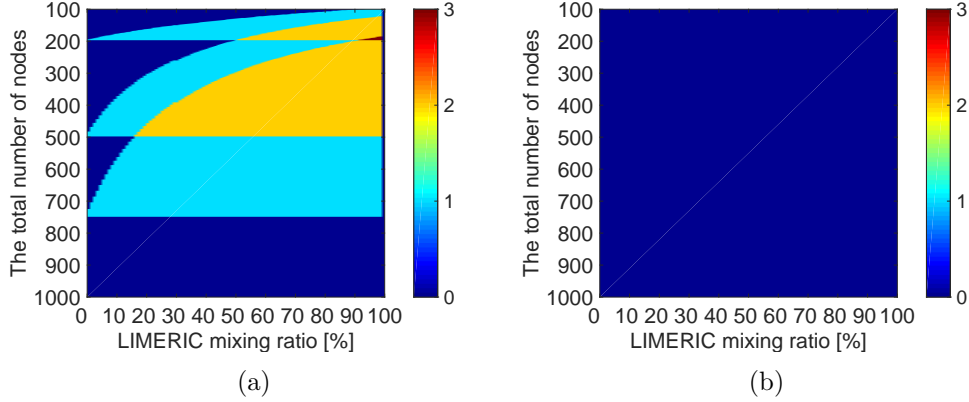
Figure 4.6: Performance degradation of CAM-DCC vehicles in terms of DCC state, allowing zero-level degradation: (a) without target adjustment; (b) with target adjustment
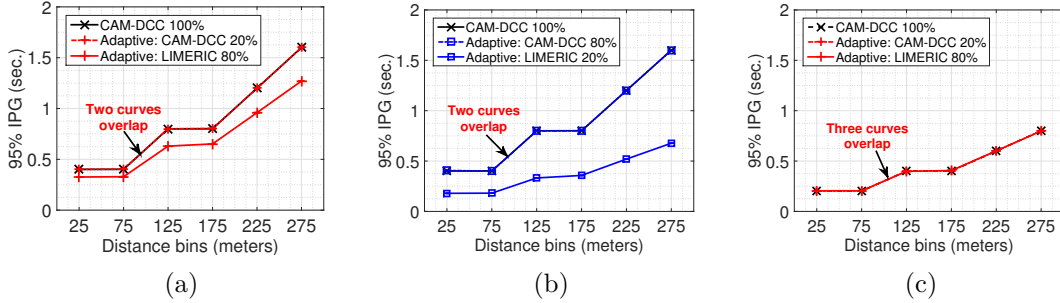
Figure 4.7: 95th percentile IPG for the mixed networks: (a) zero-level degradation, 500 vehicles with 80% LIMERIC; (b) zero-level degradation, 500 vehicles with 20% LIMERIC; (c) zero-level degradation, 250 vehicles with 80% LIMERIC

of LIMERIC nodes, the CAM-DCC nodes already operate at a highly restricted state. Fig. 4.6b shows the results of simulations where the proposed CBP target adjustment mechanism is applied and the CAM-DCC nodes only allow zero-level degradation. It is observed that across many different combinations of node density and LIMERIC's mixing ratio, the proposed mechanism helps the CAM-DCC nodes to eliminate performance degradation. This is because the proposed mechanism estimates the pure CAM-DCC state based on the collected information and the LIMERIC's CBP target is adjusted in a way such that the steady-state CBP is within the CBP range associated with the pure CAM-DCC state. Therefore, the performance degradation of the CAM-DCC nodes is eliminated.

Figure 4.8: Road topology for simulations

4.5.2 Evaluation in ns-2 Simulations

In this subsection, the performance of the proposed mechanism is evaluated via ns-2 simulations of a highway scenario. As shown in Fig. 4.8, a highway is configured as 4 km long and three lanes in each direction. The middle part of the road is set to be a winding section of linear length 375 m. The vehicle's average speed is around 30 m/s. The Nakagami model is used to model the wireless channel fading, and the model parameters are the same in [66]. The transmission power is set to 10 dBm to create a typical 500 m DSRC transmission range in the simulation. More details of the simulation configurations can be found in [65]. Note that all the presented results are based on transmissions carried out on the winding part of the road.

Fig. 4.7a shows the 95th percentile IPG results of a set of simulations with 500 vehicles and the LIMERIC's mixing ratio as 80%. Similar to the observations from the MATLAB simulations, with the proposed mechanism, the results of the CAM-DCC vehicles in the mixed network only differ by 1.4%, comparing to the results of the homogeneous CAM-DCC network (CAM-DCC 100% scenario). Recall that the degradation was two-level before the target adjustment is applied (see Fig. 4.3b). Although the LIMERIC vehicles adjust their CBP target with the purpose of controlling the performance degradation of the CAM-DCC vehicles, the LIMERIC vehicles still outperform the CAM-DCC vehicles by $\sim 20\%$.

Changing LIMERIC's Mixing Ratio

To investigate the performance of the proposed mechanism in mixed networks with different LIMERIC's mixing ratios, a set of simulations with the LIMERIC's mixing ratio as 20% is conducted. Similar to the observations from Fig. 4.7a, Fig. 4.7b shows that the performance degradation of the CAM-DCC vehicles is eliminated with the target adjustment, while the LIMERIC vehicles still perform better.

Changing the Number of Vehicles

As shown in Fig 4.7c, similar results are observed for the simulations with 250 vehicles and the LIMERIC mixing ratio as 80%. In this scenario, the degradation decreases to less than 0.1%. Note that in this scenario, the LIMERIC vehicles behave similarly to the CAM-DCC vehicles. It is because in this case, the LIMERIC vehicles conservatively determine a new CBP target which can help the CAM-DCC vehicles to control performance degradation but let the LIMERIC vehicles transmit at a lower rate than the CAM-DCC vehicles. Recall that the proposed mechanism can detect such a situation and then force the LIMERIC vehicles to transmit at the same rate as the CAM-DCC vehicles to prevent the unfairness between the LIMERIC vehicles and the CAM-DCC vehicles.
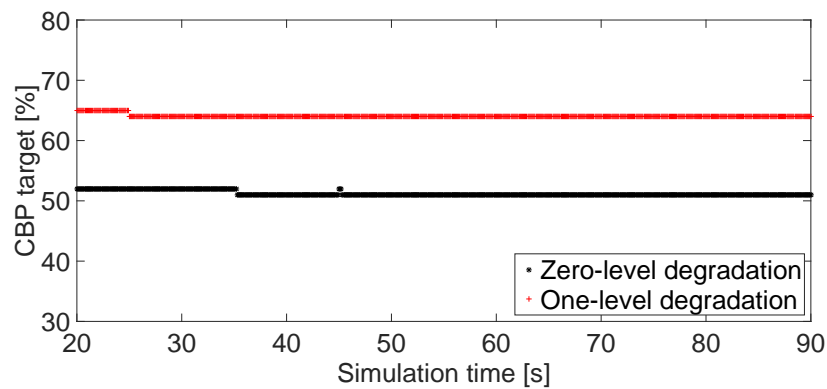
Figure 4.9: CBP target for allowing zero-level degradation and one-level degradation

Different Allowed Degradation Levels

Fig. 4.9 illustrates the CBP target of a LIMERIC vehicle which stands in the middle region of the road. It shows that the CBP target of the simulation allowing zero-level of degradation is about 13% lower than that of the simulation allowing one-level of degradation. Generally speaking, to meet a higher requirement for performance degradation, LIMERIC vehicles have to adjust to a lower target and then transmit at a lower rate. This is because the pure CAM-DCC state is normally more relaxed than the CAM-DCC state of CAM-DCC vehicles in a mixed network. Towards a more relaxed state, the CBP has to be driven to a range of smaller values.
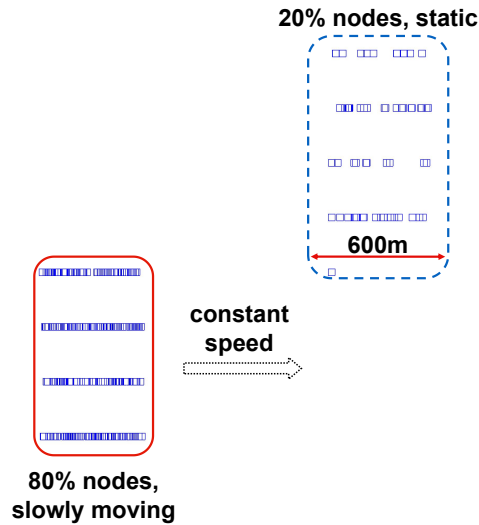
Figure 4.10: A dynamically changing topology for examining CBP target stability

4.6 Summary

We presented a CBP target adjustment mechanism for adjusting the CBP target of LIMERIC vehicles to eliminate or reduce the performance degradation of CAM-DCC vehicles to a specified level. Simulation results indicate that the performance degradation of the CAM-DCC vehicles is virtually eliminated when the target adjustment is used, while the LIMERIC vehicles still maintain similar or better performance. When no CAM-DCC vehicles are around, LIMERIC reverts to its default target and performance. This suggests that it is feasible to design vehicular congestion control algorithms so that a new algorithm can be gradually introduced without significantly degrading the performance of legacy vehicles.

Chapter 5

Impact of 5.9 GHz Spectrum Sharing on DSRC Performance

This chapter studies a coexistence scenario where DSRC devices and unlicensed Wi-Fi devices share the DSRC spectrum. Driven by the increasing congestion in the Wi-Fi channels, there is interest in both the United States and Europe to allow secondary users, such as Wi-Fi, on the 5.9 GHz band reserved for Intelligent Transportation Services. Under standard spectrum sharing rules, secondary users such as Wi-Fi are required to detect primary users such as DSRC devices and avoid interfering with their transmissions. Compared to conventional spectrum sharing scenarios, such as unlicensed devices sharing TV whitespaces, the safety-critical nature of DSRC transmissions places stricter requirements on the effectiveness of spectrum sharing mechanisms. In this chapter, we first analyze this spectrum sharing scenario to identify its fundamental challenges and derive network scenarios that can represent challenging scenarios. We also evaluate three recently proposed spectrum sharing mechanisms, Detect & Vacate, Detect & Mitigate and Re-channelization, to understand their performance in these challenging scenarios. Among these mechanisms, Detect & Vacate and Detect & Mitigate are under discussion in the European standardization group, while Re-channelization is primarily designed for using in the U.S. We identify that these mechanisms can introduce extra packet losses to DSRC transmissions and significantly degrade DSRC performance.

5.1 Motivation

Due to increasing congestion of the the 2.4 and 5.8 GHz Industrial, Scientific and Medical (ISM) bands, strong interest exists in letting Wi-Fi exploit the adjacent 5.850-5.925 GHz (5.9 GHz) band [24, 67]. This would allow usage of three additional 20 MHz channels, two 40 MHz channels or, perhaps more importantly, allow creating an additional contiguous 80 or 160 MHz Wi-Fi channel, as shown in Fig. 5.1. This motivated proposals to open the 5.9 GHz band for spectrum sharing.

However, the primary application of Dedicated Short Range Communications (DSRC) systems in the 5.9 GHz band is safety-critical, which places stricter requirements on network performance, e.g. lower packet loss rate and inter-packet delay, than in other spectrum sharing scenarios such as TV whitespaces. DSRC is an Intelligent Transportation System (ITS) technology which enables direct vehicle-to-vehicle and vehicle-to/from-infrastructure communication. It allows a vehicle to share trajectory, driving status as well prevailing road and traffic conditions with other vehicles. With the shared information, significant improvements in road safety and efficiency are expected. This potential impact had motivated the U.S. Federal Communications Commission (FCC) to reserve the 5.9 GHz band for DSRC in 1999 [10]. Such safety-related applications of primary users, raise deeper questions about the interference avoidance guarantees that spectrum sharing protocols offer and how such protocols can be evaluated—not just in the average case but also under challenging, near-worst case conditions.
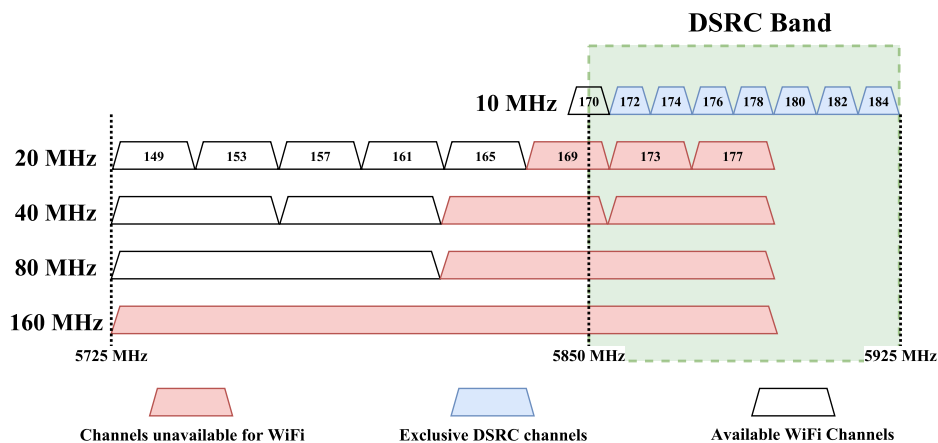
Figure 5.1: Channelization in 5.7-5.9 GHz band

While significant work has been conducted on spectrum sharing protocols (e.g., [21, 68,69]), this work has primarily focused on non-safety related applications, i.e., assuming applications in little need of low-latency and time-critical communications. For safety-related communications in the 5.9 GHz band, three sharing mechanisms, Detect & Vacate (D&V), Detect & Mitigate (D&M) and Re-channelization have been proposed by the Wi-Fi industry to share the DSRC spectrum. The details of D&V and D&M are defined in TR 103 319 [70] and they are currently under further investigation in the Broadband Radio Access Networks (BRAN) working group within the European Telecommunications Standards Institute (ETSI). While Re-channelization is primarily proposed for deployment in the U.S. Prior work has studied the performance gains that Wi-Fi can achieve through spectrum sharing [71]. However, we are not aware of any publications that carefully evaluate the impact of Wi-Fi on DSRC and, in particular, any analysis of challenging and near-worst case scenarios.

To fill this gap, in this chapter, we conduct such an analysis by identifying fundamental challenges, providing guidance on challenging scenarios, and simulating the three aforementioned spectrum sharing mechanisms under such challenging scenarios. In terms of design philosophy, D&V and D&M are significantly different from Re-channelization and they are planned to be deployed in different regions. Their performances are analyzed and studied separately.

5.2 Background Knowledge on Spectrum Sharing Techniques

This section reviews two popular spectrum sharing techniques in the wireless communication community.

5.2.1 Listen-before-talk

Listen-before-talk is a spectrum sharing technique that requires devices to monitor channel status and only transmit packets when the channel is accessed to be free of use. This Clear Channel Assessment (CCA) is acheived through two methods, Carrier Sensing (CS) and Energy Detection (ED).

Table 5.1: Channel busy thresholds defined in the IEEE 802.11 standard

Channel bandwidth	CS threshold (dBm)	ED threshold (dBm)
10 MHz	-85	-65
20 MHz	-82	-62

The CS mechanism tries to match the preamble of the received signal with a known training signal sequence. It is primarily designed to avoid interference from other devices using the same technology. The ED mechanism tries to detect whether the energy on the channel is above a certain threshold, regardless of the form of the signal. The ED mechanism can be used to prevent interference from other devices using different technologies. However, according to the IEEE 802.11 standard, the ED detection threshold is 20 dB higher than the CS detection level, see Table 5.1.

Listen-before-talk is the primary technique used to resolve backward compatibility issue between a newer version of Wi-Fi protocols and legacy Wi-Fi protocols. For example, IEEE 802.11ac standard [72] requires a legacy Wi-Fi preamble (e.g., IEEE 802.11a preamble) is included in its packet structure. Such that, a 802.11ac transmission can be detected by legacy Wi-Fi receivers via CCA. Recently, this solution is also adopted to mitigate interference when coexisting LTE and Wi-Fi. In [21], Chai et al. proposed a coexisting mechanism which integrates Wi-Fi's carrier sensing and notification mechanisms into LTE in order to achieve the mutual CCA detection between Wi-Fi and LTE.

5.2.2 Dynamic Frequency Selection

The second solution is Dynamic Frequency Selection (DFS). The purpose of DFS is to ensure compatible operation with radio determination systems by avoiding co-channel operation with these systems [73]. As the standard feature of IEEE 802.11 protocol, Wi-Fi operating in the radar band should passively scan for and select the channel not occupied by radars. If the presence of the radar waveform is detected, Wi-Fi devices are required to execute a channel switching procedure [24].

In comparison of listen-before-talk and DFS, we realize that both approaches require

detection of users' presence and deferral to ongoing transmissions in order to avoid packet collision. However, listen-before-talk does not differentiate channel users while DFS aims to detect the primary user of the channel. Also, listen-before-talk only defers to other transmissions in short term (normally a few milliseconds). But the deferral from transmissions in DFS is relatively long term (in the radar detection case, at least 30 min) [73].

To best of our knowledge, neither of the above two spectrum sharing approaches has been reported to immediately apply to the Wi-Fi and DSRC coexisting scenario. It is mainly because: 1) primary and secondary users coexisting. DSRC is the primary user of the channel, and its safety critical nature poses higher requirements of coexisting performance; 2) not radio determination systems. in most cases, the DSRC detection environment is dynamic due to the high mobility of DSRC devices.

The algorithms studied in this paper, D&V and D&M, integrate the features from the aforementioned solutions, i.e., dynamically detecting DSRC devices as the primary user of the channel but deferring to the DSRC transmissions in relative short term.

5.3 Study of D&V and D&M Mechanisms

The Physical (PHY) and Medium Access Control (MAC) protocol defined in the DSRC technology is a variation of the IEEE 802.11a standard, referred to as Wireless Access in Vehicular Environments (WAVE). This variation is specified in the IEEE 802.11p amendment [33]. While the similarity of Wi-Fi and DSRC simplifies the spectrum sharing problem, lack of mutual carrier sensing leads to inefficient detection. It is because Wi-Fi typically operates on channels with 20 MHz bandwidth while DSRC on channels with 10 MHz bandwidth. Wi-Fi is not capable of detecting DSRC via CCA directly. Therefore an extra component in a Wi-Fi device is needed to recognize DSRC operations on 10 MHz channels and mitigate accordingly. Such receiving-only hardware is called DSRC detector and has been assumed by both spectrum sharing algorithms. Note that the DSRC detector does not completely enable mutual carrier sensing between Wi-Fi and DSRC since DSRC devices still cannot detect Wi-Fi operations via the CS

mechanism.

D&V approach, proposed by Cisco, requires Wi-Fi devices to be equipped with DSRC detectors. If a Wi-Fi device operating in the DSRC band detects a DSRC transmission, it needs to vacate the entire DSRC band for a few seconds.

Similar to D&V, D&M, proposed by Broadcom, relies on the DSRC detector to monitor the appearance of DSRC transmissions. However, instead of leaving the ITS band, the approach allows a packet-by-packet spectrum sharing after the detection of DSRC transmissions. More specifically, D&M approach adjusts the medium access parameters of the IEEE 802.11 Enhanced Distributed Channel Access (EDCA) mechanism. In EDCA, the primary medium access parameters are Arbitration Interframe Space Number(AIFSN), minimum and maximum size of Contention Window (CW_{min} and CW_{max}). These parameters control the minimum time gap between two consecutive transmissions and thus provide different levels of channel access priority to traffic. Traffic with higher priority waits less before it can send a packet than traffic with lower priority. Four EDCA defined priority levels are: background (AC_BK), best effort (AC_BE), video (AC_VI), and voice (AC_VO). Upon detection of DSRC transmissions, D&M largely increases these EDCA parameters, such that the minimum gap between two consecutive Wi-Fi transmissions is prolonged as compared to that enabled by the default EDCA. The rationale behind the increased inter-packet gap is to enable an improved probability for DSRC packets to be sent before Wi-Fi packets when DSRC and Wi-Fi devices observe the same channel. In particular, Table 5.2 summarizes the post-detection EDCA parameters a Wi-Fi device needs to use for running D&M.

Table 5.2: EDCA parameters in D&M after DSRC detection

AC	CW_{min}	CW_{max}	AIFSN	Max TxOp
AC_BK	31	2047	2065	2.258 ms
AC_BE	31	2047	2059	2.258 ms
AC_VI	15	31	1029	3.008 ms
AC_VO	7	15	515	1.504 ms

In [71], D&V and D&M have been analytically evaluated with performance metrics:

spectrum efficiency and data rate. While these metrics provide insights on the characteristics of the two approaches, they do not reflect the impact of Wi-Fi transmissions on the DSRC performance which is the focus of our work in this chapter.

5.3.1 Methodology Overview

This paper, to our best knowledge, investigates for the first time the spectrum sharing mechanisms from the perspective of ITS safety applications based on systematic analysis and realistic simulations. We start the investigation by dissecting each algorithm into a pre-detection phase and a post-detection phase. The former starts from the moment at which DSRC activities appear on the channel and ends when an interfering Wi-Fi device engages its mitigation mechanism. In this phase, we focus on studying how well a Wi-Fi device can detect the presence of DSRC transmissions. We find that due to strong self-interference, a Wi-Fi device can detect the presence of DSRC transmissions only when the Wi-Fi device itself is not transmitting. The analysis for the post-detection phase focuses on studying how well a Wi-Fi device can protect DSRC transmissions after it detects one. It has been observed that due to lack of mutual carrier sensing, an unilateral hidden terminal problem can arise, causing undesired packet collision between DSRC and Wi-Fi. Based on the identified challenges, we further provide guidelines of creating challenging scenarios. The performance of D&V and D&M are then evaluated in these challenging scenarios via ns-3 simulations.

Simulation Configuration

Our main studied simulation scenario is a four-leg intersection, shown in 5.2. The main reasons for selecting an intersection scenario are: 1) Wi-Fi deployment is commonly seen in an urban intersection; 2) communications between DSRC devices in two perpendicular roads can be non-line-of-sight (NLOS). Comparing to line-of-sight (LOS) communications, the signal strength for NLOS is normally lower at the same transmitter and receiver distance, leading NLOS communications more vulnerable to interference signals [74, 75]. Specifically, in this studied intersection, we assume that one large building is located at each intersection corner and each DSRC device is mounted on

one car. Two DSRC devices are placed in two perpendicular roads of the intersection. The position and traffic volume of each Wi-Fi device are carefully configured in order to create near-worst scenarios.

Scenario 1: Pre-Detection with Wi-Fi device 1;
Scenario 2: Post-Detection with Wi-Fi device 2 and Wi-Fi device 3
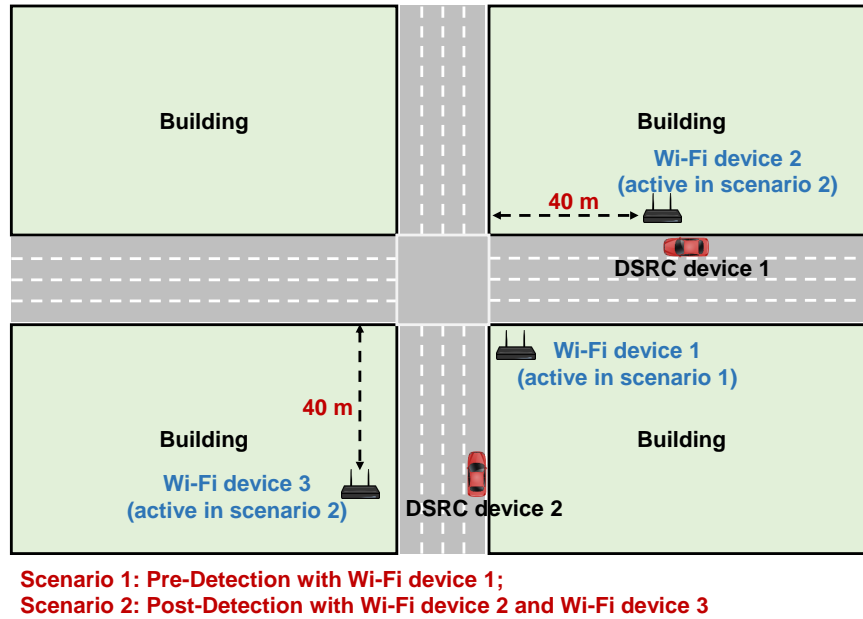
Figure 5.2: The simulation scenarios at an intersection: Wi-Fi device with red color for pre-detection analysis, with green color for post-detection analysis

We rely on network simulations to verify the theoretical observations and evaluate the performance of the proposed mechanisms. The key simulation parameters used in our simulations are listed in Table 5.3.

Evaluation Metrics

We primarily use following two metrics to evaluate the impact of Wi-Fi transmissions on the DSRC performance:

- The first contact distance to the intersection center is defined as at which distance to the intersection center, the two DSRC devices start to receive packets from each other. Generally, a larger first contact distance is preferred, since it gives more time for two cars to take any necessary actions to prevent collision.

- The DSRC PER in post-detection phase. This evaluate how well a Wi-Fi device can provide protection to DSRC transmissions after it detects the presence of

Table 5.3: Simulation configurations

Configuration items	Values
Network simulator	ns-3.25
DSRC transmit power	20 dBm
Wi-Fi transmit power	20 dBm
DSRC transmit rate	2.5 Hz
Wi-Fi transmit rate	saturate mode (packets always ready to be sent)
DSRC transmit duration	0.5 ms
Wi-Fi transmit duration	limited by maximum TxOp
DSRC detector detection threshold	-85 dBm
DSRC device decoding threshold	-92 dBm
Wi-Fi ED threshold	-62 dBm
DSRC ED threshold	-65 dBm
DSRC to/from DSRC propagation model	VirtualSource11p [7]
Wi-Fi to/from DSRC propagation model	IEEE P802.11 TGn [76] with 15dB signal attenuation per wall

DSRC devices. Ideally, once the DSRC devices are detected by the Wi-Fi devices, the DSRC devices are expected to perform as well as no Wi-Fi devices sharing the band.

5.3.2 Analysis of Pre-detection Phase

We explore in this section the challenges for Wi-Fi devices to detect the presence of DSRC devices. We show that interference from a Wi-Fi device's transmission prevents its DSRC detector from working until the transmission completes. This observation leads to identification of a near-worst setting for D&V and D&M by making a Wi-Fi device transmit with a saturated load, i.e., the Wi-Fi device always has a packet to be sent.

Figure 5.3: Wi-Fi transmission sequence

Challenge: Self-interference on DSRC Detector

A DSRC detector, upon detecting a DSRC transmission, will report a channel busy event to the host Wi-Fi device. However, this detection can only occur at moments when no transmissions from the host Wi-Fi device. This is mainly because the resultant self interference prevents any incoming DSRC preamble from being decoded at the DSRC detector. Fig. 5.3 shows an example channel access time-line for a Wi-Fi device. We can see that a Wi-Fi device releases the channel for a Short Interframe Space ("SIFS") after it finishes one transmission. If an acknowledgement (ACK) is received successfully, the Wi-Fi device will start an idle interframe period, consisting of an Arbitration Interframe Space (AIFS) and a backoff time period whose length is random within a certain range, before it can send another packet. The length of the AIFS and the backoff time period is controlled by the EDCA parameters, i.e., AIFSN and CW_{min}, respectively. The "No-packet" period in the figure represents the time duration when the Wi-Fi device has no packets ready to be sent and the device keeps idle. In this example, if we further assume that the signal strength of the ACK packet is strong enough to interfere with the detection of DSRC transmissions, the probability for a DSRC transmission to be detected then equals to the probability that the arrival time of DSRC packets falls into any of "SIFS", "AIFS", "Backoff" and "No-packet" periods, i.e., the periods when the Wi-Fi devices are not transmitting. We define sum of the four periods as an idle period. Therefore, the expected DSRC detection probability can be estimated as

$$Prob_{detection} = \frac{idle\ period}{idle\ period + WiFi\ Tx\ duration} \tag{5.1}$$

Near-worst Case Study

The above analysis shows a way to identify a near-worst case for detecting DSRC transmissions. That is to reduce the length of "No-packet" period to zero, or, in other words, to make a Wi-Fi device transmit in saturation. With the default Wi-Fi channel access parameters (AIFS = 43 μs, the average length of the backoff duration = 67.5 μs and the length of an ACK = 44μs) and 2 ms Wi-Fi transmission duration, a DSRC

preamble can be detected, on average, with a probability of only 5% in a near-worst case.

One implicit assumption behind this 5% detection probability is that the arrival time of DSRC packets at a DSRC detector is independent of the host Wi-Fi device's transmission timing. This assumption is valid in this study because the interval between two consecutive DSRC transmissions is a few hundreds of milliseconds. It is long enough to witness many Wi-Fi transmissions with a 2ms-duration. The backoff period with a random length can randomize the Wi-Fi transmission phase at which a DSRC packet arrives. With this observation, we model the DSRC detection as a Bernoulli experiment, whose trial is consider successful when a DSRC transmission is detected by the Wi-Fi device. Given our analysis setting, the probability of a successful trial, noted by p, is 5%. With this model, we can then calculate the number of trails to the first successful one, noted by n, i.e., with $n-1$ failures, the trial n is successful. The expected value of n is defined by $\frac{1}{p}$. Given $p = 5\%$, the expected value of n is 20, which means about 20 DSRC transmissions are required before one DSRC transmission can be detected by the Wi-Fi device.

To validate the above assumptions, the identified near-worst case is also created in the ns-3 simulator where two DSRC devices in Fig. 5.2 remain static, each 25 m away from the stop line. Only one Wi-Fi device is generating Wi-Fi traffic and it is located close to the intersection box, see Wi-Fi device 1 in Fig. 5.2. As a car is approaching to the intersection box, its collision risk with another car in the perpendicular road is growing and thus the communication between the two cars becomes increasingly important. Comparing to a Wi-Fi device located far from the intersection box, Wi-Fi device 1, which is located near to the intersection box, has higher potential to interfere with the transmissions from two DSRC devices and consequently results in more severe threats to driving safety.

Fig. 5.4a shows that the average number of DSRC transmissions to the first detection for D&V and D&M is similar since they share the same detection phase. However, both mechanisms require about 20 DSRC transmissions before a successful DSRC detection. The simulation results agree the theoretical analysis, indicating our modeling

assumptions are valid.

Adding an Additional Idle Period

Without a fast and effective DSRC detection, many DSRC packets can collide with Wi-Fi packets, resulting in significant performance degradation of DSRC systems. We argue that an average of 20 DSRC transmissions may impose too long detection delay. However, we have observed that by adding an additional idle period to the Wi-Fi interframe idle periods, the detection performance can be largely improved. Fig 5.4b shows the results of the simulation where we experimentally add 266 μs at the end of an AIFS period (The value of 266 μs has been introduced in [77]). Then, the expected number of DSRC transmissions to the first detection decreases to 4. Given the significant improvement, D&V has incorporated this idea into its recent design [70].
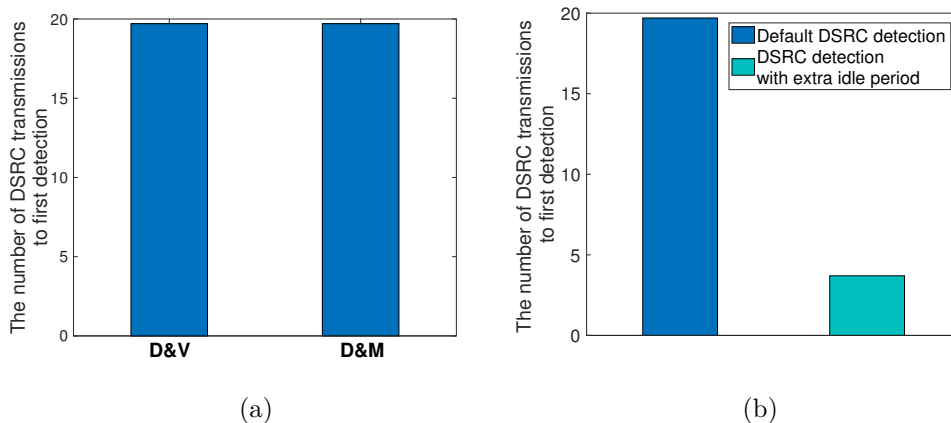
Figure 5.4: The average number of DSRC transmissions to the first detection with Wi-Fi transmission duration as 2 ms (a) D&V v.s. D&M; (b) with v.s. without extra idle period

Performance Evaluation in a Mobile Scenario

The detection performance of D&V and D&M with saturated Wi-Fi traffic is also studied in a mobile scenario, where two DSRC devices in Fig. 5.2 are moving at speed 10 m/s towards the intersection center from 200 m away. Note that in order to create a car collision threat, we set two cars move symmetrically. Fig. 5.5a and Fig. 5.5b depict the distribution of the first DSRC contact distance to the intersection center

with two DSRC signal propagation conditions. From Fig. 5.5a, it can be observed that without Wi-Fi traffic, the two DSRC devices can communicate with each other before they are 65 m away from the intersection center. However, with Wi-Fi traffic, it is possible that until 30 m away from the intersection center, the two DSRC devices talk to each other at the first time. A similar trend is also shown in Fig. 5.5b, except in this harsher DSRC propagation environment, DSRC devices have to be closer before they can communicate. Therefore, even without Wi-Fi traffic, the minimum value of the first contact distance decreases to 50 m. However, with Wi-Fi traffic, the two DSRC devices have to be only 20 m away from the intersection center before they can talk to each other at the first time.
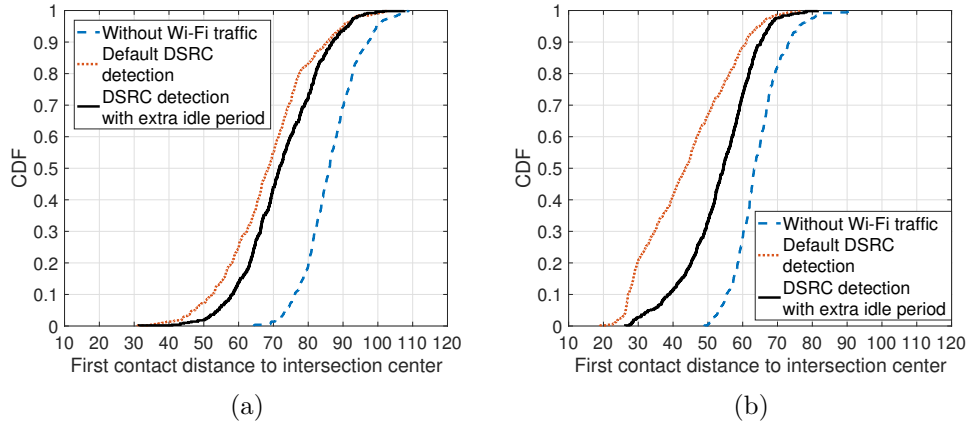
Figure 5.5: The CDF of DSRC first contact distance to the intersection center: (a) typical signal propagation environment for DSRC links [7]; (b) harsher signal propagation environment for DSRC links

Comparing Fig. 5.5a with Fig. 5.5b, we notice that the effect of adding an additional idle period is sensitive to the DSRC propagation conditions. A harsher propagation environment (Fig. 5.5b) shows a more significant gain than a typical propagation environment (Fig. 5.5a), e.g., in Fig. 5.5b, the probability of the first contact distance at 50 m increases from 30% to 70%. While in Fig. 5.5a, the gain is less than 10%. We believe the main reason for such a difference is: 1) adding an addtional idle period is expected to primarily improve the DSRC detection performance; 2) in a less harsh DSRC signal propagation environment, the signal strength of a DSRC link may be strong enough to overcome the interference from Wi-Fi transmissions, which means even with less

effective DSRC detection, the first contact between DSRC devices has chances to be established; 3) in a harsher DSRC signal propagation environment, the DSRC link is more vulnerable to the interference, such that in this environment, the first contact of DSRC devices depends more on successful DSRC detection where adding additional idle period is comparatively more useful. The DSRC signal propagation at an intersection relies heavily on the building configurations at the corner. Several harsh propagation environments have been reported in field experiments [75].

5.3.3   Analysis of Post-detection Phase

In this section, we identify the challenges for Wi-Fi devices to protect DSRC transmissions after they detect the presence of DSRC devices. We show that due to lack of mutual detection, D&M can cause extra packet losses in DSRC transmissions, while D&V requires Wi-Fi devices to leave the band, minimizing its packet on DSRC performance.

Challenge: Unilateral Hidden Terminal

Wi-Fi devices use the carrier sense mechanism for DSRC detection via the integrated DSRC detector. However, DSRC devices can sense Wi-Fi transmissions only through the energy detection mechanism. Given the higher threshold for the ED mechanism (see Table 5.1), in many cases, DSRC devices may not be able to sense and defer to Wi-Fi transmissions. This leads to a unilateral hidden terminal problem. As an example shown in Fig. 5.6, DSRC device 2 generates a new packet and the packet is ready to be sent before a Wi-Fi transmission completes. Since there is no other ongoing DSRC transmissions and the Wi-Fi signal is not strong enough to be detected through the ED mechanism, DSRC device 2 may consider the channel idle and then start its transmission, leading to a packet collision between DSRC device 2 and the Wi-Fi device. As a result, DSRC device 1 will not be able to successfully decode the packets from DSRC device 2. Until DSRC device 2 becomes close enough to the Wi-Fi device, i.e., when the ED detection becomes available, DSRC device 2 then starts to defer to the Wi-Fi transmissions.
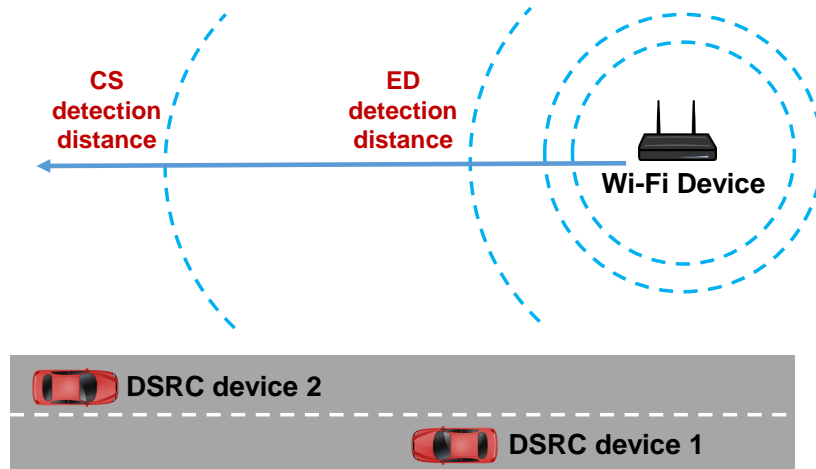
Figure 5.6: An illustration of the unilateral hidden terminal problem

Near-worst Case Study

D&V and D&M suffer from the unilateral hidden terminal problem in different levels. D&V leaves the spectrum upon detecting DSRC transmissions for several seconds. Therefore, after a successful detection, the Wi-Fi device will not affect the DSRC transmissions afterwards. On the other hand, D&M tries to squeeze Wi-Fi transmissions between DSRC transmissions after detecting DSRC transmissions. For the post-detection phase, we focus on the analysis of D&M. Considering the same example in Fig. 5.6, transmissions from DSRC device 2 may collide with transmissions from the Wi-Fi device due to the unilateral hidden terminal problem, and it is expected that *a) a longer Wi-Fi transmission duration would lead to a higher packet collision probability; b) shorter Wi-Fi interframe idle periods would also result in a higher packet collision probability.* According to the EDCA parameters of D&M for the post-detection phased in Table 5.2, the minimum Wi-Fi interframe idle periods are 18.72 ms, 9.32 ms, and 4.65 ms for AC_BE, AC_VI and AC_VO, respectively. The Wi-Fi transmission duration is limited by the defined "Max TxOp", which are 2.2 ms, 3.0 ms, and 1.5 ms for AC_BE, AC_VI and AC_VO, respectively. With these configurations, the collision probability between Wi-Fi transmissions and DSRC transmissions can be estimated based on the ratio of the Wi-Fi transmission duration to the total Wi-Fi transmission cycle (the transmission duration plus the interframe idle duration). The results are

11% for AC_BE, 24.3% for AC_VI and 24.4% for AC_VO. The calculation is based on two assumptions: 1) Wi-Fi traffic is saturated. Therefore, besides AIFS and backoff time, no other significant idle time duration between two Wi-Fi transmissions; 2) The transmission timing of Wi-Fi packets and DSRC packets is independent, i.e., when a Wi-Fi transmission occurs is independent of when a DSRC transmission starts. The calculated results identify the near-worst case occurs when AC_VO is use.

We validate the aforementioned theoretical analysis via the ns-3 simulations. The studied scenario is: two DSRC devices in Fig. 5.2 remain stationary and each one is 40 m away from the stop line. two Wi-Fi devices are located 40 m away from the stop line, see Wi-Fi device 2 and 3 labeled by "active in scenario 2" in Fig. 5.2. With this configuration, two unilateral hidden terminal pairs are created, i.e., Wi-Fi device 2—DSRC device 2 and Wi-Fi device 3—DSRC device 1. This simulation setting also ensures Wi-Fi device 2 and 3 are incapable of communicating with each other due to strong signal attenuation through walls.

Fig. 5.7a shows the PER of DSRC device 1 for different Wi-Fi ACs. It is observed that without any Wi-Fi traffic, the packet loss for the link from DSRC device 2 to DSRC device 1 is about 0.2% only. However, 11.52% extra packet loss is introduced by the Wi-Fi transmissions when AC_BE is used. The value is increased to 25.98% and 28.22% for AC_VI and AC_VO, respectively. There is a noticeable difference between the theoretical analysis and the simulation results for AC_VI and AC_VO (recall that the theoretical results are 24.3% for AC_VI and 24.4% for AC_VO). It is because a weak temporal correlation exists between DSRC transmissions and Wi-Fi transmissions since they are both periodic transmissions. The periodicity of DSRC transmissions is obvious. However, the periodicity of Wi-Fi transmissions is primarily because: 1) the Wi-Fi device always has a packet ready to be sent. Therefore, once a transmission opportunity is available to the Wi-Fi device, the packet will be sent out; 2) the transmission opportunity of D&M in the post-detection phase is dominated by the increased EDCA parameters and it occurs periodically. This temporal correlation violates one of our assumptions, causing slightly mismatch to the theoretical analysis results. Given smaller contention window sizes used in AC_VI and AC_VO, the temporal correlation

becomes stronger since less randomization between Wi-Fi transmissions is available for breaking the correlation.

One may argue that the traffic load for AC_VO and AC_VI is normally not high enough to saturate the channel. Therefore, this near-worst case primarily caused by saturated Wi-Fi traffic rarely occurs. However, we find that in the post-detection phase, the adjusted EDCA parameters by D&M becomes the dominating component that limits the Wi-Fi traffic volume on the channel. As shown in Fig. 5.7b, although only 20% of the saturated Wi-Fi traffic is generated by the device, the resulting PER is similar as that the saturated traffic can produce. This is because in both cases, the actual Wi-Fi traffic volume on the channel is similar.
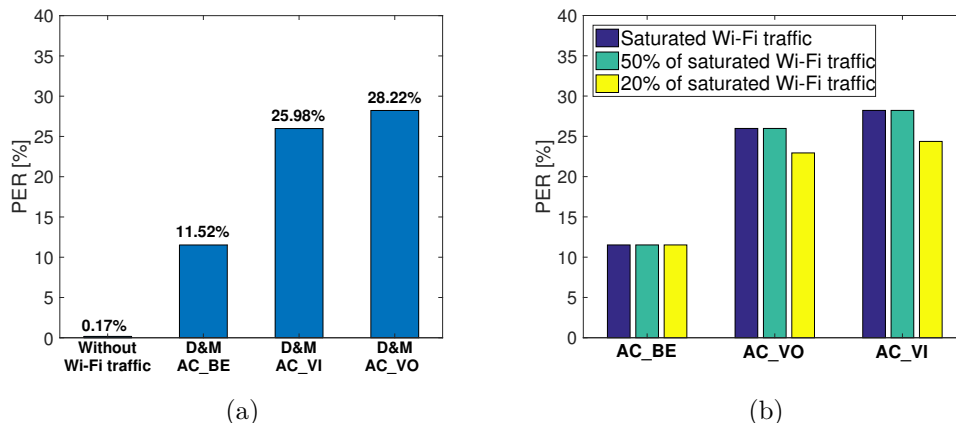
Figure 5.7: The post-detection PER of DSRC device 1 in Fig. 5.2 (a) different EDCA categories; (b) different traffic volume

Performance Evaluation in a Mobile Scenario

We have identified that the near-worst case of packet loss introduced by Wi-Fi transmissions to DSRC transmissions occurs when the Wi-Fi devices use the AC_VO category. In this subsection, we focus on studying the performance of this near-worst case in a mobile scenario. The simulated scenario is similar to the previous DSRC stationary scenario, except two DSRC devices in Fig. 5.2 are now moving towards the intersection center from 200 m away at speed 10 m/s.

Fig. 5.8a and Fig. 5.8b depict the PER of DSRC transmissions at different distances

to the intersection center with different DSRC signal propagation conditions. It is observed from both figures that at a short distance (e.g., < 25 m) or a large distance (e.g., > 85 m), the performance difference between with and without Wi-Fi traffic is not noticeable. It is because at short distances, the signal strength between the two DSRC device is strong enough to overcome the interference from the Wi-Fi device. However, even though at such short distances the DSRC devices can communicate with each other with a low packet loss rate, we argue that 25 m to the intersection center may be too short for drivers to take necessary actions to prevent car collisions. At large distances, the packet loss is dominated by the propagation loss, such that the extra packet loss introduced by the Wi-Fi traffic is not prominent in this case. However, at the distance range $25 - 75$ m, D&M introduces up to 30% extra packet loss to the DSRC transmissions. We believe this high extra packet loss can significantly degrade the DSRC performance. From Fig. 5.8b, we also observe that in a harsher propagation environment, the DSRC devices are required to be closer in order to overcome the interference from the Wi-Fi devices. And the propagation loss increases more dramatically, such at at a shorter distance (i.e., starting from 65 m) the signal propagation becomes the dominating factor for the packet loss.
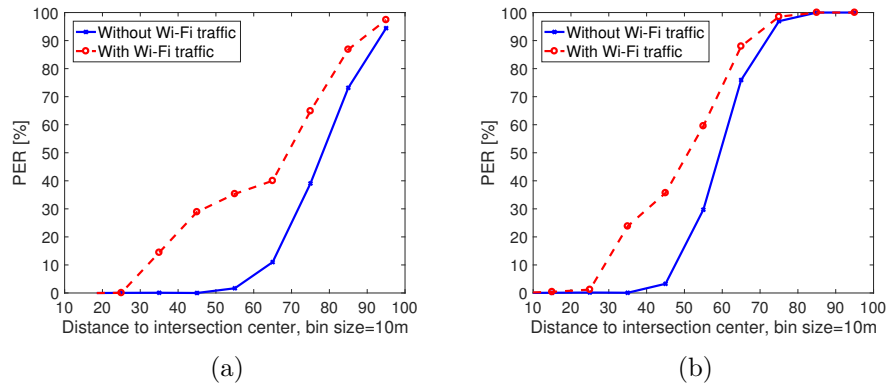
Figure 5.8: The PER of DSRC transmissions v.s. the distance of DSRC devices to intersection center: (a) typical signal propagation environment for DSRC links [7]; (b) harsher signal propagation environment for DSRC links

5.3.4   Discussion

In the previous sections, we have investigated the impact of Wi-Fi transmissions on DSRC performance in terms of the network layer metrics, e.g., PER. However, how network performance metrics can address application requirements and contribute to application performance remain challenging. To tackle the challenge, we utilize awareness, as proposed in [78], to link the DSRC network performance and the safety application performance. We believe awareness is an intermediate metric which is influenced by the network layer and understood by the application layer.
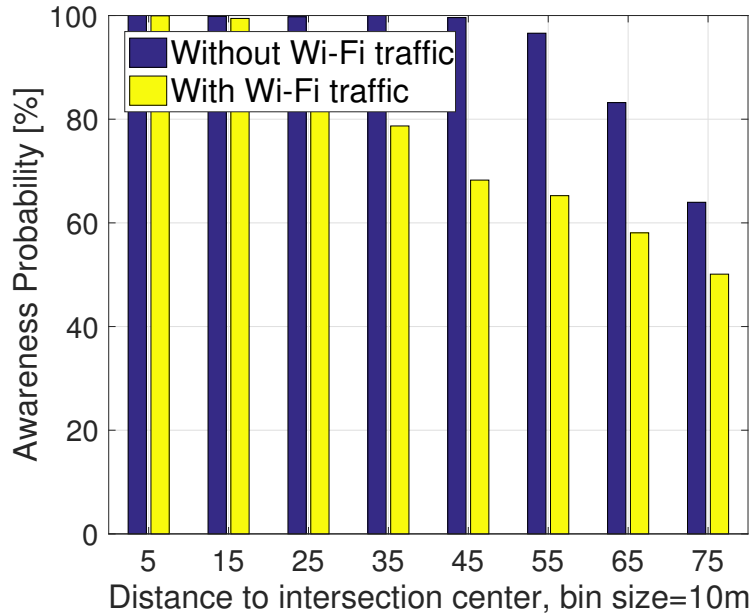
Figure 5.9: Awareness probability of D&M with AC_VO at different distances

In [78], the neighborhood awareness of a DSRC network is defined as at least n safety messages are successfully received during tolerance time window T, and the awareness probability is consequently expressed as a probability of vehicles being aware. A higher awareness probability indicates a vehicle has more chances of being aware of its neighboring vehicles and thus the safety applications which are built upon neighborhood awareness can operate with higher reliability.

To investigate how the presence of Wi-Fi traffic can change the awareness probability of DSRC networks and further affect the effectiveness of safety applications, we perform

an example study in the simulation scenario 2 described in Fig. 5.2 with two DSRC devices moving at 10 m/s. We focus on studying the post-detection performance of D&M. Different safety application may require different level of awareness, i.e., different n and T. In our study, we assume $n = 1$ and $T = 0.5s$, which matches the requirements of the collision avoidance application described in [78]. Fig. 5.9 shows the awareness probability of simulations with and without Wi-Fi traffic at different distances to the intersection center. The Wi-Fi devices operate in a typical propagation environment with traffic in AC_VO category. We can observe that the awareness probability is degraded when the Wi-Fi traffic is introduced into the network, especially at 45 m and 55 m, the awareness probability is reduced by more than 30%. If a safety application requires more than 90% awareness probability, the safety application may be no longer effective with the presence of Wi-Fi traffic at these distance bins.
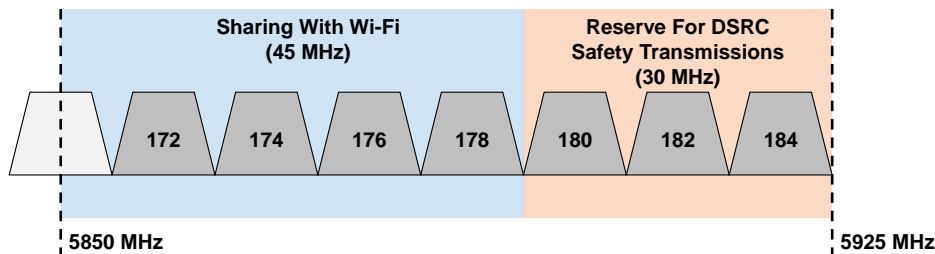
Figure 5.10: Illustration of the Re-channelization proposal for sharing the DSRC band between DSRC devices and Wi-Fi devices

5.4 Study of Re-channelization Mechanism

As illustrated in Fig. 5.10, the Re-channelization mechanism looks at reorganization of the DSRC band and channel usage plan. More specifically, it re-designates the seven channels, squeezing all safety-critical services that are currently spread out across all seven channels to the upper 30MHz of the band without acknowledging the possibility of severely elevated DSRC self-interference. In addition, the proposal aligns the lower 45MHz of the DSRC band with existing U-NII-3 Wi-Fi channels and requires DSRC to use two 20 MHz channels instead of four 10 MHz channels. The proponents of Re-channelization assert that by doing so, DSRC can achieve mutual detection with Wi-Fi (neglecting that mutual detection with non-Wi-Fi U-NII will not exist). In an recent

FCC filing[1], Broadcom suggested several possible Wi-Fi channel access priority modes for testing, as shown in Table 5.4. Each gives Wi-Fi a certain priority relative to DSRC.

Table 5.4: Wi-Fi operation modes in the Re-channelization proposal

Mode	CW_{min}	CW_{max}	**AIFSN**
Mode 1	15	1023	3
Mode 2	15	1023	6
Mode 3	31	1023	6
Mode 4	31	1023	8
Mode 5	31	1023	10

Simulation Study Configuration & Metric

We evaluate the impact of the Re-channelization proposal on the DSRC's performance via ns-3 network simulations. The main studied scenario is a four-leg intersection, as shown in Fig. 5.11. The motivation by using this scenario is two-fold: a) Wi-Fi exists within and/or near a building. Portable Wi-Fi devices may be used in vehicles. b) A pivotal set of safety critical scenarios addressed by DSRC, beyond the capability of other vehicle on-board sensors, is related to intersection where victims of a potential vehicle crash come from perpendicular streets. As a result, the simulation configuration in Fig. 2 represents a number of realistic scenarios where Wi-Fi and DSRC may encounter each other. Note that we may not use all the Wi-Fi devices in a particular simulation since we aim to uncover underlying technical characteristics for Re-channelization and a simpler Wi-Fi topology will facilitate this goal. Hence, further specification of usage of these Wi-Fi devices will be provided in corresponding sections to follow. Similarly, PER is selected as the primary metric to evaluate the impact of the Wi-Fi operation on the DSRC performance.

5.4.1   Cross-channel Interference from Wi-Fi to DSRC

Under Re-channelization, safety-critical DSRC services would move to channel 180, 182 and 184. There are many concerns over this migration idea which by analysis will cause

---

[1]FCC docket 13-49, Broadcom ex parte of April 6, 2017
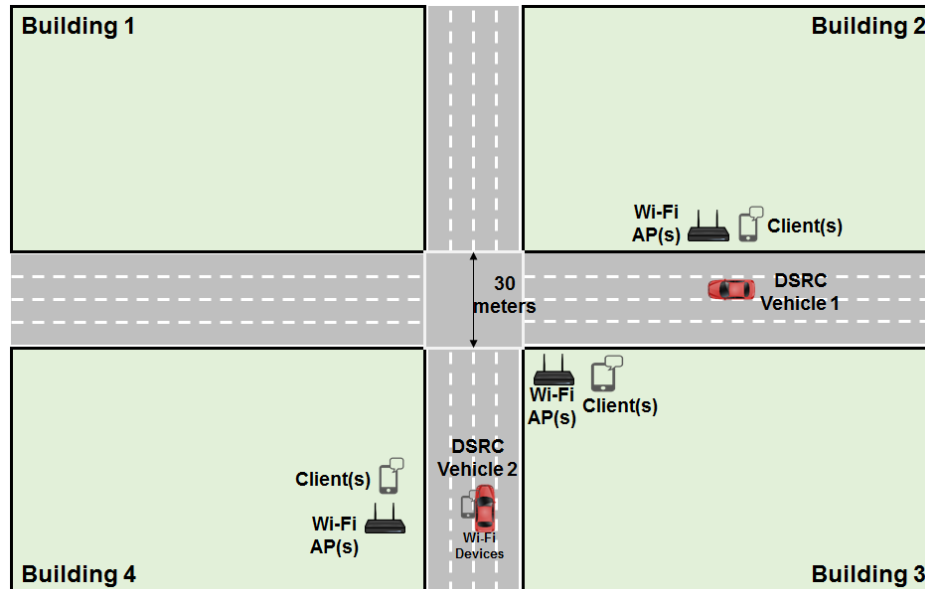
Figure 5.11: The primary simulation scenario of Re-channelization mechanism study

significant impact to DSRC safety communications [79] . The simulation in this section evaluates one of the concerns, which is the impact of cross-channel interference from Wi-Fi in the shared band on the quality of DSRC safety critical services replaced to channels 180, 182 and 184. The goal is to assess the magnitude of DSRC packet loss due to leaked energy from Wi-Fi transmissions in the shared band.

To set up the simulation, based on what is described in Section III we keep the Wi-Fi devices in vehicle 2 active and turn down the others in the scenario. The rationale behind such a configuration is that the cross-channel interference for vehicle 2 would be dominated by the transmissions of Wi-Fi devices in the vehicle since they are much closer to the DSRC radio. If negligible impact on DSRC performance is observed in this case, there should be a less of concern about Wi-Fi operations in the building. In this simulation, Wi-Fi exchanges data on channel 177 over a 20MHz channel width and DSRC uses channel 180 to send Basic Safety Messages per SAE J2945/1. Evaluation results for other Wi-Fi-DSRC channel choices are not included in the paper due to the space limitation.

We configure the mobility trace of vehicles to mimic one potentially leading to a T-bone accident. More specifically, the two vehicles move towards the intersection center

from the same distance on their respective streets with identical speed. They will meet at the intersection as if they were going to collide. Furthermore, we assume that vehicle 1 is the violator of traffic rules, e.g. by running a stop sign or ignoring a traffic light turning from yellow to red. We hope to see that vehicles 2, via BSMs of vehicle 1, can predict the potential of a vehicle crash.
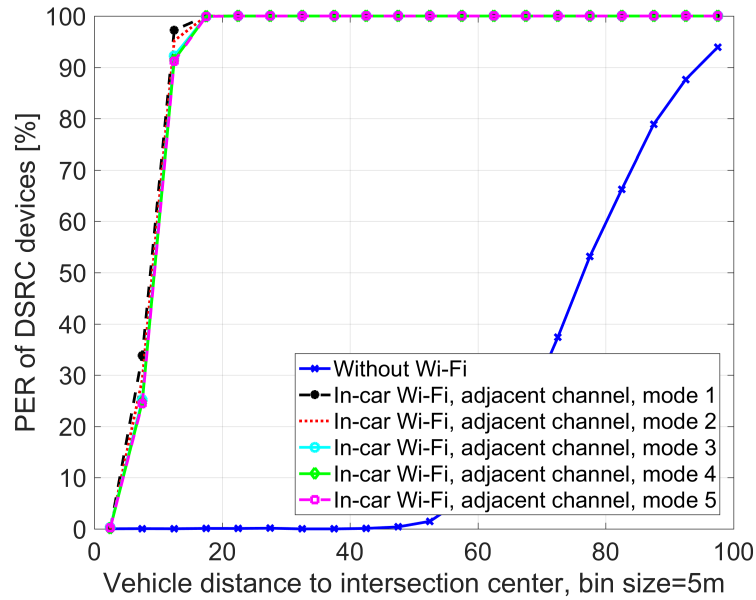
Figure 5.12: PER for vehicle 1's BSMs sent to vehicle 2, with/without Wi-Fi present on adjacent channels

Fig. 5.12 shows the packet reception performance for vehicle 1's BSMs at vehicle 2, with and without Wi-Fi operations. It is starkly clear that Wi-Fi usage causes devastating impact to DSRC performance. In particular, all BSMs from vehicle 1 are lost before the two vehicles proceed to around 15 meters away from the intersection center when Wi-Fi is enabled. Considering that the width of the intersection is 30 meters, this means that vehicle 2 is not aware of vehicle 1 until they become Line-Of-Sight (LOS), too late for vehicle 2 to take appropriate actions to avoid a collision. In contrast, without Wi-Fi there are plenty of chances for vehicle 2 to receive vehicle 1's BSMs that will facilitate vehicle 2 to infer the likelihood of a vehicular collision and plan accordingly.

The harmful impact as reflected in Fig. 5.12 is particularly concerning. It proves

that one fundamental assumption of the Re-channelization proposal, i.e., DSRC safety critical service would have a better communication environment after the migration to channel 180 and above, is not always true. Meanwhile, Fig. 5.12 suggests that the cross-channel interference significantly discounts the core value of DSRC for road safety, which is to expand drivers' awareness of the traffic situation from LOS to None Line-of-Sight (NLOS). It is shown that the NLOS communication performance of DSRC has largely degraded due to Wi-Fi sharing the adjacent channels.

One additional thing to note is that the impact on BSM communication perfor-mance by different EDCA options, suggested in Table 5.4, is very similar. This should be straightforward to understand since these EDCA modes intend to prioritize DSRC channel access in the shared band and have no consideration of cross-channel inter-ference. In the following section, we will evaluate their impact on the performance of DSRC transmissions carried out in the shared band.

5.4.2 Co-channel interference from Wi-Fi to DSRC

Another key point of the Re-channelization proposal is that it can enable mutual detec-tion between Wi-Fi and DSRC. The supporters of the proposal assert that this mutual detection will facilitate protection of DSRC traffic from harmful interference in the shared band. However, it needs to be recognized that this mutual detection assump-tion violates the spirit of technology neutrality. Any non-Wi-Fi U-NII technology (e.g, Long Term Evolution-Advanced) will not sense the presence of DSRC on the shared band like the CS mechanism enables for Wi-Fi devices. However, even in the context where Wi-Fi is the sole unlicensed technology in the shared band, we need to evaluate the level of protection the Re-channelization proposal provides for DSRC traffic.

Hidden Terminal

It is a well-known fact that hidden terminals degrade the performance of a communi-cation system. The hidden terminal problem, in one of its simplest forms, reflects a communication topology where two transmitter nodes without knowing the existence of the other are transmitting to the same receiving node. This is called mutual hidden. A

packet reception may fail if two transmitter nodes have their transmissions overlapped.

The hidden terminal problem is commonly observed in daily communication scenarios. In fact, the Wi-Fi community invented Request-to-Send and Clear-to-Send messages to mitigate the impact of the hidden terminal problem. However, these messages are not suitable for broadcast services. In addition, they may not be used even for unicast links because in Wireless Local Area Networks (WLAN), a receiver device may be much closer to its desired transmitter than to the hidden interfering nodes. In that case where a packet reception involves interference from the hidden nodes, the desired signal may be strong enough to overcome the interference, leading to a success packet reception.

Within the context of the Re-channelization proposal, Wi-Fi devices could well play as hidden terminals to DSRC transmissions due to signal attenuation caused by concrete walls and/or obstructing metal car body. To understand the impact of these hidden Wi-Fi devices on the performance of DSRC broadcasting services, we configure, in Fig. 5.11, a pair of Wi-Fi devices in Building 4 to be mutually hidden to the DSRC transmitter in vehicle 1. The other Wi-Fi devices are turned off in this evaluation.
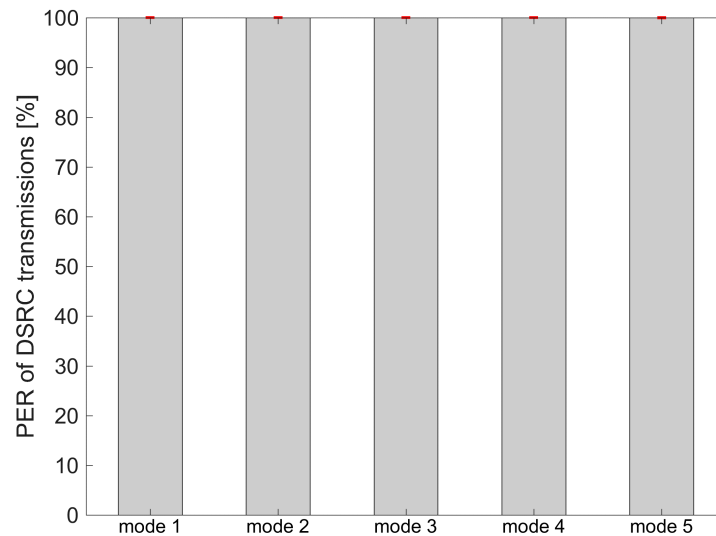
Figure 5.13: PER of vehicle 1's transmissions due to hidden terminal problem

Fig. 5.13 shows the PER of vehicle 1's packets at vehicle 2 (Both vehicles are stationary during the evaluation). Independent of the EDCA mode in Table 5.4, all of vehicle 1's transmissions failed. The reason is two-fold: a) Lack of mutual detection between the two technologies in this case makes the Wi-Fi interference always present at vehicle 2 (as listed in Table 2, Wi-Fi operates in saturation mode) when vehicle 1's transmissions occurs. b) Vehicle 2 is closer to Wi-Fi interferers than to vehicle 1. In a packet collision, the strength of a DSRC packet cannot overcome the stronger Wi-Fi interference.

Unfortunately, this second aspect of the reason is commonly seen for vehicular communications. More specifically, a sender vehicle and its receiver vehicles are often spread out across a space much wider than that for a WLAN where communicating nodes are constrained to a few meters. This topology difference leads receiver vehicles more likely (than Wi-Fi users in a WLAN) to observe hidden interfering source (e.g., Wi-Fi devices transmitting on the shared band) at a distance much closer than that to the desired transmitter. As an effort to illustrate the region in which hidden Wi-Fi devices may exist, we moved around the Wi-Fi devices in Fig. 5.11 to evaluate where signal strength of packets from vehicle 1 falls under the CS threshold of Wi-Fi, and vice versa. The results are plotted in Fig. 5.14. Note that to not over complicate the evaluation, we turned off the fading component in our channel models.

Fig. 5.14 plots several different zones, describing the mutual detection relationship between Wi-Fi devices and vehicle 1 when the former appear at different locations in the scenario. The first type of zone is called mutual hidden zone. It represents the set of locations at which appeared Wi-Fi devices are mutually hidden to the DSRC device in vehicle 1. Note that this zone only includes places from which Wi-Fi signal is strong enough to fail vehicle 1's packet reception at vehicle 2 during a packet collision. Other mutual hidden places are painted white since they are less interesting to the discussion. As we can see, the mutual hidden zone occupies a sizable portion of the scenario in Fig. 5.11, including places inside and outside the buildings. Wi-Fi devices present in this zone cause significant DSRC packet loss as shown in Fig. 5.13.

As we test different locations, we observe another set of places at which appeared
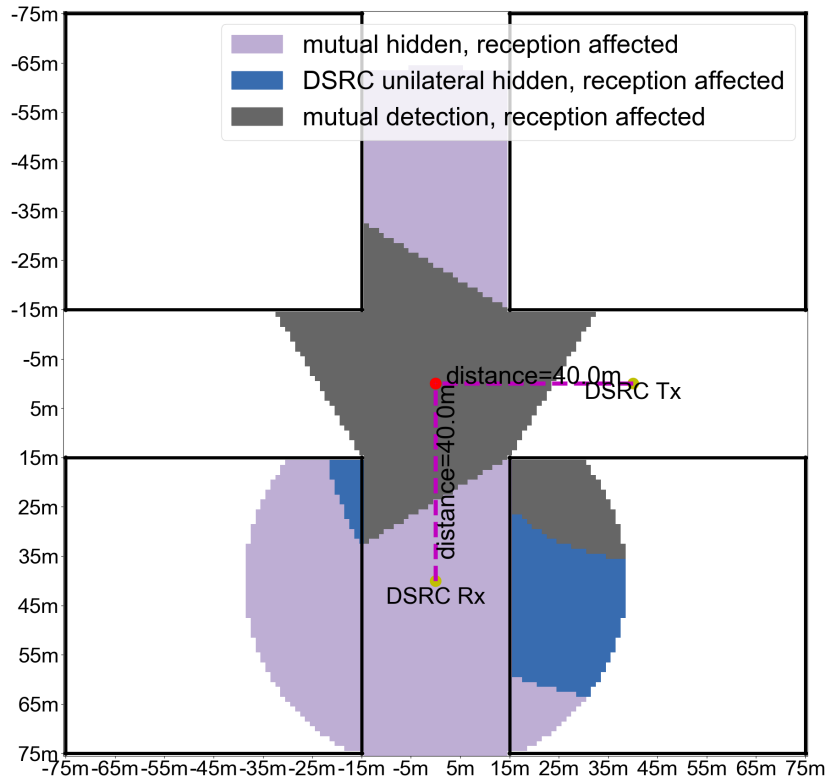
Figure 5.14: Potential impact regions on the DSRC performance with Wi-Fi device at various locations

Wi-Fi devices could not sense the transmission of vehicle 1 but the reverse is false. In other words, vehicle 1 could sense Wi-Fi activities. This happens because the CS mechanisms of the two technologies use different thresholds, -92dBm for DSRC and -82dBm for Wi-Fi. Such a mismatching provides a unique relationship among the two technologies which we call unilateral hidden terminal. From vehicle 2's perspective, this means that when Wi-Fi transmissions are on the air, vehicle 1 could sense them and defer its transmission according to CSMA. However, when vehicle 1 starts a transmission, the Wi-Fi devices will not sense that and therefore could potentially cause interference. In Fig. 6, we marked out a region where the unilateral hidden terminal exits as "DSRC unilateral hidden". Again, this region only includes places from which Wi-Fi transmission's signal is strong to fail a DSRC packet reception at vehicle 2 during a packet collision.

To understand the scale of impact of unilateral hidden terminal on DSRC performance, we leverage a pair of Wi-Fi devices in Building 3 in Fig. 5.11. We place them at a place in the building where they form a unilateral hidden terminal relationship with vehicle 1, and we turn off the other Wi-Fi devices in the scenario. Note that channel fading is re-adopted in the evaluation and both vehicles are stationary. The performance results are shown in Fig. 5.15. One can observe that unilateral hidden terminal leads to 100% PER for vehicle 1's transmissions, independent of the EDCA modes used, as in the case of mutual hidden terminal. The reason is that although vehicle 1 can adjust its transmission timing based on CSMA and Wi-Fi activities, Wi-Fi devices may continue usage of the channel since they are not aware of the presence of the DSRC device in vehicle 1.
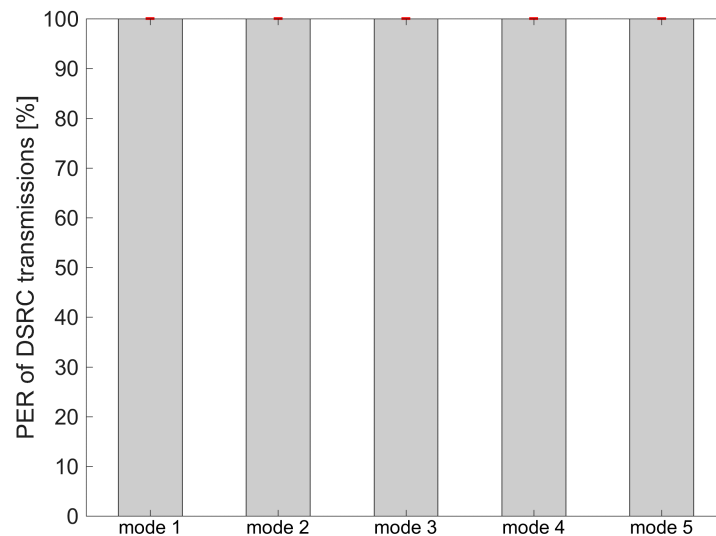
Figure 5.15: PER of vehicle 1's transmissions due to unilateral hidden terminal problem

The third type of zone in Fig. 5.14 is called mutual detection zone which means Wi-Fi devices, if present in the zone, could form a mutual detection with vehicle 1. This zone, as compared to others, is closer to the location of vehicle 1. We will evaluate in the next subsection if and how much of DSRC communication would be impacted.

Impact of mutual detection on DSRC communications

In this subsection, we will show that even the assumption of mutual detection between DSRC and Wi-Fi is able to achieve, the impact of Wi-Fi traffic on DSRC transmissions is not negligible. In the IEEE 802.11 based on MAC protocols, one key component to avoid packet collision is to let stations wait for a period of time before they can start a transmission. The length of the waiting time is randomly selected based on the EDCA parameter, Contention Window (CW). However, it is possible that different stations choose the same length of the waiting time. As a result, two stations start the transmissions at the same time, leading to a packet collision. We call this problem as countdown collision which may apply to coexistence of Wi-Fi and DSRC . For example, a Wi-Fi transmitter and a DSRC transmitter choose the same length of the waiting time after a channel busy period. The packet collision between DSRC and Wi-Fi may result in a packet loss at the DSRC receiver. Note that the probability of the packet collision increases with the Wi-Fi traffic load. Therefore, with the saturated Wi-Fi traffic, it is possible to create the near-worst case of the DSRC packet losses.

Our simulation employs some of the Wi-Fi devices in Building 3 to generate Wi-Fi traffic in the scenario. The devices (one Access Point (AP) and one user) are placed at a location inside the building where they can detect vehicle 1, and vice versa. Evaluation results are shown in Fig. 5.16. One can observe that as the less aggressive mode is applied (from mode 1 to mode 5, the level of aggressiveness of Wi-Fi channel access decreases), the impact of Wi-Fi traffic on DSRC transmissions is decreased. In addition, it can be noticed that the PER of DSRC transmissions is dramatically increased as the Wi-Fi devices switch from UDP traffic to TCP traffic. The main reason is that according to the TCP protocol, the transmitted data packets by the Wi-Fi AP will be acknowledged by the Wi-Fi client. These TCP ACK packets, as compared to UDP traffic, will compete for the channel access with DSRC and generate additional backoff countdown collisions with DSRC packets, leading to more packet losses.

We also evaluated the impact of different number of Wi-Fi users on DSRC's performance, as shown in Fig. 5.17. More specifically, we increased the number of Wi-Fi
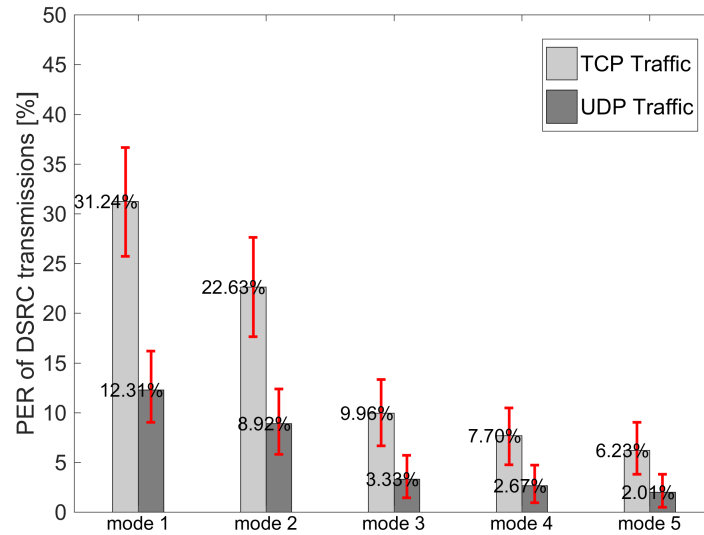
Figure 5.16: Packet loss of DSRC transmissions due to backoff countdown collisions between DSRC and Wi-Fi, TCP and UDP traffic

devices in Building 3 from one pair of AP and user to 4 pairs and adopted mode 2 in Table 1 as Wi-Fi's EDCA parameters. One can observe that as the number of AP-Client pairs increases, more and more DSRC packets are lost due to the packet collision. These packet losses as well as those in Fig. 5.16 show Wi-Fi cause harmful inference to DSRC operations even in contexts where mutual detection is achieved for both technologies.

5.5 Summary

In this chapter, we studied the performance of three mechanisms for sharing the ITS band between DSRC devices and Wi-Fi devices. The two mechanisms, D&V and D&M, are actively discussed in the European standardization group for possible deployment. Different from D&V and D&M, Re-channelization requires fundamental changes to the current DSRC channelization scheme and it is planed to be deployed in the U.S.

For D&V and D&M, we identify that the Wi-Fi devices may suffer from strong self-interference, leading to a delayed detection of the presence of the DSRC devices in both mechanisms. However, by adding an extra idle period to the Wi-Fi inter-frame space, the performance of the DSRC detection can be significantly improved. After
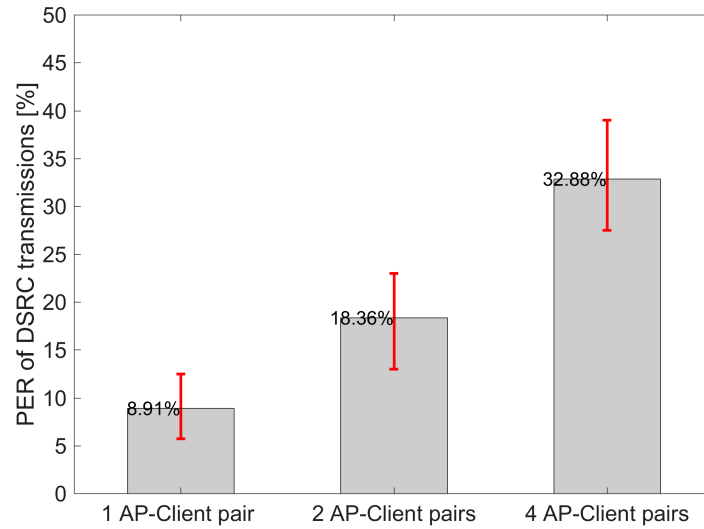
Figure 5.17: Packet loss of DSRC transmissions due to backoff countdown collisions between DSRC and Wi-Fi for the Re-channelization mode 2 with different numbers of AP-Client pairs, UDP traffic

detection, we observe that D&M can introduce more than 30% extra DSRC packet loss in certain cases, compared to none for D&V, which appears undesirable. We also observe that the degraded network performance could further affect the effectiveness of safety applications that are built upon V2V communications, e.g., in our example study, the extra DSRC packet loss introduced by the Wi-Fi traffic can cause up to 30% decrease in the neighboring vehicle awareness probability. Such a large decrease in awareness may lead to failures of many safety applications. One key observation is that even though DSRC and Wi-Fi use similar medium access control mechanisms, this mechanism is less effective when these technologies operate over different bandwidths (10MHz in DSRC and 20+MHz for Wi-Fi). Devices are not able to perform mutual preamble detection for carrier sensing, which leads to less effective channel access decisions. This explains the lower performance of the D&M mechanism, whose mitigation strategy appears to assume mutual detection.

For Re-channelization, we showed that Wi-Fi transmissions, if sharing DSRC band, could harmfully impact safety-critical DSRC transmissions in channels 180, 182, and 184, due to cross-channel interference. Our study proves the claims of Re-channelization

proponents that those three channels will be interference-free from Wi-Fi operations are false. The second question we investigated is if the mutual detection between DSRC and Wi-Fi claimed by Re-channelization proponents protects DSRC from harmful interference. Our study shows that in many scenarios DSRC and Wi-Fi devices will suffer from mutual and unilateral hidden terminal problems, which means that the claimed benefits of mutual detection will not generally be realized. Furthermore, even in an ideal scenario where no hidden terminals are present, backoff countdown collisions that are inherent to the IEEE 802.11 MAC protocol can still lead to a noticeable amount of packet collisions between DSRC and Wi-Fi. We also note that TCP Wi-Fi traffic creates more interference than UDP Wi-Fi traffic.

Chapter 6

DSRC-assisted MmWave Sensor Data Sharing

In this chapter, we study a multi-technology and multi-band V2V scenario where DSRC and mmWave coexist on the same car. Due to its large bandwidth and high throughput, the mmWave communication technology is considered a promising solution for sharing a large volume of sensor data between vehicles. One intuitive strategy for mmWave to share sensor data is to let each vehicle broadcast its sensing information to nearby line-of-sight neighbors. However, due to the necessity of directional communications, these neighbors have to be contacted sequentially after the previous transmission ends and thus the transmission delay is sequentially increased. Furthermore, it is also a fact that the value of a mmWave transmitter's sensing information is different for different mmWave receivers. For example, a vehicle's sensor data is more useful for trailing vehicles to extend their perception range but is less useful for vehicles that are far ahead. Without considering the information usefulness, it is very likely that a vehicle can blindly schedule the less useful transmissions first and delay or even cancel the transmissions with more useful information. Therefore, we argue that simply broadcasting sensor data to neighboring vehicles without considering the usefulness of the shared sensor data is inefficient. We then propose an information usefulness-aware sensor data sharing mechanism that estimates the usefulness of a mmWave transmitter's sensing information to its intended receiver and prioritizes the scheduling of mmWave transmissions carrying more useful information. Via ns-3 simulations, we evaluate the performance of the proposed mechanism and compare it with a baseline approach using a simple broadcast strategy. The simulation results verify that our approach prioritizes the mmWave transmissions with high information usefulness scores and therefore efficiently improves the sensor data sharing efficiency by up to 50%.

6.1 Motivation

Thanks to the rapid development of recent technologies, driving has become increasingly automated. These automated vehicles primarily depend on its sensor data to make decisions and take actions. Therefore, the quality and quantity of sensing information about environments are essential for correct and safe vehicle control [80]. To collect high quality and quantity of sensing information, automated vehicles are equipped with different types of sensors, e.g., LIDAR, radar, and camera. The rich sensor information would significantly enhance the vehicle's perception capability.

However, even equipped with multiple sensors, automated vehicles still fundamentally perceive the environment from a single point of view. A major challenge associated with such a single point of view system is the limited sensing range. That is, sensors, like radars, LIDARs and cameras, can provide information only about objects within the line of sight (LOS) region of the sensors. Also, these sensors are only effective up to a certain distance, beyond which they cannot provide useful information any more. One solution to this challenge is collaborative perception. In a collaborative perception system, vehicles leverage the vehicle-to-vehicle communication (V2V) technology and share the sensing information between each other. With the shared sensing information from neighboring vehicles, a vehicle can extend its perception range to reveal hidden objects which were visually blocked or beyond the sensing range [81]. However, as listed in Table 6.1, each sensor can generate a large amount of data per second. Therefore, to share the sensor data in real-time, data rates of several megabytes per second for each user are required. Due to its large bandwidth, the millimeter wave (mmWave) communication technology is a promising solution to realize this high data rate requirement.

Table 6.1: The sensor data rates of automotive radar, camera and LIDAR [2]

Sensor Type	Data Rate
Radar	< 1 Mbps
Camera	$100 - 700$ Mbps for raw images, $10 - 90$ Mbps for compressed images
LIDAR	$10 - 100$ Mbps

One intuitive strategy using mmWave communications to share sensor data is simply allowing each vehicle to periodically broadcast its sensor data to its neighboring vehicles, as periodic Basic Safety Message broadcasting. However, the directional nature of mmWave communications inherently requires point-to-point transmissions such that the neighboring vehicles have to be contacted sequentially and therefore the transmission delay for the scheduled neighbors is sequentially increased [82]. Moreover, due to different relative positions, a mmWave transmitter's sensing information shows different values for different mmWave receivers. For example, vehicle A may be less interested in the sensor data of vehicles that are far behind it or multiple lanes away from it, since normally, the sensor data of these vehicles have a very limited contribution to vehicle A's perception accuracy and decision making. Thereby, blindly broadcasting sensing information without considering the information usefulness can lead a vehicle to schedule less useful information first and consequently delay or even cancel the transmissions carrying more useful information. Also, one physical event (such as the traffic condition of one road segment, an unexpected pedestrian crossing the intersection, etc.) may be already sensed by vehicle A's local sensors and other nearby vehicles. Simply broadcasting these observations would lead to duplication of sensor data, causing a significant waste of channel resources on sharing sensing information whose value is low to vehicle A. Therefore, efficient mmWave data sharing remains challenging.

The envisioned multi-band and multi-technology V2V scenarios provide opportunities to improve the efficiency of mmWave sensor data sharing. In [83, 84], the authors discussed the feasibility of exploiting out-of-band information, such as the periodic DSRC information, to reduce the mmWave transmission overhead. In this work, we further utilize the DSRC information to estimate the information usefulness. Specifically, for each vehicle, we define a Region-of-Interest (RoI) to quantify a vehicle's interest in the environment. With sufficient knowledge about a vehicle's RoI, the vehicle is expected to plan its future path better. The concept of information usefulness builds on top of RoI and it is to quantitatively evaluate the usefulness of a vehicle A's sensing information to another vehicle B in developing the knowledge of vehicle B's

RoI. Based on the information shared via DSRC, each vehicle can estimate the information usefulness for all possible mmWave transmitter-receiver pairs of its neighboring vehicles. Thereby, each vehicle can locally build a directed and weighted mmWave transmission graph with the neighboring mmWave transmitters/receivers as vertices, the directional mmWave links as edges and the information usefulness scores as edge weights. Moreover, since the transmission range of DSRC is typically much larger than that of mmWave, a group of mmWave neighbors can collect the same DSRC information and therefore build the same mmWave transmission graph. This virtually centralized graph can further facilitate the scheduling of mmWave transmissions by grouping the edges into non-conflict *compatible sets* and prioritizing the compatible sets with higher average usefulness scores. With such a mmWave transmission schedule, the spatial reuse is achieved by enabling the simultaneous transmissions of mmWave links in the same compatible set and the usefulness-awareness is realized by prioritizing transmissions according to their information usefulness scores.

We evaluate the proposed mechanism via ns-3 simulations, and the evaluation results indicate that the proposed mechanism can significantly improve the mmWave sensor data sharing efficiency by up to 50%, comparing to a mechanism using a simple broadcast strategy.

6.2 Background

Although DSRC enables basic message exchange between road users with a range of up to 1000 m (in near-ideal conditions), its data rates are normally as low as 2 - 6 Mbps, which are not sufficient for sharing large volumes of sensor data. Thanks to the large bandwidth channels in mmWave bands, mmWave is a promising candidate to realize the high data rates [85].

MmWave refers to the spectrum between 30 to 300 GHz. In these frequencies, channels can exploit a larger bandwidth. By combining the large bandwidth with advanced modulation techniques, mmWave significantly increases the data rates. As stated in the IEEE 802.11ad standard [86], mmWave can achieve up to 7 Gbps data

rates with 2.16 GHz of bandwidth in the unlicensed 60 GHz band. While achieving high data rates, mmWave communications are subject to severe propagation path-loss and are vulnerable to blockage. To overcome these effects, mmWave communications require a directional link between the transmitter and receiver. The directional link is achieved by using narrow beams with high antenna gains. These narrow beams are commonly formed by using a large number of small antennas at the transmitter and the receiver, and applying beamforming techniques. Due to its low complexity and cost, in this work, we assume mmWave devices are applying the analog beamforming. However, the analog beamforming also limits the mmWave operation to single-user transmissions, i.e., a mmWave transmitter can only contact one mmWave receiver in each transmission. Moreover, as the use of narrow beams, the beam alignment between the transmitter and the receiver is critical in mmWave communications. In the context of V2V, the beam alignment becomes even more challenging due to the high mobility of vehicles. However, as aforementioned, several works have considered using DSRC information from neighboring vehicles to reduce the beam alignment overhead. DSRC messages provide rich information such as the absolute position, velocity, and heading of vehicles. Using the information, a vehicle can deduce the relative position information of the neighboring vehicles and therefore speed up the beam alignment process. In this work, we also apply this DSRC-assisted beam alignment technique to establish mmWave communication links.

The width of narrow beams is a key factor affecting the transmission interference area. In many studies, this area is modeled as a cone-shaped area. As in Fig. 6.1, the beamwidth is defined by the sector angle γ and the cone depth is defined by the mmWave transmission range R.

6.3 Information Usefulness-aware Scheduling

The design goal of the information usefulness-aware scheduling is to utilize the frequently exchanged DSRC messages and estimate the information usefulness of mmWave transmissions. Then the transmissions carrying more useful information are scheduled with higher priorities. To achieve this goal, two sub-tasks need to be accomplished:
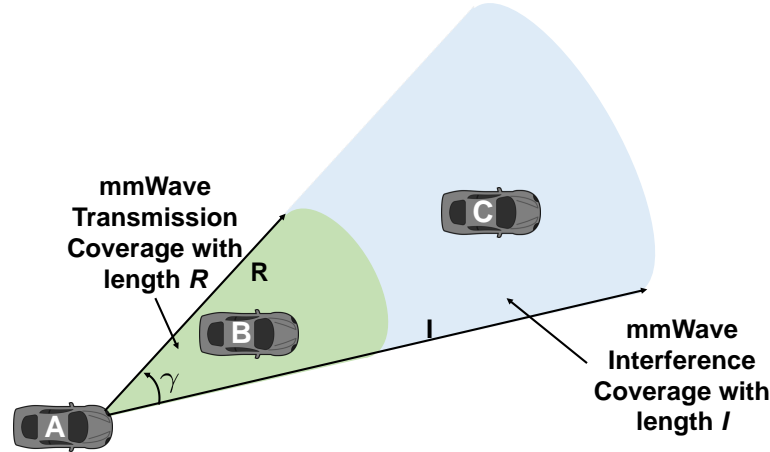
Figure 6.1: mmWave transmission coverage

1) quantitatively modeling the information usefulness; 2) efficiently prioritizing the transmissions considering both information usefulness and spatial reuse. For the first sub-task, we model the information usefulness based on the concepts of a vehicle's region-of-interest and region-of-detection as well as the age of information. For the second sub-task, we propose an algorithm which groups mmWave links into compatible sets and prioritizes the transmissions of links in these compatible sets sharing more useful information. The links in the same compatible set can be scheduled simultaneously, such that the proposed mechanism achieves both usefulness-awareness and spatial reuse. Before introducing the details of the proposed mechanism, we first describe the used assumptions and definitions.

6.3.1   Assumptions and Definitions

Assumptions

Following assumptions are made in the proposed information-awareness scheduling:

- Each vehicle is equipped with both DSRC and mmWave devices. Vehicles use DSRC to periodically broadcast its position, heading, moving speed, etc.

- It is assumed that immediate mmWave links are possible only when the mmWave transmitters and receivers are in LOS. As an example shown in Fig. 6.4, a mmWave link exists between vehicle A and vehicle B. But there are no mmWave links

between vehicle A and vehicle C since vehicle B blocks the LOS between them.

- On-board sensors take samples synchronously across different vehicles, such that a vehicle knows when the sensor data was generated at another vehicle.

- Each vehicle is aware of neighboring vehicles' interests in the environment. This can be achieved by pre-defining rules for building RoI for all vehicles or piggy-backing the information of a vehicle's perception interests in DSRC messages. We will present our model of RoI shortly.
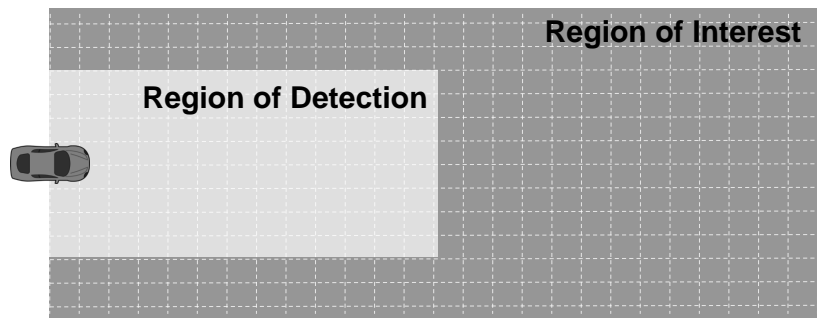
Figure 6.2: An illustration of a vehicle's region of interest and region of detection

Vehicle's Region of Interest and Region of Detection

For each vehicle, we define two regions: the region of interest and the region of detection. For a vehicle, it needs the knowledge about the region of interest (RoI) to take necessary actions in time and plan the future route. The vehicle's local sensor measurements can cover a part of the vehicle's RoI. This region is defined as the region of detection. In this study, we model the two regions as 2D rectangles, see Fig. 6.2 for an illustration. Further, both regions are discretized into small cells with the default cell size of $1m \times 1ml$. This leads to a straightforward representation of both regions as matrices with N_{RoI} rows, M_{RoI} columns for the region of interest, and N_{RoD} rows, M_{RoD} columns for the region of detection. If a vehicle receives a piece of fresh sensing information about a cell via either local sensor measurements or remote sensing information sharing, its knowledge about that cell is then updated. However, the value of the sensing information decreases as the age of information increases. To measure the

value of the sensing information, we define an *information score* as follows.

Definition 6.3.1. *Information score. For a cell at location (x, y) of vehicle k's RoI, the information score of that cell at time t is*

$$S_t^k(x, y) = e^{-\lambda \tau} \tag{6.1}$$

where τ is the age of information, which measures the elapsed time between the current time and the moment when the information was obtained. λ defines how fast the information score decreases with τ.

The information score transforms the unbounded age of information to a bounded value in the range of [0, 1]. This transformation facilitates the following calculation of the information usefulness. For different applications, information with the same age may present different values. In a more time-sensitive application, the usefulness of information may decreases faster as the age of information increases. In our model, we use different values of λ to capture the different application requirements. The information score of cells can be updated in two ways:

1. The sensing information of cells within a vehicle's RoD is primarily updated by local sensor measurements. Each vehicle updates its local sensor measurements periodically and accordingly updates the information scores of cells within the vehicle's RoD.

2. The sensing information of cells can also be updated by receiving the sensing information from remote vehicles. See Fig 6.3 as an example, vehicle B's RoD intersects with vehicle A's RoI. This indicates that the sensing information of vehicle B is helpful for updating the information scores of these cells within the intersection region of vehicle A's RoI and vehicle B's RoD. Let (x', y') represent a cell within the intersection region of vehicle A's RoI and vehicle B's RoD. $S_t^B(x', y')$ is the information score of cell (x', y') at vehicle B at time t. Similarly, $S_t^A(x', y')$ is the information score of the same cell at vehicle A at time t. By sharing the sensing information from vehicle B to vehicle A, $S_t^A(x', y')$ can be
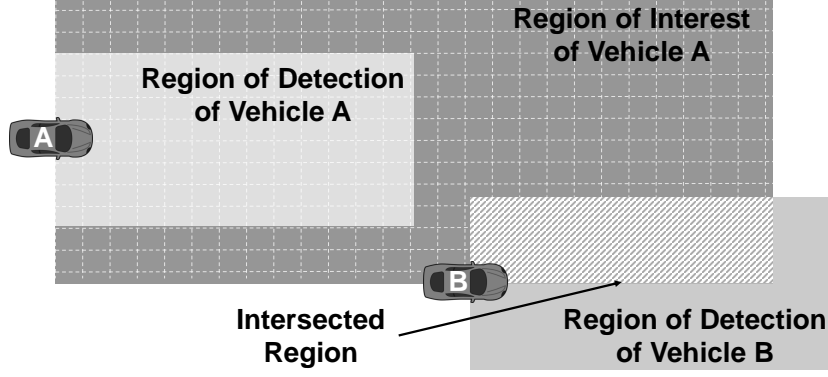
Figure 6.3: An example of updating information score in the region of interest

replaced by $S_t^B(x', y')$, if $S_t^B(x', y') > S_t^A(x', y')$. As a result, the information score of cell (x', y') at vehicle A is increased by

$$\Delta_t^{B \to A}(x', y') = S_t^B(x', y') - S_t^A(x', y')$$

Information Usefulness

Upon the updated information score of each cell in the intersection region, we define the information usefulness score of sharing sensing information from vehicle B to vehicle A as:

Definition 6.3.2. *Information usefulness score. The usefulness of vehicle B's sensing information to vehicle A is estimated by the sum of the updated information scores of all cells in the intersection region of vehicle A's RoI and vehicle B's RoD, i.e.,*

$$\text{Information Usefulness} = \sum_{(x', y') \in U_t^{AB}} \Delta_t^{B \to A}(x', y')$$

where $U_t^{AB} = RoI_A \cap RoD_B$ represents the intersection region of vehicle A's RoI and vehicle B's RoD.

Note if $RoI_A \cap RoD_B = 0$, i.e., vehicle A' RoI and vehicle B's RoD are not intersected, the information usefulness score is zero.

6.3.2 Information Usefulness-aware Scheduling Algorithm

The directional nature of mmWave communications also provides the opportunities of exploiting the significantly enhanced spatial reuse to improve the data sharing efficiency.

In this work, we first group mmWave links into compatible sets with considering the information usefulness scores and then schedule the concurrent transmissions to maximize both the spatial reuse and the information usefulness scores. A compatible set consists of mmWave links that can transmit packets simultaneously without interfering each other. Consider the example in Fig 6.4. mmWave link $A \rightarrow D$ and $B \rightarrow C$ are in the same compatible set since two links are mutually non-interfering. However, in the reversed direction, link $D \rightarrow A$ and $C \rightarrow B$ may not be compatible. It is because transmissions from vehicle C to vehicle B may interfere the receptions at vehicle A [87]. In this work, we conservatively assign link $D \rightarrow A$ and $C \rightarrow B$ to different compatible sets since vehicle A is within the interference range of vehicle C.
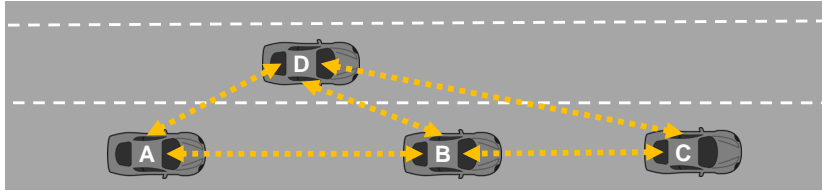
Figure 6.4: An example of mmWave links

To find a collection of compatible sets for all possible neighboring mmWave links, we consider this problem in the context of a directed and weighted graph, $G = (V, E)$, where E represents the set of mmWave links and V for the set of mmWave transmitters and receivers. An edge $e_{s,d}$ indicates that the transmitter of the corresponding mmWave link is vehicle s and its intended receiver is vehicle d. The weight of this edge, $w(e_{s,d})$, is defined as the information usefulness score of vehicle s's sensing information to vehicle d. Therefore, the problem of finding a collection of compatible sets is equivalent to finding a non-conflict partition of the edge set E, i.e., finding $\mathbf{S} = \{S_1, S_2, ..., S_k\}$ where $\bigcup_{i=1}^{k} S_i = E$. Here S_k corresponds to a compatible set, and $\mathbf{S}$ represents the collection of compatible sets. This problem can then be solved by the edge coloring. The edge coloring is a well-studied problem, while the conventional edge coloring does not typically take edge weights into consideration [88, 89]. In our model, the edge coloring is not only to find the minimum number of colors needed to color all edges but also to maximize the total weights of edges with the same color. The details of the proposed algorithm are described in Algorithm 3.

Algorithm 3 Search Compatible Sets Algorithm

1: **Input:** $G(V', E')$ ▷ V' is the set of vertices with the associated edges in E'. E' is a subset of $'E$, containing the remaining edges that haven been assigned to any compatible set in **S**

2: $w(E')$ ▷ The set of weight of edges in set E'

3: **Output: S**   ▷ The output of the algorithm is the collection of compatible sets

4: $E' = E$ ▷ Initialize E' to E, the set of all edges of $G(V, E)$

5: $\mathbf{S} = \emptyset$

6: **while** $E' \neq \emptyset$ **do**

7:      $e = \arg\max w(E')$ ▷ Pick e whose weight is the largest in E'

8:      **if** $w(e) > 0$ **then**

9:          **for** compatible set S_i in **S do**

10:             **if** e compatible with all edges in S_i **then**

11:                $S_i = S_i \cup e$

12:             **end if**

13:          **end for**

14:          **if** e is not assigned to any existing sets **then**

15:             $S_k = \{e\}$ ▷ Create a new compatible set for edge e

16:             $\mathbf{S} = \mathbf{S} \cup S_k$ ▷ Add the newly created set to **S**

17:          **end if**

18:          $E' = E' - e$

19:      **end if**

20: **end while**

In Algorithm 3, line 1-2 present the inputs of the algorithm: the first one is a graph $G(V', E')$, whose edges have not been included in the collection **S** yet and the second one is the weight of each edge in graph $G(V', E')$. The output of the algorithm is a collection of compatible sets, **S**. The edge set E', and the collection **S** are initialized in line 4 and 5. Line 6 - 15 are a loop to check every edge that has not been included in **S**. The edges are examined according to the decreasing order of their weights, i.e., the edge with a larger weight is examined first (line 7). In line 8, the algorithm first checks whether the weight of the selected edge is zero. A zero-weighted edge indicates that the transmitter of the corresponding mmWave link cannot help improve the environmental perception of the receiver. This is primarily because the transmitter's RoD does not overlap with the receiver's RoI. In line 9 - 11, the algorithm iterates each existing compatible set in **S** and checks whether the currently being examined edge, e, is compatible with any of these existing compatible sets. If such a compatible set exists, the edge e is then added to that set. Otherwise, the algorithm initializes a new compatible set for edge e (line

12-13). The collection **S** includes the newly created compatible set in line 14. After the examination, edge e is thus removed from the edge set E'. The loop repeats to examine the next edge.

After obtaining the collection of compatible sets, we rank these compatible sets according to their average information usefulness score. The transmissions are then scheduled following this order. In this way, the mmWave transmissions carrying more useful information are scheduled with higher priorities.

6.4 Information Usefulness-aware Scheduling Implementation

In this section, we discuss the details for each vehicle to implement the proposed information usefulness-aware scheduling. The implementation consists of three phases: 1) vehicles exchanging and collecting information via DSRC; 2) distributively determining a mmWave transmission schedule; 3) at the scheduled time slot, establishing the mmWave connection and transmitting the packets.
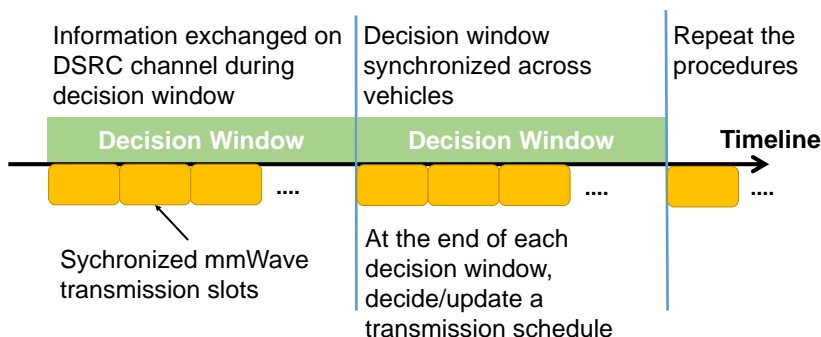
Figure 6.5: The procedure of sensing information sharing mechanism

6.4.1 Collecting Information via DSRC

Each vehicle periodically shares its driving status with neighboring vehicles. The driving status includes the vehicle's current position, heading, and moving speed, etc. Each vehicle collects the shared information of its neighboring vehicles within *decision windows*. The decision window is set to be synchronized across different vehicles [1]. In

---

[1] The synchronized time window can be realized by applying the GPS global timestamps

this way, the neighboring vehicles are expected to collect the information for the same period. The collected information is useful for the DSRC receiver to construct the DSRC transmitter's RoD and RoI. Additionally, if its RoI and RoD cannot be inferred directly, a vehicle can also include the description of its RoI and RoD in DSRC messages. Since the transmission frequency of DSRC is typically high (e.g., 10 times per second), vehicles are thus frequently updating their knowledge about each neighboring vehicle's RoI and RoD. With such knowledge, vehicles can further estimate the information usefulness of mmWave links.

6.4.2 Determining a MmWave Transmission Schedule

As depicted in Fig. 6.5, at the end of each decision window, each vehicle determines a schedule for the future mmWave transmissions based on the received DSRC information in the current decision window. Although the schedule is determined in a distributed manner, potential mmWave transmitters, receivers and their interferers utilize the same DSRC shared information to determine the mmWave transmission schedule, which makes the schedule is virtually centralized. This is primarily because the transmission range of DSRC is typically more than 500m in a highway scenario [90] and the transmission range of mmWave is only tens of meters (the measurements in [91, 92] suggest that the transmission range of mmWave is about 75m under the LOS condition with the transmission power as 30 dBm). The transmission range of DSRC is sufficiently large for a mmWave transmitter, its intended receiver and its interferers to be within the same transmission range.

To determine a usefulness-aware schedule, two steps are necessary: 1) constructing a mmWave transmission graph; 2) finding the collection of compatible sets in that constructed graph and deciding their scheduling orders.

Construct a MmWave Transmission Graph

Based on the collected information within the current decision window, a vehicle (called host vehicle) estimates direct mmWave links for all neighboring vehicles according to their relative positions. For a vehicle pair (v, u), the host vehicle examines whether

there are other vehicles blocking the LOS between vehicle v and u. In this checking process, the vehicles are considered a rectangle on a 2D plane. The size of the rectangle is adjusted according to the type of the vehicles. If the LOS of vehicle v and u is not violated and the distance between vehicle v and u is less than the mmWave transmission range (the default value of the mmWave transmission range is 75m), two mmWave links can be constructed, one starting from v to u and the other starting from u to v. The process is repeated until all the node pairs in the collected information have been examined. These direct mmWave links and their vertices then form a graph $G(V, E)$. Fig. 6.4 is an example of such a graph. Each vehicle constructs a mmWave transmission graph locally. As previously discussed, since they are spatially close to each other and within the same DSRC transmission range, vehicle A – vehicle D will generate the same graph like the one depicted in the figure.

Find a Collection of Compatible Sets and its Order

Taking the graph $G(V, E)$ from the previous step as input, each vehicle applies Algorithm 3 to generate a collection of compatible sets $\mathbf{S}$. The average weight of each compatible set is used as the index to rank the compatible sets in $\mathbf{S}$ in decreasing order. Following the ranking order, each compatible set is then allocated to one non-overlapping time slot after the current decision window. Since the decision window is synchronized across different vehicles, the time slots are, therefore, synchronized as well. We believe the synchronized time slots are easier for different vehicles to schedule and coordinate their transmissions.

6.4.3 Conduct MmWave Transmissions

With the determined transmission schedule, a mmWave transmitter and its intended receiver then know at which time slot to transmit and receive. When reaching the scheduled time slot, the mmWave transmitter and the receiver switch their beams and establish the connection. With the vehicle position information shared via DSRC, the mmWave transmitter and receiver would know the correct direction to point the beam to. Similar techniques have been applied and mentioned in [82, 83] to reduce the

mmWave's beam alignment overhead. Once the connection is established, the scheduled mmWave transmitter starts to transmit packets and the transmission lasts for one time slot. If the mmWave transmission fails, the receiver then broadcasts an acknowledgment to the neighboring vehicles via DSRC, such that nearby vehicles would know the sensing information of cells within the intersection region of the mmWave transmitter's RoD and the receiver's RoI has not been updated. This will be further taken into consideration when estimating the information usefulness score to this mmWave receiver in the following decision windows. If the mmWave transmission completes successfully, the received information is used to update the information score of the receiver's RoI. Without hearing any acknowledgment of the failed transmissions, the neighboring vehicle would assume the information score of the related cells has been updated.

The above procedures are repeated at the end of the next decision window. Based on the information collected in the new decision window, vehicles will update their mmWave transmission schedule. In this way, the vehicles can adapt their schedule to reflect the changes in the mmWave links.

6.5 Simulation Evaluation

In this section, we evaluate the performance of the proposed information usefulness-aware scheduling and compare it with a broadcast based approach proposed in [82] via ns-3 simulations.

6.5.1 Evaluation Scenario and Metrics

Simulation Configurations

We select a 2km highway as the main evaluation scenario, since the highway is a common driven scenario. Also, 2km is long enough to well-distribute the simulated cars and cover several times of the DSRC transmission range. In each direction, cars are moving in 6 lanes with speed in the range of 20 m/s to 25 m/s. The movement of these simulated cars is generated by the SUMO simulator [93]. The simulated cars are all passenger cars with width × length as 3m × 5m.

The DSRC module at each simulated car broadcasts DSRC messages every 100 ms with 20 dBm transmission power. The received power at DSRC receivers is calculated by using the propagation model proposed in [94]. The mmWave module at each car is implemented based on the models proposed in [95]. The directional antenna used in the mmWave module has 30 sectors, i.e., beamwidth=12° for each sector. We apply the model defined in [96] to calculate the signal propagation loss from the mmWave transmitter to its receiver. For the calculations in the information usefulness-aware scheduling, we set the mmWave transmission range as 75m and its interference range as 150m. The primary simulation configurations are summarized in Table 6.2.

Table 6.2: Simulation configurations

Parameters	Values
DSRC Tx power	20 dBm
DSRC Tx frequency	10 Hz
DSRC data rate	6 Mbps
DSRC packet size	340 Bytes
mmWave Tx power	30 dBm
mmWave data rate	693 Mbps
mmWave transmission slot	50 ms
mmWave beamwidth	12°
mmWave packet size	1500 Bytes
mmWave decision window	200 ms
Size of RoI	Width $\times$ Depth $= 36m \times 100m$
Size of RoD	Width $\times$ Depth $= 18m \times 50m$
simulation time	20 seconds

Evaluation Metric

A cell in a vehicle's RoI is considered *covered* at time t, if the age of information in that cell at time t is less than a pre-defined coverage threshold $\tau_{threshold}$. Further, we define the coverage ratio of a vehicle's RoI at time t as

$$Ratio_{coverage}(t) = \frac{N_{covered}(t)}{N_{ideal}(t)}$$

where $N_{covered}(t)$ is the number of cells that are currently being covered at time t. Given the positions of a vehicle and its neighboring vehicles, $N_{ideal}(t)$ represents the number of cells whose information score can be possibly updated via either the local sensor measurements or the remote sensor data sharing. Ideally, all N_{ideal} cells can be

covered at time t. However, due to the communication limitations, some cells may not be able to meet the coverage threshold. The coverage ratio reflects the impact of the communication limitations on the perception capability of a vehicle.

Baseline Approach

The mmWave transmission mechanism proposed in [82] is selected as the baseline approach in comparison with our usefulness-aware scheduling. It is because our approach and this baseline approach use the same DSRC-assisted method to align the mmWave beams and then establish the connections. However, the baseline approach simply broadcasts a vehicle's sensing information to its LOS neighbors without considering the usefulness of the shared sensing information. By comparing the baseline approach and our proposed approach, we can focus on studying the benefits of considering the information usefulness while scheduling the mmWave transmissions.

6.5.2 Consistency of MmWave Transmission Schedule

In the proposed information usefulness-aware scheduling, vehicles produce a mmWave transmission schedule in a distributed manner. But, since the DSRC information can be shared within a larger region, the mmWave transmitter, its intended receiver and interferers are expected to generate the same schedule. To verify this claim, we first simulate a specifically designed scenario where 20 cars are distributed in one lane with 60m as the separation distance between two adjacent cars. In this scenario, the useful sensing information is mostly shared from one car to its immediate trailing car, which simplifies the structure of the mmWave transmission graph.

Fig. 6.6 shows the average successful mmWave reception rate of different vehicles. One can observe that the successful rate of each vehicle's mmWave receptions is 100%, indicating that mmWave transmissions were scheduled without any conflicts or strong interference. This is mainly because a mmWave transmission's transmitter, receiver and interferers follow the same transmission schedule, which was generated based on the widely shared DSRC information.
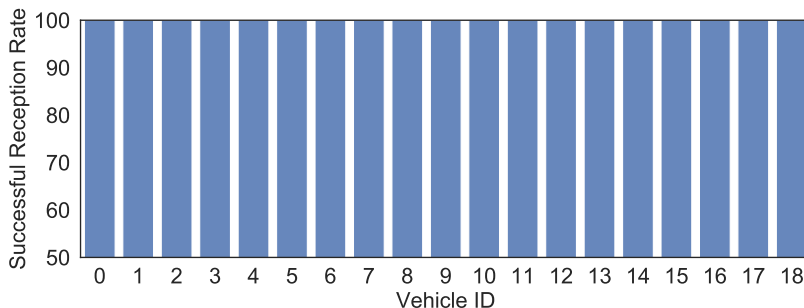
Figure 6.6: The average successful mmWave reception rate of different vehicles

6.5.3 Different Coverage Thresholds

Different applications could pose different requirements on the information freshness. We use the coverage threshold, $\tau_{threshold}$, to quantify the requirements on the information freshness. Only if the age of information of a cell is smaller than the threshold $\tau_{threshold}$, the sensing information of the cell is useful. Otherwise, it is outdated and less valuable. As previously mentioned, the requirements on the information freshess are also reflected on the decay rate λ in Eq. 6.1. For different values of $\tau_{threshold}$, the value of λ is adjusted according to $\lambda = \frac{log(T)}{-\tau_{threshold}}$ where T is arbitrarily set to 0.1 as an example in this evaluation. The rationale behind this setting is straightforward, i.e., when the age of information reaches to $\tau_{threshold}$, the corresponding information score is set to T.

In this subsection, we study the impact of different values of $\tau_{threshold}$ on the performance of the proposed mechanism. Fig. 6.7 depicted the average coverage ratio of 100 cars over time under the value of $\tau_{threshold}$ as 0.25, 0.5 and 1.0. Two curves, one for the baseline approach and the other one for the proposed approach, are presented in each subplot. For a specific time point, the width of each curve's shadow area represents the standard deviation of the coverage ratio across different cars. From Fig. 6.7, one can observe that the proposed approach achieves more than 90% coverage for the three thresholds and it outperforms the baseline approach by up to 32%. Also, it can be noticed that the results of the proposed approach show a much smaller variation than that of the baseline approach. This is because the proposed approach can schedule the mmWave transmissions fairly and thus maintains a high coverage ratio for the majority
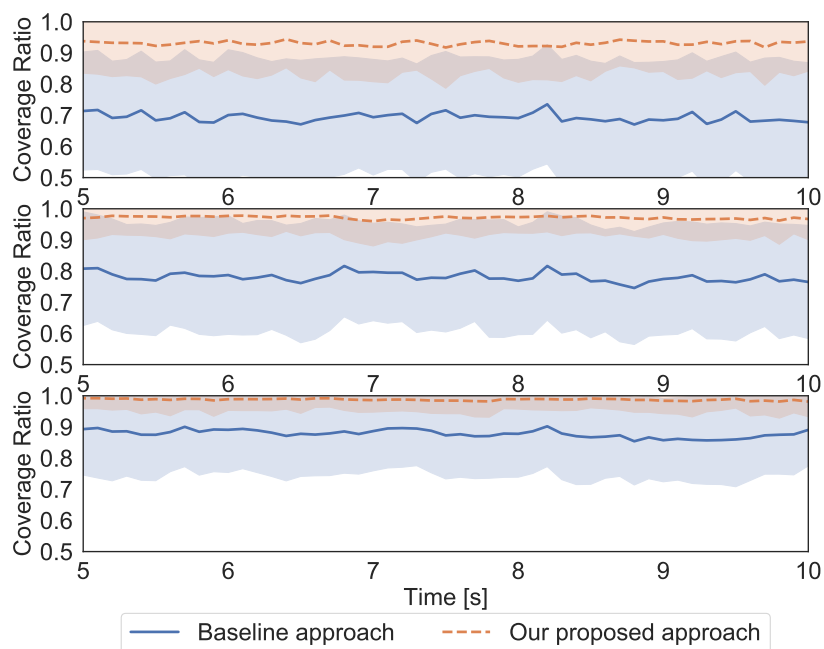
Figure 6.7: The average coverage ratio of 100 vehicles v.s. time, with different coverage ratio threshold $\tau_{threshold}$, top: $\tau_{threshold} = 0.25$; middle: $\tau_{threshold} = 0.5$; bottom $\tau_{threshold} = 1.0$
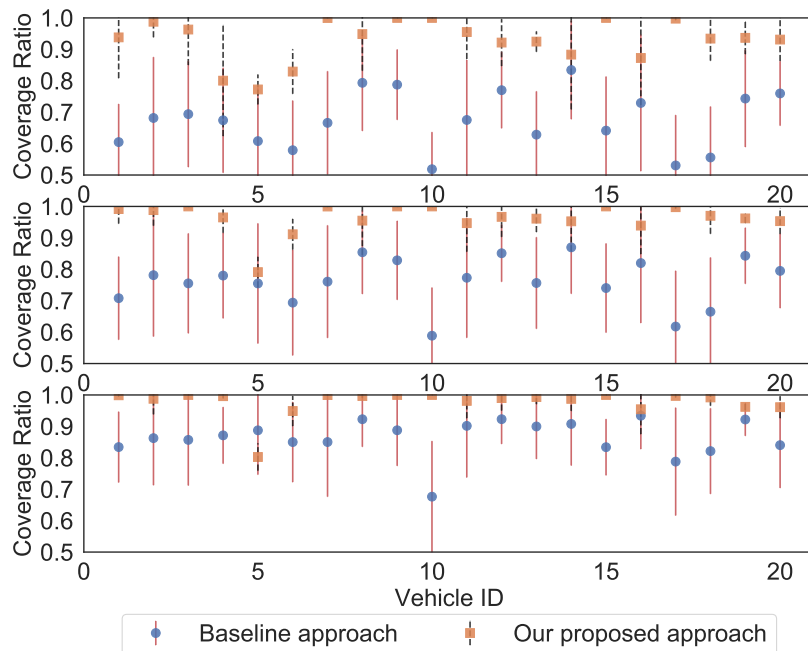

Figure 6.8: The average coverage ratio of different vehicles, with different $\tau_{threshold}$, top: $\tau_{threshold} = 0.25$; middle: $\tau_{threshold} = 0.5$; bottom $\tau_{threshold} = 1.0$

of cars.

Fig. 6.8 shows the results from the perspective of each car. In this figure, we randomly sample 20 cars and compare the average coverage ratio of the baseline approach with that of the proposed approach with $\tau_{threshold}$ values of 0.25, 0.5 and 1.0, respectively. The error bars represent the standard deviation of a car's coverage ratio over time. Similar to the observations of Fig. 6.7, one can observe that for the same car with the same mobility and the same set of LOS neighbors, the proposed approach produces a higher coverage ratio for all sampled cars. The improvement is up to 50%. Also, the proposed approach generates coverage ratios with smaller variations.

Both Fig. 6.7 and Fig. 6.8 show that the proposed approach can produce better coverage ratio results than the baseline approach. The improvements are primarily due to the consideration of the information usefulness while scheduling mmWave transmissions in our approach. To support the conclusion, we plot, in Fig. 6.9, the cumulative distribution of the information usefulness score of mmWave transmissions in the simulation with 100 cars and $\tau_{threshold} = 0.25$. The usefulness score was averaged over the number of cells that are within the intersection region of the mmWave transmitter's RoD and its receiver's RoI. From Fig. 6.9, we observe that over 40% of mmWave transmissions in the baseline simulation have a zero information usefulness score. This implies that the sensing information carried in these mmWave transmissions is less useful to the receivers in terms of improving the knowledge about their RoI. We found two main cases that are contributing to zero usefulness scores. One case is shown in Fig 6.10a, where two cars are moving in the opposite directions and they are moving away from each other. In this case, it is impossible for one car's RoD to overlap with the other car's RoI, which leads to zero usefulness scores. This is intuitively reasonable because two cars are moving away from each other and thus one car's sensing information is unlikely to be useful for the other car's future movements. The other case is presented in Fig 6.10b, where car A is the mmWave transmitter and it is following car B. In this case, car A's RoD largely overlaps with car B's RoD. Therefore, sharing car A's sensing information to car B is unlikely to introduce new knowledge to car B's RoI. Moreover, the sensor view of car A is partially blocked by car B. The quality of car A's

sensing information could be potentially affected. Hence, sharing sensing information from car *A* to car *B* may not be useful. Additionally, these transmissions occupy the transmission opportunities that could be used for transmitting more useful and valuable sensing information, causing a waste of the network resource. Our approach minimizes the number of transmissions with low usefulness scores and achieves the median value of the information usefulness score as 50 in Fig. 6.9. This significant improvement is because in our approach, a mmWave transmitter estimates its information usefulness to the intended receivers and then prioritizes the scheduling of mmWave transmissions with higher usefulness scores. By receiving the mmWave transmissions with higher usefulness scores, the mmWave receivers can efficiently improve the coverage of its local RoI. We can also notice that the prioritized scheduling is also fair. After a mmWave receiver recently receives a mmWave transmission and updates the knowledge about its RoI, the sensing information from another potential mmWave transmitter, covering the similar region as the previous mmWave transmitter, will be less useful to the receiver at this time. The transmission of this potential transmitter-receiver pair will have a low scheduling priority. Other mmWave links that have not been transmitted but with high usefulness scores will be scheduled with a higher priority. This round-robin like scheduling helps reduce the variations of the coverage ratio in different time and across different cars, as observed in Fig. 6.7 and Fig. 6.8.

From Fig. 6.7 and Fig. 6.8, it is also easy to observe that as the value of the coverage threshold decreases from 1.0 to 0.25, the coverage ratio of both the baseline and the proposed approach decreases. It is because even with the same number of LOS neighbors, if the threshold $\tau_{threshold}$ is tight, it is possible that a car is not able to receive information updates from neighboring vehicles before the information of the corresponding cells gets outdated, leading to a lower coverage ratio.

6.5.4 Different Vehicle Densities

In this subsection, we evaluate the performance of the proposed mechanism under different vehicle densities. Fig. 6.11 shows the results of simulations with 100 vehicles, 200 vehicles, and 300 vehicles, respectively. Independent of node densities, our proposed
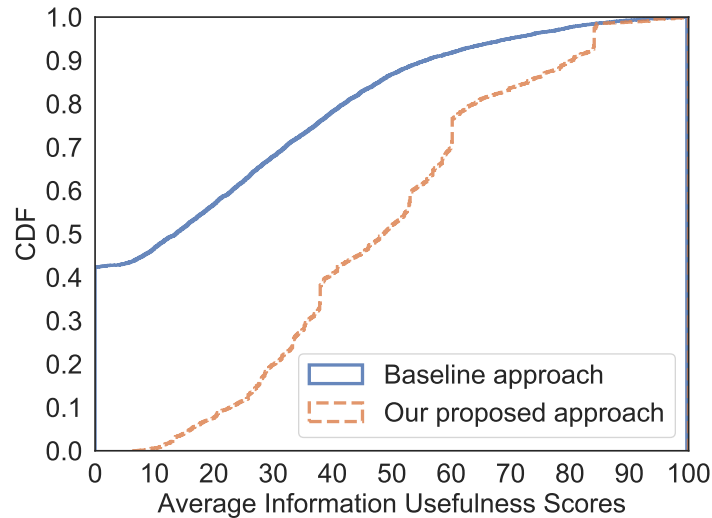
Figure 6.9: The distribution of information usefulness score of mmWave transmissions in the simulation with 100 cars and $\tau_{threshold} = 0.25$
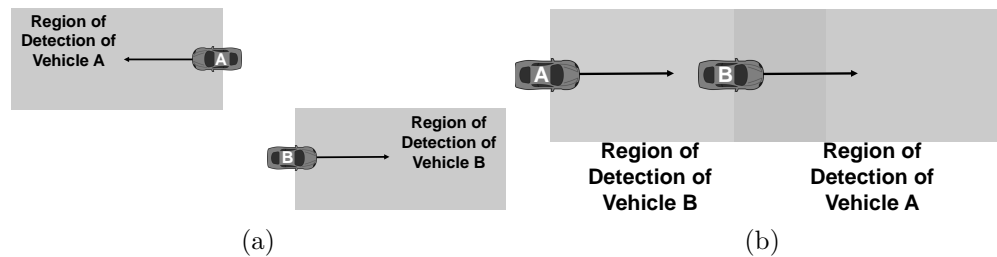
Figure 6.10: Cases with zero usefulness scores: (a) two cars are moving away from each other, (b) the mmWave transmitter is behind and in the same lane with the mmWave receiver

approach outperforms the baseline approach by up to 42%. However, it is also observed that the coverage ratio of the two approaches decreases as the vehicle density increases. It is primarily because, with more and more vehicles in the neighborhood, a vehicle may not be able to receive the updated sensor information from a neighboring vehicle in time due to the time slots are currently used by other vehicles. Therefore, the information of the corresponding cells becomes outdated. However, even in such challenging scenarios, our approach can still maintain about 90% coverage ratio.
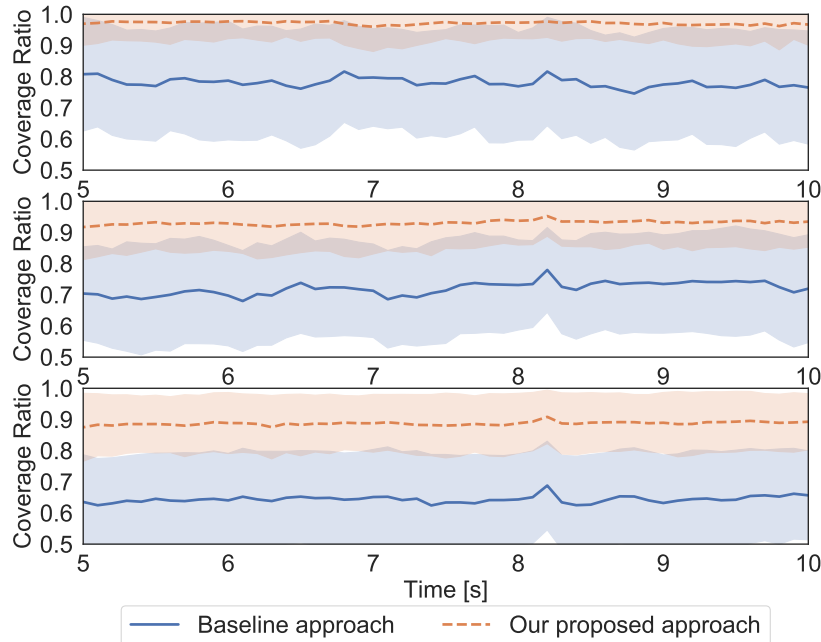
Figure 6.11: The average coverage ratio of different number of cars over time with $\tau_{threshold} = 0.5$, top: 100 cars; middle: 200 cars; bottom 300 cars

6.6 Discussion and Limitations

6.6.1 Information Score Calculation

We believe the definitions for the information usefulness, such as RoI, RoD, the information score calculation equation and the information usefulness score calculation equation, should be predefined and identical to all vehicles. The rationales for this setting are: 1) in this way, a vehicle can know how to calculate the information score and the information usefulness score for other vehicles; 2) moreover, we believe this is necessary to guarantee the fairness between vehicles. Although we have mentioned that a vehicle can include its customized information usefulness calculation in DSRC message to inform other vehicles of applying the customized models for calculating its information usefulness, this also poses a possibility that the vehicle would use the customized calculation to benefit its own transmissions, causing an unfair schedule to other vehicles. Therefore, we think unless the vehicles reach a consensus that some of them can apply the customized information usefulness calculation, the vehicles should follow the predefined information usefulness calculation.

6.6.2 Environment Perception

In this work, we assume that if a vehicle A can receive the sensor data from a remote vehicle B, the information of the corresponding cells at vehicle A will be updated. Vehicles follow this rule to estimate the information usefulness score for vehicle A. However, we acknowledge that a more accurate estimation is desired since it is possible that vehicle B's sensor view has been partially blocked by other objects (e.g., a car or a building) and consequently, the information of certain cells at vehicle A should not be updated based on vehicle B's sensor data. In our current model, we have not considered theses blockage effects or actual detection results in vehicle B's sensor data yet. To solve this issue, more information should be shared between vehicles via DSRC. We will consider this improvement in future work.

6.7 Summary

This work proposes a DSRC-assisted mmWave data sharing mechanism. Different from previous works that primarily exploit DSRC information for reducing mmWave beam alignment overhead, we further extend the usage of DSRC information for estimating the usefulness of sensing information contained in mmWave transmissions. We first define the information usefulness score to quantify the usefulness of a mmWave transmission based on the definition of RoD and RoI. With knowing the information usefulness score of mmWave links, we then propose the information usefulness-aware scheduling which can group the mmWave links into non-conflicting compatible sets and prioritize the mmWave transmissions according to their information usefulness scores. The proposed approach is evaluated in a highway scenario via ns-3 simulations, and the simulation results show that our approach increases the average coverage ratio of vehicles' RoI by up to 50% when comparing to a baseline approach using the broadcast strategy. The significant improvements are primarily due to our approach prioritize the mmWave transmissions carrying more useful sensing information and allocate the network resource efficiently.

Chapter 7

Conclusion

In this dissertation, we conducted a series of simulation studies on the DSRC performance in challenging scenarios where the legacy DSRC coexists with other technologies or protocols. As the primary research tool of this dissertation, we first developed and calibrated a V2V network simulator based on the extensive data collected in a set of field experiments with up to 400 DSRC transmitters. Our simulator calibration efforts focused on two main components of the simulator, i.e., the signal propagation modeling and the receiver behavior modeling. We then investigated how different models for the two components can affect the simulation accuracy. We found that with well-calibrated simulation models, it is possible to achieve 88% simulation accuracy with a marginal increase in the simulation runtime.

With the calibrated simulator, three DSRC coexistence scenarios were studied in this dissertation: 1) different versions of DSRC protocols coexisting in one network; 2) DSRC and Wi-Fi sharing the DSRC spectrum; 3) DSRC and mmWave coexisting on the same car enabled by the multi-technology and multi-band V2V deployment.

For the first coexistence scenario, we used two DSRC congestion control protocols as an example to understand the impact of introducing an evolved DSRC protocol to the network on the performance of the legacy DSRC. CAM-DCC is considered the legacy DSRC protocol since it is expected to be deployed for day one applications, and LIMERIC is regarded as the evolved DSRC protocol as it is a good candidate for day two deployment. We first identified that the CAM-DCC vehicles can experience noticeable performance degradation after LIMERIC is introduced. The primary reasons for the performance degradation are: 1) LIMERIC, as an adaptive control algorithm, tries to push the channel load to a comparatively high target; 2) CAM-DCC, as a

reactive control algorithm, reacts to the increased channel load and then reduces its transmission rate, leading to an increased packet latency. Based on the analyzed reasons, we proposed an adaptive mechanism that can automatically adjust LIMERIC's channel load target such that the performance degradation of CAM-DCC is controlled to a desired level. As shown in Chapter 4, with the proposed adaptive mechanism, the performance degradation of CAM-DCC can be approximately removed with only a negligible impact on the performance of LIMERIC vehicles.

In the second coexistence scenario, we primarily discussed the challenges of sharing the DSRC spectrum with Wi-Fi devices, and investigated the impact of Wi-Fi transmissions on the DSRC performance. Mainly, we evaluated the performance of three recently proposed mechanisms for sharing the DSRC spectrum to Wi-Fi devices, i.e., D & V, D & M, and Re-channelization. We identified that Wi-Fi devices may suffer from strong self-interference, leading to delayed detection of the presence of the DSRC transmissions in D & V and D & M. The delayed detection can cause packet collisions between DSRC transmissions and Wi-Fi transmissions. However, by adding an extra idle period to the Wi-Fi inter-frame period, the performance of Wi-Fi detecting the presence of DSRC transmissions can be significantly improved. This idea has been incorporated in the newer version of D&V. In the post-detection phase, D & M can introduce more than 30% extra DSRC packet losses compared to none for D & V. Therefore, we believe Wi-Fi devices leaving the DSRC band after DSRC detection is a more suitable solution to provide adequate protection to the legacy DSRC. Different from D & V and D & M, Re-channelization overhauls the current DSRC channelization. Our study showed that in many scenarios DSRC and Wi-Fi devices suffer from hidden terminal problems. Furthermore, even in an ideal situation where no hidden terminals are present, backoff countdown collisions that are inherent to the IEEE 802.11 MAC protocol can still cause 32% extra packet losses of DSRC transmissions.

In the third coexistence scenario, we studied a multi-technology and multi-band V2V scenario, where DSRC and the emerging mmWave technology coexist. In this case, DSRC is employed as the control channel for mmWave and shares information that can facilitate the sensor data sharing via mmWave. Different from previous work

that primarily exploits DSRC information for reducing beam alignment overhead of mmWave, the DSRC information is further utilized to estimate the usefulness of the shared information. With knowing the information usefulness of mmWave links, the problem of efficiently scheduling mmWave transmissions for each vehicle is modeled as the problem of finding a ranked collection of compatible sets in a directed weighted graph with information usefulness scores as weights. We then proposed a simple yet efficient algorithm to solve this problem as well as the protocols for implementing this algorithm at each vehicle. The evaluation results showed that our approach increases the average coverage ratio of vehicles' RoI by up to 50% more than a baseline approach simply using the broadcast strategy. The significant improvement is primarily due to our approach prioritize the transmissions with higher information usefulness scores and allocate the network resource efficiently.

In summary, this dissertation quantifies the DSRC performance degradation after introducing a second protocol/technology to the network via accurate simulations. It has been shown that the performance degradation is significant, which can jeopardize the effectiveness of safety applications built upon DSRC. To control the degradation to an acceptable level, these newly introduced protocols/technologies are required to adjust their parameters carefully and design their access strategy to the DSRC network more conservatively. Furthermore, we showed that DSRC can help coordinate the transmissions of the emerging technologies in a multi-technology and multi-band V2V scenario and largely improve the data sharing efficiency of the emerging technologies.

Appendix A

Transmission Rate of LIMERIC in Mixed Networks

This appendix describes the calculation of LIMERIC's transmission rate in mixed networks. According to eq. 4.1, each LIMERIC vehicle uses

$$r_j(k) = (1 - \alpha)r_j(k - 1) + \beta(r_g - r_C(k - 1)) \tag{A.1}$$

for adapting the rate, where r_g is the target, and $r_C(k - 1)$ is the aggregate channel capacity allowed to all vehicles.

Each CAM-DCC vehicle updates its rate based on the table look-up. It can be modeled as

$$r_i(k) = F(r_C(k - 1)) \tag{A.2}$$

where $F(*)$ defines the mapping function between measured channel loads and transmission rates. However, since CAM-DCC uses inertia to prevent frequent transitions between states and LIMERIC facilitates the CBP convergence, the rate of CAM-DCC vehicles gets converged to one value easily (even before LIMERIC reaches to final steady state), i.e. $r_i(k) = r_i(k - 1)$. Based on the assumptions above, the rates of K vehicles can be formatted in a vector

$$\mathbf{R(k)} = \begin{pmatrix} \mathbf{R_{limeric}(k)} \\ \mathbf{R_{camdcc}(k)} \end{pmatrix} \tag{A.3}$$

where $\mathbf{R_{limeric}(k)}$ and $\mathbf{R_{camdcc}(t)}$ are the rate vector of LIMERIC and CAM-DCC vehicles, respectively. Then, applying the rate adaption equation for LIMERIC and CAM-DCC vehicles, eq. A.3 can be rewritten as:

$$\mathbf{R(t)} = \begin{pmatrix} \mathbf{A_1} & \mathbf{A_2} \\ \mathbf{0} & \mathbf{I} \end{pmatrix} \begin{pmatrix} \mathbf{R_{limeric}(k - 1)} \\ \mathbf{R_{camdcc}(k - 1)} \end{pmatrix} + \beta \begin{pmatrix} \mathbf{R_g} \\ \mathbf{0} \end{pmatrix} \tag{A.4}$$

where

$$\mathbf{A_1} = \begin{pmatrix} 1-\alpha-\beta & -\beta & -\beta & ... & -\beta \\ -\beta & 1-\alpha-\beta & -\beta & ... & -\beta \\ -\beta & -\beta & 1-\alpha-\beta & ... & -\beta \\ . & . & . & ... & . \\ . & . & . & ... & . \\ -\beta & -\beta & -\beta & ... & 1-\alpha-\beta \end{pmatrix} \quad (A.5)$$

$$\mathbf{A_2} = \begin{pmatrix} -\beta & -\beta & -\beta & ... & -\beta \\ -\beta & -\beta & -\beta & ... & -\beta \\ -\beta & -\beta & -\beta & ... & -\beta \\ . & . & . & ... & . \\ . & . & . & ... & . \\ -\beta & -\beta & -\beta & ... & -\beta \end{pmatrix} \quad (A.6)$$

The size of matrix $\mathbf{A1}$ and $\mathbf{A2}$ are $K_{limeric} \times K_{limeric}$ and $K_{limeric} \times K_{camdcc}$, respectively. Matrix $\mathbf{0}$ is a zero matrix with size $K_{camdcc} \times K_{limeric}$, and matrix $\mathbf{I}$ is a unit matrix with size $K_{camdcc} \times K_{camdcc}$. Note that

$$\mathbf{A}^k = \begin{pmatrix} \mathbf{A_1}^k & \mathbf{A_1}^{k-1}\mathbf{A_2} + \mathbf{A_1}^{k-2}\mathbf{A_2} + ... + \mathbf{A_2} \\ \mathbf{0} & \mathbf{I} \end{pmatrix} \quad (A.7)$$

and

$$\mathbf{A_1}^{k-1}\mathbf{A_2} = -\beta(1-\alpha-\beta K_{limeric})^{k-1} \begin{pmatrix} 1 & 1 & ... & 1 \\ 1 & 1 & ... & 1 \\ . & . & ... & . \\ . & . & ... & . \\ 1 & 1 & ... & 1 \end{pmatrix} \quad (A.8)$$

Recall that

$$\mathbf{R(k)} = \mathbf{A}^k\mathbf{R(k_0)} + \beta \sum_{i=0}^{k-1} \mathbf{A}^{k-i-1}\mathbf{B}, where\ \mathbf{B} = \begin{pmatrix} \mathbf{R_g} \\ \mathbf{0} \end{pmatrix} \quad (A.9)$$

Thus, the converged rate of one LIMERIC vehicle in mixed network can be derived

as

$$r_j = lim_{k \to \infty} r_j(k) = \frac{\beta(r_g - r_i K_{camdcc})}{\alpha + \beta K_{limeric}} \quad (A.10)$$

Where r_i is the converged rate of CAM-DCC vehicles.

According to the theoretical analysis above, eq. 4.2 can be rewritten as the following equation for mixed networks:

$$CBP_{con} = \frac{\beta K_{limeric}(CBP_{target} - CBP_{camdcc})}{20\alpha + \beta K_{liemric}} \qquad \text{(A.11)}$$

where CBP_{camdcc} is the channel load that is contributed by CAM-DCC vehicles in the mixed network.

References

[1] "IEEE standard for information technology–telecommunications and information exchange between systems local and metropolitan area networks–specific requirements part 11: Wireless lan medium access control (mac) and physical layer (phy) specifications," *IEEE Std 802.11-2012 (Revision of IEEE Std 802.11-2007)*, pp. 1–2793, March 2012.

[2] J. Choi, V. Va, N. Gonzalez-Prelcic, R. Daniels, C. R. Bhat, and R. W. Heath, "Millimeter-wave vehicular communication to support massive automotive sensing," *IEEE Communications Magazine*, vol. 54, no. 12, pp. 160–167, December 2016.

[3] T. Zhang and L. Delgrossi, *Vehicle Safety Communications: Protocols, Security, and Privacy*, ser. Information and Communication Technology Series,. Wiley, 2012.

[4] J. B. Kenney, "Dedicated Short-Range Communications (DSRC) standards in the united states," *Proceedings of the IEEE*, vol. 99, no. 7, pp. 1162–1182, July 2011.

[5] Q. Chen, F. Schmidt-Eisenlohr, D. Jiang, M. Torrent-Moreno, L. Delgrossi, and H. Hartenstein, "Overhaul of IEEE 802.11 modeling and simulation in ns-2," in *Proceedings of the 10th ACM Symposium on Modeling, Analysis, and Simulation of Wireless and Mobile Systems*, ser. MSWiM '07. ACM, 2007, pp. 159–168.

[6] T. Bingmann, "Accuracy enhancements of the 802.11 model and edca qos extensions in ns-3," Master's thesis, University of Karlsruhe, 2009.

[7] T. Mangel, O. Klemp, and H. Hartenstein, "5.9 GHz inter-vehicle communication at intersections: a validated non-line-of-sight path-loss and fading model," *EURASIP Journal on Wireless Communications and Networking*, vol. 2011, no. 1, p. 182, 2011.

[8] U.S. Department of Transportation National Highway Traffic Safety Administration. Traffic safety facts, 2015 data. https://crashstats.nhtsa.dot.gov/Api/Public/ViewPublication/812412.

[9] Association for Safe International Travel. (2015) http://asirt.org/Initiatives/Informing-Road-Users/Road-Safety-Facts/Road-Crash-Statistics.

[10] T. F. C. C. (FCC), "FCC 03-324 report and order," December 2003.

[11] F. Ahmed-Zaid, F. Bai, S. Bai, C. Basnayake, B. Bellur, S. Brovold, G. Brown, L. Caminiti, D. Cunningham, and e. a. H. Elzein, "Vehicle Safety Communications-Applications(VSC-A) final report," National Highway Traffic Safety Administration (NHTSA), Tech. Rep., 2011.

[12] J. Harding, G. Powell, R. Yoon, J. Fikentscher, C. Doyle, D. Sade, M. Lukuc, J. Simons, and J. Wang, "Vehicle-to-vehicle communications: Readiness of V2V technology for application," National Highway Traffic Safety Administration (NHTSA), Tech. Rep., 2014.

[13] W. G. Najm, J. D. Smith, and M. Yanagisawa, "Pre-crash scenario typology for crash avoidance research," National Highway Traffic Safety Administration (NHTSA), Tech. Rep., 2007.

[14] Safety Pilot websit, University of Michigan Transportation Research Center, Ann Arbor, Michigan. http://www.safetypilot.us/.

[15] U.S. Department of Transportation National Highway Traffic Safety Administration. Collaborative connected vehicle research update. https://www.its.dot.gov/presentations/pdf/V2V_Collaborative_Research_MikeLukuc2013.pdf.

[16] "V2V notice of proposed rulemaking," National Highway Traffic Safety Administration (NHTSA), Tech. Rep., 2016.

[17] S. M. Kim and T. He, "Freebee: Cross-technology communication via free side-channel," in *Proceedings of the 21st Annual International Conference on Mobile Computing and Networking*, ser. MobiCom '15. New York, NY, USA: ACM, 2015, pp. 317–330.

[18] C.-J. M. Liang, N. B. Priyantha, J. Liu, and A. Terzis, "Surviving Wi-fi interference in low power zigbee networks," in *Proceedings of the 8th ACM Conference on Embedded Networked Sensor Systems*, ser. SenSys '10. New York, NY, USA: ACM, 2010, pp. 309–322.

[19] S. Gollakota, F. Adib, D. Katabi, and S. Seshan, "Clearing the rf smog: Making 802.11n robust to cross-technology interference," in *Proceedings of the ACM SIGCOMM 2011 Conference*, ser. SIGCOMM '11. New York, NY, USA: ACM, 2011, pp. 170–181.

[20] A. M. Cavalcante, E. Almeida, R. D. Vieira, S. Choudhury, E. Tuomaala, K. Doppler, F. Chaves, R. C. D. Paiva, and F. Abinader, "Performance evaluation of LTE and Wi-Fi coexistence in unlicensed bands," in *2013 IEEE 77th Vehicular Technology Conference (VTC Spring)*, June 2013, pp. 1–6.

[21] E. Chai, K. Sundaresan, M. A. Khojastepour, and S. Rangarajan, "LTE in unlicensed spectrum: Are we there yet?" in *Proceedings of the 22Nd Annual International Conference on Mobile Computing and Networking*, ser. MobiCom '16. New York, NY, USA: ACM, 2016, pp. 135–148.

[22] S. Sagari, S. Baysting, D. Saha, I. Seskar, W. Trappe, and D. Raychaudhuri, "Coordinated dynamic spectrum management of LTE-U and Wi-Fi networks," in *2015 IEEE International Symposium on Dynamic Spectrum Access Networks (DySPAN)*, Sept 2015, pp. 209–220.

[23] M. H. Ng, S. D. Lin, J. Li, and S. Tatesh, "Coexistence studies for 3GPP LTE with other mobile systems," *IEEE Communications Magazine*, vol. 47, no. 4, pp. 60–65, April 2009.

[24] Y. Park and H. Kim, "On the coexistence of IEEE 802.11ac and WAVE in the 5.9 GHz band," *IEEE Communications Magazine*, vol. 52, no. 6, pp. 162–168, June 2014.

[25] M. J. Marcus, "Unlicensed cognitive sharing of tv spectrum: the controversy at the federal communications commission," *IEEE Communications Magazine*, vol. 43, no. 5, pp. 24–25, May 2005.

[26] "Vehicle Safety Communications project: Task 3 final report:identify intelligent vehicle safety applications enabled by DSRC," National Highway Traffic Safety Administration (NHTSA), Tech. Rep., 2005.

[27] DRIVE-C2X. http://www.drive-c2x.eu.

[28] L. Cheng, B. E. Henty, D. D. Stancil, F. Bai, and P. Mudalige, "Mobile vehicle-to-vehicle narrow-band channel measurement and characterization of the 5.9 GHz dedicated short range communication (DSRC) frequency band," *IEEE Journal on Selected Areas in Communications*, vol. 25, no. 8, pp. 1501–1516, Oct 2007.

[29] A. Tanenbaum, *Computer Networks*, 4th ed. Prentice Hall Professional Technical Reference, 2002.

[30] "IEEE standard for wireless access in vehicular environments (wave) – multi-channel operation," *IEEE Std 1609.4-2016 (Revision of IEEE Std 1609.4-2010)*, pp. 1–94, March 2016.

[31] "ISO/IEC/IEEE international standard - information technology – telecommunications and information exchange between systems – local and metropolitan area networks - specific requirements – part 2: Logical link control," *IEEE Std 8802-2-1994*, pp. 1–174, Dec 1994.

[32] "IEEE standard for wireless access in vehicular environments (wave) – networking services," *IEEE Std 1609.3-2010 (Revision of IEEE Std 1609.3-2007)*, pp. 1–144, Dec 2010.

[33] "IEEE standard for information technology– local and metropolitan area networks– specific requirements– part 11: Wireless lan medium access control (mac) and physical layer (phy) specifications amendment 6: Wireless access in vehicular environments," *IEEE Std 802.11p-2010 (Amendment to IEEE Std 802.11-2007 as amended by IEEE Std 802.11k-2008, IEEE Std 802.11r-2008, IEEE Std 802.11y-2008, IEEE Std 802.11n-2009, and IEEE Std 802.11w-2009)*, pp. 1–51, July 2010.

[34] NHTSA, "Federal motor vehicle safety standards: Vehicle-to-vehicle (v2v) communications advance notice of proposed rulemaking," Tech. Rep., August 15 2014.

[35] U.S. department of transportation announces decision to move forward with vehicle-to-vehicle communication technology for light vehicles. http://www.nhtsa.gov/About+NHTSA/Press+Releases/2014/USDOT+to+Move+Forward+with+Vehicle-to-Vehicle+Communication+Technology+for+Light+Vehicles.

[36] D. B. Johnson, "Validation of wireless and mobile network models and simulation," in *DARPA/NIST Network Simulation Validation Workshop*, 1999.

[37] S. Ivanov, A. Herms, and G. Lukas, "Experimental validation of the ns-2 wireless model using simulation, emulation, and real network," in *Communication in Distributed Systems (KiVS), 2007 ITG-GI Conference*, Feb 2007, pp. 1–12.

[38] S. Jansen and A. McGregor, "Performance, validation and testing with the network simulation cradle," in *Modeling, Analysis, and Simulation of Computer and Telecommunication Systems, 2006. 14th IEEE International Symposium on*, Sept 2006, pp. 355–362.

[39] N. Baldo, M. Requena-Esteso, J. Núñez Martínez, M. Portolès-Comeras, J. Nin-Guerrero, P. Dini, and J. Mangues-Bafalluy, "Validation of the IEEE 802.11 mac model in the ns3 simulator using the extreme testbed," in *Proceedings of the 3rd International ICST Conference on Simulation Tools and Techniques*, ser. SIMUTools '10, 2010, pp. 64:1–64:9.

[40] S. Papanastasiou, J. Mittag, E. Strom, and H. Hartenstein, "Bridging the gap between physical layer emulation and network simulation," in *Wireless Communications and Networking Conference (WCNC), 2010 IEEE*, April 2010, pp. 1–6.

[41] Q. Sun, S. Tan, and K. Teh, "Analytical formulae for path loss prediction in urban street grid microcellular environments," *Vehicular Technology, IEEE Transactions on*, vol. 54, no. 4, pp. 1251–1258, July 2005.

[42] C.-X. Wang, X. Cheng, and D. Laurenson, "Vehicle-to-vehicle channel modeling and measurements: recent advances and future challenges," *Communications Magazine, IEEE*, vol. 47, no. 11, pp. 96–103, 2009.

[43] I. Sen and D. Matolak, "Vehicle-vehicle channel models for the 5 GHz band," *Intelligent Transportation Systems, IEEE Transactions on*, vol. 9, no. 2, pp. 235–245, June 2008.

[44] J. Karedal, N. Czink, A. Paier, F. Tufvesson, and A. Molisch, "Path loss modeling for vehicle-to-vehicle communications," *Vehicular Technology, IEEE Transactions on*, vol. 60, no. 1, pp. 323–328, Jan 2011.

[45] M. Boban, J. Barros, and O. Tonguz, "Geometry-based vehicle-to-vehicle channel modeling for large-scale simulation," *Vehicular Technology, IEEE Transactions on*, vol. 63, no. 9, pp. 4146–4164, Nov 2014.

[46] C. Sommer, D. Eckhoff, R. German, and F. Dressler, "A computationally inexpensive empirical model of IEEE 802.11p radio shadowing in urban environments," in *Wireless On-Demand Network Systems and Services (WONS), 2011 Eighth International Conference on*, Jan 2011, pp. 84–90.

[47] T. Rappaport, *Wireless Communications: Principles and Practice*, 2nd ed. Upper Saddle River, NJ, USA: Prentice Hall PTR, 2001.

[48] V. Erceg, L. J. Greenstein, S. Y. Tjandra, S. R. Parkoff, A. Gupta, B. Kulic, A. A. Julius, and R. Bianchi, "An empirically based path loss model for wireless channels in suburban environments," *IEEE Journal on Selected Areas in Communications*, vol. 17, no. 7, pp. 1205–1211, Jul 1999.

[49] S. Kokalj-Filipovic, L. J. Greenstein, B. Cheng, and M. Gruteser, "Methods for extracting V2V propagation models from imperfect rssi field data," in *Vehicular Technology Conference (VTC Fall), 2015 IEEE 82nd*, Sept. 2015.

[50] E. Ben Hamida, G. Chelius, and J. M. Gorce, "Impact of the physical layer modeling on the accuracy and scalability of wireless network simulation," *Simulation*, vol. 85, no. 9, pp. 574–588, Sep. 2009.

[51] G. Pei and T. Henderson, "Validation of OFDM error rate model in ns-3 simulation," *Boeing Research Technology*, pp. 1–15, 2010.

[52] S. Kokalj-Filipovic and L. Greenstein, "EM-based channel estimation from crowdsourced rssi samples corrupted by noise and interference," in *49th Conf. on Information Systems and Sciences (CISS)*, Mar. 2015.

[53] "Intelligent Transport Systems (ITS); vehicular communications; basic set of applications; part 2: Specification of cooperative awareness basic service," *ETSI EN 302 637-2 V1.3.2*, November 2014.

[54] "Dedicated short range communications (DSRC) message set dictionary," *SAE Std J2735*, November 2009.

[55] C. L. Huang, Y. P. Fallah, R. Sengupta, and H. Krishnan, "Intervehicle transmission rate control for cooperative active safety system," *IEEE Transactions on Intelligent Transportation Systems*, vol. 12, no. 3, pp. 645–658, Sept 2011.

[56] J. Jose, C. Li, X. Wu, L. Ying, and K. Zhu, "Distributed rate and power control in DSRC," in *Information Theory (ISIT), 2015 IEEE International Symposium on*, June 2015, pp. 2822–2826.

[57] T. Tielert, D. Jiang, H. Hartenstein, and L. Delgrossi, "Joint power/rate congestion control optimizing packet reception in vehicle safety communications," in *Proceeding of the Tenth ACM International Workshop on Vehicular Inter-networking, Systems, and Applications*, ser. VANET '13, 2013, pp. 51–60.

[58] M. Sepulcre, J. Gozalvez, O. Altintas, and H. Kremo, "Adaptive beaconing for congestion and awareness control in vehicular networks," in *Vehicular Networking Conference, IEEE*, Dec 2014, pp. 81–88.

[59] "Intelligent Transport Systems (ITS); cross layer dcc management entity for operation in the ITS G5A and ITS G5B medium," *ETSI TS 103 175, V1.1.1*, Jun 2015.

[60] "Intelligent Transport Systems (ITS): Decentralized congestion control mechanisms for intelligent transport systems operating in the 5 GHz range; access layer part," *ETSI TS 102 687, V1.1.1*, July 2011.

[61] G. Bansal, J. B. Kenney, and C. E. Rohrs, "LIMERIC: A linear adaptive message rate algorithm for dsrc congestion control," *Vehicular Technology, IEEE Transactions on*, vol. 62, no. 9, pp. 4182–4197, Nov 2013.

[62] "C-ITS platform final report," C-ITS Deployment Platform of the European Commission, Tech. Rep., January 2016.

[63] T. Tielert, D. Jiang, Q. Chen, L. Delgrossi, and H. Hartenstein, "Design methodology and evaluation of rate adaptation based congestion control for vehicle safety communications," in *Vehicular Networking Conference (VNC), 2011 IEEE*, Nov 2011, pp. 116–123.

[64] G. Bansal, J. Kenney, and A. Weinfield, "Cross-validation of DSRC radio testbed and ns-2 simulation platform for vehicular safety communications," in *Vehicular Technology Conference (VTC Fall), 2011 IEEE*, Sept 2011, pp. 1–5.

[65] B. Cheng, A. Rostami, M. Gruteser, J. B. Kenney, G. Bansal, and K. Sjoberg, "Performance evaluation of a mixed vehicular network with CAM-DCC and LIMERIC vehicles," in *Proceedings of Workshop of SmartVehicles at IEEE WoWMoM*. IEEE, 2015, pp. 1–6.

[66] G. Bansal, H. Lu, J. B. Kenney, and C. Poellabauer, "EMBARC: Error model based adaptive rate control for vehicle-to-vehicle communications," in *Proceeding of the Tenth ACM International Workshop on Vehicular Inter-networking, Systems, and Applications*, ser. VANET '13. ACM, 2013, pp. 41–50.

[67] J. Lansford, J. B. Kenney, and P. Ecclesine, "Coexistence of unlicensed devices with DSRC systems in the 5.9 GHz its band," in *2013 IEEE Vehicular Networking Conference*, Dec 2013, pp. 9–16.

[68] I. F. Akyildiz, W. y. Lee, M. C. Vuran, and S. Mohanty, "A survey on spectrum management in cognitive radio networks," *IEEE Communications Magazine*, vol. 46, no. 4, pp. 40–48, April 2008.

[69] P. V. Bahl, R. Murty, T. Moscibroda, and R. Chandra, "Senseless: A database-driven white spaces network," *IEEE Transactions on Mobile Computing*, vol. 11, pp. 189–203, 2011.

[70] "BRAN technical report 103 319," Tech. Rep., 2016.

[71] J. Wang, T. Wu, Y. Liu, W. Deng, and H. Oh, "Modeling and performance analysis of dynamic spectrum sharing between dsrc and wi-fi systems," *Wireless Communications and Mobile Computing*, vol. 16, no. 16, pp. 2743–2758.

[72] "IEEE standard for information technology– telecommunications and information exchange between systemslocal and metropolitan area networks– specific requirements–part 11: Wireless lan medium access control (mac) and physical layer (phy) specifications–amendment 4: Enhancements for very high throughput for operation in bands below 6 GHz." *IEEE Std 802.11ac-2013 (Amendment to IEEE Std 802.11-2012, as amended by IEEE Std 802.11ae-2012, IEEE Std 802.11aa-2012, and IEEE Std 802.11ad-2012)*, pp. 1–425, Dec 2013.

[73] "Coexistence of 5 Ghz RLAN with ITS," *M74_13R0_SE24*, 2013.

[74] T. Mangel, F. Schweizer, T. Kosch, and H. Hartenstein, "Vehicular safety communication at intersections: Buildings, non-line-of-sight and representative scenarios," in *2011 Eighth International Conference on Wireless On-Demand Network Systems and Services*, Jan 2011, pp. 35–41.

[75] T. Mangel and H. Hartenstein, "5.9 GHz IEEE 802.11p inter-vehicle communication: Non-line-of-sight reception under competition," in *2011 IEEE Vehicular Networking Conference (VNC)*, Nov 2011, pp. 155–162.

[76] "IEEE p802.11wireless LANs TGn channel models," Tech. Rep., 2014.

[77] "IEEE p802.11 wireless LANs: Proposal for 5850-5925 mhz unlicensed devices," Tech. Rep.

[78] N. An, T. Gaugel, and H. Hartenstein, "VANET: Is 95% probability of packet reception safe?" in *2011 11th International Conference on ITS Telecommunications*, Aug 2011, pp. 113–119.

[79] J. Kenney, H. Lu, and B. Cheng, "Technical challenges of sharing dsrc band at 5.9 GHz in US," in *ITS World Congress*, 2017.

[80] J. Leonard, J. How, S. Teller, M. Berger, S. Campbell, G. Fiore, L. Fletcher, E. Frazzoli, A. Huang, S. Karaman, O. Koch, Y. Kuwata, D. Moore, E. Olson, S. Peters, J. Teo, R. Truax, M. Walter, D. Barrett, A. Epstein, K. Maheloni, K. Moyer, T. Jones, R. Buckley, M. Antone, R. Galejs, S. Krishnamurthy, and J. Williams, "A perception-driven autonomous urban vehicle," *J. Field Robot.*, vol. 25, no. 10, pp. 727–774, Oct. 2008.

[81] S. W. Kim, B. Qin, Z. J. Chong, X. Shen, W. Liu, M. H. Ang, E. Frazzoli, and D. Rus, "Multivehicle cooperative driving using cooperative perception: Design and experimental validation," *IEEE Transactions on Intelligent Transportation Systems*, vol. 16, no. 2, pp. 663–680, April 2015.

[82] B. Coll-Perales, J. Gozalvez, and M. Gruteser, "Sub-6GHz assisted mac for millimeter wave vehicular communications," *arXiv preprint arXiv:1809.02455*, 2018.

[83] V. Va, T. Shimizu, G. Bansal, and R. W. H. Jr., "Millimeter wave vehicular communications: A survey," *Foundations and Trends in Networking*, vol. 10, no. 1, pp. 1–113, 2016.

[84] N. Gonzalez-Prelcic, A. Ali, V. Va, and R. W. Heath, "Millimeter-wave communication with out-of-band information," *IEEE Communications Magazine*, vol. 55, no. 12, pp. 140–146, Dec 2017.

[85] T. Rappaport, R. Heath, R. Daniels, and J. Murdock, *Millimeter Wave Wireless Communications*, ser. Prentice Hall Communications Engineering and Emerging Technologies Series from Ted Rappaport. Pearson Education, 2014.

[86] "IEEE standard for information technology–telecommunications and information exchange between systems–local and metropolitan area networks–specific requirements-part 11: Wireless lan medium access control (MAC) and physical layer (PHY) specifications amendment 3: Enhancements for very high throughput in the 60 ghz band," *IEEE Std 802.11ad-2012 (Amendment to IEEE Std 802.11-2012, as amended by IEEE Std 802.11ae-2012 and IEEE Std 802.11aa-2012)*, pp. 1–628, Dec 2012.

[87] E. Anderson, G. Yee, C. Phillips, D. Sicker, and D. Grunwald, "The impact of directional antenna models on simulation accuracy," in *2009 7th International Symposium on Modeling and Optimization in Mobile, Ad Hoc, and Wireless Networks*, June 2009, pp. 1–7.

[88] I. Holyer, "The np-completeness of edge-coloring," *SIAM Journal on computing*, vol. 10, no. 4, pp. 718–720, 1981.

[89] J. Song and K.-W. Chin, "A survey of single and multi-hop link schedulers for mmwave wireless systems," *Ad Hoc Networks*, vol. 33, pp. 269 – 283, 2015.

[90] F. Bai, D. D. Stancil, and H. Krishnan, "Toward understanding characteristics of Dedicated Short Range Communications (DSRC) from a perspective of vehicular network engineers," in *Proceedings of the Sixteenth Annual International Conference on Mobile Computing and Networking*, ser. MobiCom '10. New York, NY, USA: ACM, 2010, pp. 329–340.

[91] S. Takahashi, A. Kato, K. Sato, and M. Fujise, "Distance dependence of path-loss for millimeter wave inter-vehicle communications," in *2003 IEEE 58th Vehicular Technology Conference. VTC 2003-Fall*, vol. 1, Oct 2003, pp. 26–30 Vol.1.

[92] P. Kumari, J. Choi, N. González-Prelcic, and R. W. Heath, "IEEE 802.11ad-based radar: An approach to joint vehicular communication-radar system," *IEEE Transactions on Vehicular Technology*, vol. 67, no. 4, pp. 3012–3027, April 2018.

[93] "Simulation of urban mobility (sumo)," http://sumo.dlr.de/index.html.

[94] B. Cheng, A. Rostami, and M. Gruteser, "Experience: Accurate simulation of dense scenarios with hundreds of vehicular transmitters," in *Proceedings of the 22nd Annual International Conference on Mobile Computing and Networking*. ACM, 2016, pp. 271–279.

[95] H. Assasa and J. Widmer, "Implementation and evaluation of a WLAN IEEE 802.11 ad model in ns-3," in *Proceedings of the Workshop on ns-3*. ACM, 2016, pp. 57–64.

[96] A. Yamamoto, K. Ogawa, T. Horimatsu, A. Kato, and M. Fujise, "Path-loss prediction models for intervehicle communication at 60 ghz," *IEEE Transactions on vehicular technology*, vol. 57, no. 1, pp. 65–78, 2008.